SUPERCONDUCTIVITY, HIGH-TEMPERATURE SUPERCONDUCTIVITY

Effect of electron-magnon coupling on the electronic spectrum of weakly doped high-T_c compounds

M. A. Ivanov

Kurdyumov Institute of Metal Physics of the Ukrainian National Academy of Sciences, 36 Vernadskii Prs., 252142 Kiev-142, Ukraine

V. M. Loktev

*Bogolyubov Institute for Theoretical Physics of the Ukrainian National Academy of Sciences, 14-b Metrologichna Str., 252143 Kiev-143, Ukraine**

Yu. G. Pogorelov

Departamento de Fisica, Universidad do Porto, 4150 Porto, Portugal
(Submitted March 2, 1998)
Fiz. Nizk. Temp. **24**, 615–620 (July 1998)

A theoretic analysis of magnon-induced damping Γ of quasiparticle states in the normal phase of doped copper-oxide high-T_c materials is developed, based on a microscopic model which accounts for the specific $2D$ structure of their electron and magnon spectra. Among the obtained energy and temperature dependencies of Γ in different regimes, the most peculiar is the anomalously early onset of linear temperature dependence $\Gamma \propto T$ with a doping-independent coefficient. © *1998 American Institute of Physics.* [S1063-777X(98)00107-8]

1. INTRODUCTION

The studies of coexistence and interplay between magnetic and electric properties of layered copper oxides are one of the most immediate problems in high-T_c superconductivity (HTSC). The general scenario for development of phase states in these systems with their doping was already established from the very early experimental data.[1] The initial compounds are AFM-ordered Mott insulators with sufficiently high Néel temperature T_N, but this long-range magnetic order is very rapidly lost under small doping c, as evidenced by a sharp drop of T_N with c (until the AFM phase gets absorbed by the low temperature spin-glass and further spin-liquid phases); this process is followed by the insulator-metal transition. However, the metallic phase of HTSC compounds cannot be considered as ordinary paramagnetic one in the usual sense, since it still preserves the short-range AFM order which is clearly revealed in its either static and dynamic properties (see, e.g., Refs. 2–6 and also the reviews[7,8]). It should be stressed that, in copper-oxide materials, unlike common magnetic metals, there are two different kinds of fermions responsible for the conducting and magnetic properties. The conductivity is mainly determined by the charge carriers (holes, either mobile or localized) from the doping, whereas the strong magnetic correlations are mainly produced by the localized ''core'' spins. Also, these two kinds of particles are spatially separated: the carriers predominantly occupy the oxygen sites, and the core spins are those at copper sites. Notably, the destroying of long-range magnetic order in cuprate CuO_2 layers precedes the appearance of metallic conductivity in them; hence, at low concentration c of dopants, the HTSC compounds are still typical doped semiconductors with shallow acceptor levels and hopping type of conductivity (in particular, for the lanthanum system this is true at $c<5\%$, while the acceptor binding energy is $\varepsilon_0 \approx 35$ meV).[9,10] It follows from the aforesaid that the proper theoretic description of the breakdown of magnetic order and of the insulator-metal transition in HTSC (at least, for small c) perhaps cannot be based on commonly used translationally-invariant models. (The very number of such models, including different magnetic mechanisms of pairing, is too long to be counted, many of them are discussed in the reviews, Refs. 11–15).

At the same time, attempts have been made[16,17] (see also Refs. 18 and 19) to consider these problems, starting from the primordial importance of disordered (impurity) character of weakly doped HTSC compounds. Initially, mainly due to the change of the oxygen component, the acceptor levels with localized holes on them appear in AFM-ordered cuprate planes (this localization is greatly facilitated by the striking $2D$ character of HTSC electronic properties). At low c, these ''impurity'' holes give rise to a disordered spin subsystem on which the regular spin excitations (magnons) are scattered and hence damped. As a result, the long-range magnetic order gets destroyed and there appears such a minimum value $k_{\min}$ of wavevector that the magnons with $k<k_{\min}$ cannot exist because of strong damping. At lower concentrations this value is estimated as $k_{\min} \sim ca^{-1}$, but at higher concentrations (metallic ones including (see Ref. 20)) it is changed

for $k_{\min}\sim\sqrt{c/c_f}\lambda_B^{-1}$, where λ_B is the Bloch domain wall width and c_f is the concentration where the decaying $T_N(c)$ meets the freezing temperature of spin-glass transition. Hence the material can be considered magnetically disordered at distances $r>k_{\min}^{-1}\equiv\xi_{\mathrm{mag}}$, where ξ_{mag} is the magnetic correlation length. This finite length is determined by the doping rather than by the temperature. Nevertheless, magnons with $k>k_{\min}$ still exist and the magnetic order at distances $r<\xi_{\mathrm{mag}}$ is preserved (at least, at time scale $<\xi_{\mathrm{mag}}/v_s$, where v_s is the magnon velocity).

When the concentration grows up to $c>c_0$, where $c_0=\varepsilon_0/W$ is the characteristic concentration for insulator-metal transition (W is the whole conduction bandwidth), the Fermi level of free (hole) carriers is formed, manifesting the onset of metallic conductivity. It was shown that, within the scope of Lifshitz's impurity model, which is appropriate for HTSC materials, the $2D$ systems are in fact more favorable (at small c) for this transition than the $3D$ ones.[17]

However, the two above mentioned problems were treated in Refs. 16–18 independently: the destroying of magnetic order was calculated with neglect of the band of free carriers (the indirect interaction between localized hole spins was only considered as mediated by the spin-wave band). On the other hand, the localized core spins were ignored as possible scatterers for electronic excitations in calculating the characteristic concentration c_0. Undoubtedly, a more conclusive description of HTSC compounds should take both factors into account simultaneously: scattering of free carriers on localized spins and indirect interaction between localized spins via the conduction band (in real cuprates, the valence band). This determines the purpose of the present work, to study the influence of magnetic order in cuprate layers on electronic processes at metallization.

The consideration below is restricted to only effects by magnon (Bloch-like) excitations with $k>k_{\min}$, leaving mostly aside the low-energy spin excitations which are not described by the wavevector (spin fluctuation states). In other words, we consider the presence of magnon excitations in addition to the delocalized charge carriers, although the long-range magnetic order is absent. The main results of this analysis are the energy and temperature dependencies for the magnon-controlled inverse lifetime Γ of electronic quasiparticles near the Fermi level, specific for $2D$ system. In particular, a linear temperature dependence $\Gamma(T)$ is found to be concentration independent and to begin from lower temperatures than follows from the known estimates in literature. This behavior can contribute considerably to the broadly discussed linear temperature resistivity in the normal phase of high-T_c materials.

2. HAMILTONIAN AND GREEN FUNCTIONS

We choose the basic model which joins in a simple way the models previously used for description of the magnetic[16] and electronic[17] parts of the HTSC system (bearing in mind for instance the compound $La_2CuO_{4+\delta}$):

$$H=H_{\mathrm{el}}+H_s+H_{s-\mathrm{el}},$$

$$H_{\mathrm{el}}=\sum_{\mathbf{k},\sigma}\varepsilon_{\mathbf{k}}a^+_{\mathbf{k},\sigma}a_{\mathbf{k},\sigma}-\frac{\Delta\varepsilon}{N}\sum_{p,\mathbf{k},\mathbf{k}',\sigma}e^{i(\mathbf{k}-\mathbf{k}')\mathbf{p}}a^+_{\mathbf{k},\sigma}a_{\mathbf{k}',\sigma},$$

$$H_s=\sum_{\mathbf{q},j}\Omega_j(\mathbf{q})b^+_{\mathbf{q}j}b_{\mathbf{q}j}, \tag{1}$$

$$H_{s-\mathrm{el}}=\sum_{\mathbf{k},\mathbf{q},j}[\gamma_1(\mathbf{q})(a^+_{\mathbf{k},\uparrow}a_{\mathbf{k}-\mathbf{q},\downarrow}-a^+_{\mathbf{k},\downarrow}a_{\mathbf{k}-\mathbf{q},\uparrow})\times(b_{\mathbf{q}1}-b^+_{-\mathbf{q}1})+\gamma_2(\mathbf{q})(a^+_{\mathbf{k},\uparrow}a_{\mathbf{k}-\mathbf{q},\downarrow}+a^+_{\mathbf{k},\downarrow}a_{\mathbf{k}-\mathbf{q},\uparrow})\times(b_{\mathbf{q}2}+b^+_{-\mathbf{q}2})].$$

Here N is the number of elementary cells in the lattice, $a_{\mathbf{k},\sigma}$ and $b_{\mathbf{q}j}$ are respectively the Fermi and Bose operators for electronic and magnon excitations. They are labelled by two-dimensional wavevectors $\mathbf{k}$ and $\mathbf{q}$, with $\sigma=\uparrow,\downarrow$ related to the carrier spin states and $j=1,2$ to FM-like and AFM-like magnon branches, and characterized by the isotropic dispersion laws in the long wavelength region: $\varepsilon_{\mathbf{k}}=\hbar^2\mathbf{k}^2/2m$ and $\Omega_j^2(\mathbf{q})=\Omega_{gj}^2+\hbar^2v_s^2\mathbf{q}^2$. The effective mass m, the magnon velocity v_s and the spin-wave gaps Ω_{gj} can be expressed in terms of microscopic interaction parameters:

$$m=2\hbar^2/ta^2,\quad v_s=Ja/\hbar,$$

$$\Omega_{g1}=sz\sqrt{2J\Delta J_{\mathrm{rh}}},\quad \Omega_{g2}=sz\sqrt{2J\Delta J_t}\,. \tag{2}$$

For illustrative purposes, we shall use throughout this paper the parameter values for La_2CuO_4: the oxygen-oxygen hopping matrix element $t\approx0.6$ eV, the AFM exchange constant $J\approx0.1$ eV, the rhombic anisotropy $\Delta J_{\mathrm{rh}}\approx10^{-3}$ meV, the tetragonal anisotropy $\Delta J_t\approx8\times10^{-3}$ meV, the Cu^{2+} spin $s=1/2$, the in-plane coordination number $z=4$, and magnetic lattice parameter $a\approx5.4$ Å. This gives m of the order of the free electron mass, the bandwidth $W=\pi t\approx2$ eV, $\Omega_{g1}\approx1$ meV, $\Omega_{g2}\approx2.5$ meV, and $v_s\approx10^7$ cm/s (note that the latter value is comparable to typical values of the Fermi velocity v_F in the metallic phase of HTSC compounds). Finally, $\Delta\varepsilon>0$ in (1) is the shift of the local oxygen level from its initial position because of Coulomb field of the doped ions (see Ref. 17).

The spin-electron coupling $H_{s-\mathrm{el}}$ is derived from the standard Shubin–Vonsovsky model, using the specifics of spin structure for La_2CuO_4,[16] then the coupling parameters are

$$\gamma_j(\mathbf{q})\approx J'\left(\frac{z\Omega_j(\mathbf{q})}{2NJ}\right)^{1/2}, \tag{3}$$

where J' is the exchange parameter between the core spin and a carrier spin at the nearest neighbor oxygen site (it is supposed to be of the order of or even greater than J). Thus, formally this interaction is quite similar to the common electron-phonon coupling in metals, which was studied in detail by Yu. Kagan and co-workers (see, for example, Ref. 21). However, as will be seen below, the model under consideration possesses certain specifics, due to the $2D$ dispersion of either electron and magnon bands and to the absence of the usual adiabatic relation between the corresponding

velocities. Of course, one can also derive the electron-electron coupling (*d*-wave superconducting) from $H_{s-\mathrm{el}}$ but the analysis below will be restricted only to normal phases.

In addition to the above discussed translationally-invariant terms, the Hamiltonian, Eq. (1), namely, its H_{el} part, also contains the perturbation from dopants on oxygen sites **p**, distributed chaotically with concentration c (the minus sign before $\Delta\varepsilon$ accounts explicitly for attraction of carriers to charged dopants resulting in hole conductivity). In this study we focus mainly on the effects in electronic spectrum, so that impurity perturbations (such as, e.g., modification of the parameters J and J' near impurity sites, due to the evident shifts of the on-site electronic levels) are not included in H_s and $H_{s-\mathrm{el}}$. The corresponding effects can be accounted for implicitly by restricting the sums in the magnon wavevector to $q>k_{\min}$ and adding instead certain sums over (chaotic) spin fluctuation excitations. But to begin with such a so complicated problem, we shall at this first stage simply ignore the disorder effects in spin spectrum, and, only after obtaining the physical results, they will be checked with respect to the effects of spin disorder.

As usual, we shall infer the single-particle electronic properties from the Fourier-transformed two-time Green's functions (GF)

$$g_{\mathbf{k}}(\varepsilon)=\langle\langle a_{\mathbf{k},\sigma}|a^{+}_{\mathbf{k},\sigma}\rangle\rangle_{\varepsilon}=i\int_0^{\infty}\mathrm{e}^{i(\varepsilon+i0)t}\langle\{a_{\mathbf{k},\sigma}(t),a^{+}_{\mathbf{k},\sigma}\}\rangle dt, \tag{4}$$

where {.,.} is the anticommutator and $\langle ...\rangle$ the quantum-statistical average. Their poles in the complex energy plane determine the energy spectrum and damping of quasiparticles.

A necessary pre-requisite for studying the impurity effects is a detailed knowledge of dynamics for the ''background'' uniform system (often this presents an independent problem in complex systems such as HTSC compounds). Hence, as a first step, we omit the impurity term even in H_{el}. Then the equations of motion for GF, Eq. (4), to the lowest order in spin-electron coupling, readily yield the result:

$$\begin{aligned} g_{\mathbf{k}}(\varepsilon)&=[\varepsilon-\varepsilon_{\mathbf{k}}-\Pi_{\mathbf{k}}(\varepsilon)]^{-1},\\ \Pi_{\mathbf{k}}(\varepsilon)&=\sum_{\mathbf{q},j}\gamma_j^2(\mathbf{q})\left(\frac{1-f_{|\mathbf{k}-\mathbf{q}|}+n_{\mathbf{q}j}}{\varepsilon_{\mathbf{k}}-\varepsilon_{|\mathbf{k}-\mathbf{q}|}-\Omega_j(\mathbf{q})}\right.\\ &\left.+\frac{f_{|\mathbf{k}-\mathbf{q}|}+n_{\mathbf{q}j}}{\varepsilon_{\mathbf{k}}-\varepsilon_{|\mathbf{k}-\mathbf{q}|}+\Omega_j(\mathbf{q})}\right), \end{aligned} \tag{5}$$

where $f_{\mathbf{k}}=\{\exp[(\varepsilon_{\mathbf{k}}-\varepsilon_F)/T]+1\}^{-1}$ and $n_{\mathbf{q}j}=\{\exp[\Omega_j(\mathbf{q})/T]-1\}^{-1}$ are the Fermi and Bose occupation numbers, and ε_F is the Fermi energy of the free holes; this coincides with the well-known expressions, e.g., from Ref. 22. Below we consider in detail how the properties of electron and magnon spectra, specific for our system, are reflected in the behavior of this otherwise comprehensively studied self-energy term $\Pi_{\mathbf{k}}(\varepsilon)$. Firstly we consider the broadening of electronic states close to the very Fermi level at zero temperature, due to inelastic electron-electron scattering with creation of magnons. Then we pass to the damping of electronic states on the Fermi level itself at finite temperatures, including processes with thermal magnons.

3. DAMPING NEAR THE FERMI LEVEL AT $T=0$

As long as we neglect the impurity perturbation $\Delta\varepsilon$, but consider some finite doping level c, a well-defined Fermi level $\varepsilon_F=cW/2$ exists in the $2D$ electronic spectrum.[17,18] The broadening $\Gamma_{\mathbf{k}}$ of quasiparticle levels close to ε_F is given by $\Gamma_{\mathbf{k}}=\mathrm{Im}\,\Pi_{\mathbf{k}}(\varepsilon_{\mathbf{k}})$. However, bearing in mind that, in fact, the metallic state in HTSC compounds onsets well after the breakdown of long-range magnetic order, we should not consider quasiparticle energies closer to ε_F than to the lower boundary energy of magnons, $\Omega_{\min}$. Since the latter value exceeds both spin-wave gaps Ω_{gj},[16] we can take the magnon dispersion law in the relevant region to be identical for the two branches and linear: $\Omega_j(\mathbf{q})=\Omega_g\approx\hbar v_s q$. Moreover, we extend this law to the whole magnon band, forgetting for a moment the long-wave limitation (we shall recall it at the end of this Section). Then, using Eq. (5) at $T=0$, and taking into account the $2D$ character of spin-wave spectrum, we arrive at:

$$\begin{aligned} \Gamma_{\mathbf{k}}=\Gamma_0 a\int_0^{q_{\max}}q\,dq\int_0^{2\pi}d\varphi[\,&\delta(2k\,\cos\,\varphi-q+2k_s)\\ &\times\theta(\varepsilon_F-\varepsilon_{\mathbf{k}}-\hbar v_s q)+\delta(2k\,\cos\,\varphi-q-2k_s)\\ &\times\theta(\varepsilon_{\mathbf{k}}-\varepsilon_F-\hbar v_s q)], \end{aligned} \tag{6}$$

where $\Gamma_0=4\pi z J'^2/W$, $k_s=\beta k_F$, and $\beta\equiv v_s/v_F$. The Fermi velocity depends directly on the doping level c: $v_F=v_a\sqrt{c}$, where $v_a=\sqrt{\pi/2}\,a(t/\hbar)$, and, with our choice of parameters, $v_a\approx 7\times 10^7$ cm/s. The v_F is close to v_s (the ratio β is close to unity) for c being a few percent (this is in striking contrast with the usual situation for electron-phonon coupling in conventional metals where the sound velocity is about three orders of magnitude lower than v_F). After elementary integration, Eq. (6) yields an analytic result:

$$\begin{aligned} \Gamma_{\mathbf{k}}=2\Gamma_0 a\left[\sqrt{k^2-k_s^2}-\sqrt{k^2-(k_s-q_{\mathbf{k}})^2}+k_s\left(\arcsin\frac{k_s}{k}\right.\right.\\ \left.\left.-\arcsin\frac{k_s-q_{\mathbf{k}}}{k}\right)\right]\theta(k-k_s)\,\theta(k-k_s+q_{\mathbf{k}}), \end{aligned} \tag{7}$$

where $q_{\mathbf{k}}=(\varepsilon_{\mathbf{k}}-\varepsilon_F)/(2\beta\hbar v_F)$. The θ-functions in Eq. (7) determine that $\Gamma_{\mathbf{k}}$ drops to zero below certain threshold quasimomentum value, namely: for $k<(8k_s^2+k_F^2)^{1/2}-2k_s$ if $\beta<1$, and for $k<k_s$ if $\beta>1$. Close to the Fermi surface (at $\beta<1$) we obtain a quadratic dependence of $\Gamma_{\mathbf{k}}=\Gamma(\varepsilon)$ on the quasiparticle energy $\varepsilon=\varepsilon_{\mathbf{k}}-\varepsilon_F$:

$$\Gamma(\varepsilon)\approx\frac{\Gamma_0}{ak_F\sqrt{1-\beta^2}}\left(\frac{\varepsilon}{4J}\right)^2, \tag{8}$$

which is characteristic of $2D$ dispersion, unlike the usual ε^3 law in $3D$ systems.[22] Note that, since the relation $ak_F=\sqrt{2\pi c}$, this function increases with *decreasing* concentration. In no way does the presence of the enhancement factor $(1-\beta^2)^{-1/2}$ in the latter formula mean divergence of $\Gamma(\varepsilon)$ in

the ''relativistic'' limit $\beta \to 1$ (reached when the concentration decreases down to $c \to c_s = 2\pi(J/W)^2$): in this case the quadratic law, Eq. (8), is simply changed for a $\varepsilon^{3/2}$ law: $\Gamma(\varepsilon, c_s) \approx 0.6(J'/J)^2 W^{-1/2} \varepsilon^{3/2}$. With the parameter values adopted in Sec. 2, we come to the conclusion (at least, when $T=0$) that the usual Fermi-liquid condition $\Gamma(\varepsilon)/\varepsilon < 1$ is well assured for the considered magnon-induced damping in a rather broad vicinity of the Fermi surface at all relevant concentrations $c > c_0$.

To conclude this Section, we estimate the region of validity of Eqs. (7) and (8) with respect to the above mentioned neglection of spin fluctuation states. In fact, the integration over q in Eq. (6) is only legal for $q > k_{\min}$ (see Sec. 1), hence the result, Eq. (7), will not make sense if $q_{\mathbf{k}} \lesssim 2k_{\min}$. Then, with the estimate $k_{\min} \sim c(J'/J)^2 a^{-1}$ for a minimum magnon wavevector at $T=0$ [Ref. (16)] the formula, Eq. (8), is found to fail only within a narrow fluctuation region: $|\varepsilon| \lesssim \varepsilon_f \sim cJ'^2/J$. At the boundary of this region, we have the Fermi-liquid ratio $\Gamma(\varepsilon_f)/\varepsilon_f \sim \sqrt{\pi c/2}\, J'^4/WJ^3$, which is considerably smaller than unity. At least, the simplest assertion on the behavior of Γ within the fluctuation region is obtained by changing the ''magnon density of states'' factor q in Eq. (6) by a constant value $\sim k_{\min}$ at $q < k_{\min}$, which gives $\Gamma(\varepsilon) \sim \Gamma(\varepsilon_f)$ at $|\varepsilon| \lesssim \varepsilon_f$, when it is impossible to speak about undamped quasiparticles.

4. DAMPING OF FERMI STATES AT FINITE TEMPERATURES

Using explicitly the δ-function relations in the occupation numbers $f_{|\mathbf{k}-\mathbf{q}|}$ and $n_{\mathbf{q}j}$ in $\mathrm{Im}\,\Pi_{\mathbf{k}}(\varepsilon_{\mathbf{k}})$ at $\varepsilon_{\mathbf{k}} = \varepsilon_F$, the temperature dependent broadening at the very Fermi level can be obtained from Eq. (5) in the simple form:

$$\Gamma_F(T) = 2\Gamma_0 a k_F \left[\int_0^{1-\beta} \frac{x\,dx}{\sinh(2Jak_F x/T)\sqrt{1-(\beta+x)^2}} + \int_0^{1+\beta} \frac{x\,dx}{\sinh(2Jak_F x/T)\sqrt{1-(\beta-x)^2}} \right]. \quad (9)$$

This expression exhibits a crossover from quadratic function of temperature:

$$\Gamma_F(T) \approx \frac{\Gamma_0}{2ak_F\sqrt{1-\beta^2}} \left(\frac{\pi T}{J}\right)^2 \quad (10)$$

at low temperatures: $T \ll 2Jak_F$ (which decreases as a function of c alike $\Gamma(\varepsilon)$, Eq. (8)), to linear function of temperature at $T \gg 2Jak_F \equiv 2\Omega_j(\mathbf{k}_F)$ which, remarkably, is concentration independent:

$$\Gamma_F(T) \approx \Gamma_0 \frac{\pi T}{J}. \quad (11)$$

Such a crossover is rather clear, if we notice that the thermal magnon wavevector $q_T = T/\hbar v_s$ exceeds the diameter $2k_F$ of the Fermi circle just at $T > 2Jak_F$, but the independence of Eq. (11) on $\mathbf{k}_F$ is another characteristic feature of $2D$ dispersion, also in striking contrast with $3D$ systems. The crossover temperature found from comparison of the values, Eqs. (10) and (11), is $T_{c-o} = 2Jak_F\sqrt{1-\beta^2}/\pi$. In fact, this crossover, as seen from direct numeric calculations, using Eq. (9) and the parameter values chosen in Sec. 2 (Fig. 1), occurs even earlier, at about $0.6T_{c-o}$, which is essentially lower than the commonly considered value $T_{c-o} \sim J$.[23]

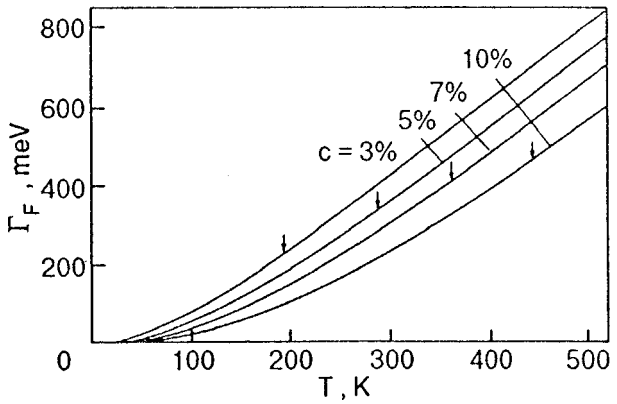

FIG. 1. Temperature dependence of quasiparticle broadening at the Fermi level for different dopant concentrations. The arrows indicate the calculated values of crossover temperature T_{c-o}, but the visible linearity extends to even lower temperatures.

Taking into mind the estimate, in the end of the previous section, for the fluctuation limit $\Gamma(\varepsilon_f)$ of the broadening close to the Fermi level, it follows that this constant limit can be reached for $\Gamma_F(T)$, with lowering temperature, at some value $T_f \sim \sqrt{c}(J'/J)T_{c-o}$, which is yet much lower than the crossover temperature value.

ACKNOWLEDGMENTS

We are pleased to devote this paper to the seventieth anniversary of Prof. Yu. Kagan whose contribution to the physics of disordered systems in general and high-T_c superconductors in particular cannot be overestimated. Taking this opportunity we would like to acknowledge Prof. Yu. Kagan for his numberless discussions and benevolent criticisms of our results which always were useful and helpful for us.

One of us (Yu.G.P.) thanks the support from the Portuguese Program PRAXIS XXI through the project BCC/6428/95.

*E-mail:vloktev@gluk.apc.org

[1] R. J. Birgeneau and G. Shirane, in *Physical Properties of High-T_c Superconductors*, I, 151 (1990).
[2] D. Vakhnin, S. K. Sinha, D. E. Monston, D. C. Johnston, J. M. Newsom, C. R. Safenya, and J. H. E. King, Phys. Rev. Lett. **58**, 2802 (1987).
[3] T. Thio, T. R. Thurston, N. W. Preyer, P. J. Picone, M. A. Kastner, H. P. Jenssen, D. R. Gabbe, C. Y. Chen, R. J. Birgeneau, and A. Aharony, Phys. Rev. B **38**, 905 (1988).
[4] S.-W. Cheong, Z. Fisk, and J. O. Willis, Solid State Commun. **65**, 111 (1988).
[5] H. Fai Fong, Phys. Rev. Lett. **75**, 316 (1995).
[6] S. M. Hayden, G. Aeppli, H. A. Mook, T. G. Perring, I. E. Mason, S.-W. Cheong, and Z. Fisk, Phys. Rev. Lett. **76**, 1344 (1996).
[7] G. Shirane, R. J. Birgeneau, Y. Endoh, and M. A. Kastner, Physica B **197**, 158 (1994).
[8] V. M. Loktev, Fiz. Nizk. Temp. **22**, 3 (1996) [Low Temp. Phys. **22**, 1 (1996)].
[9] N. W. Preyer, R. J. Birgeneau, C. Y. Chen, D. R. Gabbe, H. P. Jenssen, M. A. Kastner, P. J. Picone, and T. Thio, Phys. Rev. B **39**, 11563 (1989).
[10] J. P. Flack, A. Levy, M. A. Kastner, and R. J. Birgeneau, Phys. Rev. Lett. **69**, 1109 (1992).

[11] Yu. A. Izyumov, Phys. Usp. **165**, 403 (1995).
[12] W. E. Pickett, Rev. Mod. Phys. **61**, 433 (1989).
[13] A. P. Kampf, Phys. Rep. **249**, 219 (1994).
[14] W. Brenig, Phys. Rep. **251**, 153 (1995).
[15] D. Pines, Tr. J. Phys. **20**, 535 (1996).
[16] M. A. Ivanov, V. M. Loktev, and Yu. G. Pogorelov, Zh. Éksp. Teor. Fiz. **101**, 596 (1992) [Sov. Phys. JETP **74**, 317 (1992)].
[17] M. A. Ivanov, V. M. Loktev, Yu. G. Pogorelov, and Yu. V. Skripnik, Fiz. Nizk. Temp. **17**, 716 (1991) [Sov. J. Low Temp. Phys. **17**, 377 (1991)].
[18] M. A. Ivanov, V. M. Loktev, and Yu. V. Skripnik, Fiz. Nizk. Temp. **22**, 1186 (1996) [Low Temp. Phys. **22**, 907 (1996)].
[19] V. M. Loktev and Yu. G. Pogorelov, Fiz. Nizk. Temp. **22**, 1018 (1996) [Low Temp. Phys. **22**, 776 (1996)].
[20] V. M. Loktev, Supercond., Phys., Chem., Technol. **4**, 2293 (1991).
[21] Yu. M. Kagan and A. P. Zhernov, Sov. Phys. JETP **23**, 737 (1966).
[22] L. D. Landau and E. M. Lifshitz, *Course of Theoretical Physics*, Vol. 9: E. M. Lifshitz and L. P. Pitaevskii, *Statistical Physics*, Part II, Pergamon Press, Oxford (1980).
[23] H. Kohno and K. Yamada, Prog. Theor. Phys. **85**, 13 (1991).

This article was published in English in the original Russian journal. It was edited by R. T. Beyer.

Mechanisms of critical current limitation in YBCO thin film structures

Š. Beňačka, V. Štrbik, Š. Chromik, R. Adam, M. Darula, and Š. Gaži

*Institute of Electrical Engineering, Slovak Academy of Sciences, 842 39 Bratislava, Slovak Republic**

(Submitted March 10, 1998)
Fiz. Nizk. Temp. **24**, 621–623 (July 1998)

The limitation of critical current in high T_c superconducting YBCO thin films has a varied nature according to the quality of YBCO films. Our results showed that in strips from granular films the weak links of superconductor–normal metal–superconductor and superconductor–constriction–superconductor types were responsible for critical current limitation. In the YBCO strips with improved (preferential) crystallographic orientation a flux-creep critical current limitation was found and in the highly oriented YBCO strips the Ginzburg–Landau depairing mechanism approximated the critical current limitation for temperature close to T_c.
 [S1063-777X(98)00207-2]

1. INTRODUCTION

The critical current (or critical current density) is one of the most important parameters of the transport electrical properties of high temperature superconducting thin film strips. Various critical current limiting mechanisms (CCLM) take part according to the thin film quality. The nature of CCLM can be recognized from the critical current vs. temperature dependence $[I_c(T)]$. The important contribution to these problems in low T_c film strips have been made by the I. M. Dmitrenko group from Kharkov (see the excellent review paper[1] and papers cited therein). In this contribution we review some of our results concerning $I_c(T)$ studies on high T_c superconducting thin films, strips and junctions, stimulated by Prof. I. M. Dmitrenko's results and personal contacts.

2. EXPERIMENTAL, RESULTS AND DISCUSSION

The $YBa_2Cu_3O_{7-x}$ (YBCO) thin films were deposited by dc magnetron sputtering or vacuum coevaporation method on MgO, $SrTiO_3$, or YSZ and CeO_2 buffered Al_2O_3 single crystal substrates. The strips were patterned by wet or ion beam etching.

In Fig. 1 we summarize $I_c(T)$ dependencies in normalized units, where $I_c(T)/I_c(0) \equiv j_c(T)/j_c(0)$ and $t = T/T_c$. We analyzed the $j_c(t)$ dependencies of superconducting strips prepared from granular YBCO films (solid and open circles in dependencies *a*, *b*) in terms of weak link connections between grains, where the power dependence $j_c(t) = j_c(0)(1-t)^{\alpha}$ occurs and α characterizes the type of current transport through weak links. The fitted dependencies with $\alpha \geqslant 2.5$ (dashed line, curve *a*) are characteristic for YBCO films with depressed T_c and low critical current density $[j_c(0) < 10^3$ A/cm^2 at self-field conditions] and can be ascribed to nonhomogeneous superconductors with large dispersion of individual connections in weak link network of our granular films.[2,3] In case of YBCO films, where $\alpha \approx 1.5$–2 (dashed line *b* in Fig. 1), weak links of ScS (superconductor–constriction–superconductor) or SNS (superconductor–normal metal–superconductor) type dominate. The maximal critical current density of these samples was $j_c(0) \approx 10^4$ A/cm^2. On the basis of experimental observations one can conclude that the dc transport properties of granular films are determined by weak links between the superconducting grains, thus strongly reducing much higher critical current density of film grains.[2]

The temperature dependence of critical current density of stripes, patterned from preferentially oriented YBCO thin films, exhibits downward curvature of $j_c(t)$ (solid and open triangles on curve *c*). In this case a new mechanism of critical current limitation begins to dominate. We ascribe this CCLM to the flux creep, and the full line (curve *c*) represents the fit of experimental data computed from relation[4,5]

$$j_c(t) = j_c(0)(1 - mt - nt^2), \tag{1}$$

where $m = 0.5$, $n = 0.53$, and $j_c(0) = 2.6 \times 10^6$ A/cm^2. Because this type of $j_c(t)$ is characteristic for samples with $j_c(0) \approx 10^6$ A/cm^2 we suppose that the intergranular weak links are not responsible for critical current limitation. The current-voltage (I-V) characteristics of these samples in the low voltage range (just above I_c) also confirmed the flux-creep dissipation process.[5]

The strips patterned from YBCO thin films epitaxially grown on $SrTiO_3$ single crystal substrate $[j_c(0) \geqslant 10^7$ A/cm$^2]$ usually displayed the $j_c(t)$ dependence corresponding to curve *d* in Fig. 1. The study of these temperature dependencies of critical current indicated a Ginzburg–Landau (GL) depairing mechanism in the temperature range close to T_c.[6] The critical current of the microstrip approaches GL depairing current $I_d(t)$[1,7] when the width w and thickness d of the strip are smaller or comparable to the transverse magnetic penetration depth of the thin film

$$\lambda_{\perp} = \lambda \coth(d/2\lambda), \tag{2}$$

where λ is London penetration depth. If we consider the temperature dependence of magnetic field penetration depth $\lambda(t) = \lambda(0)/(1-t^4)^{1/2}$ for temperature close to T_c we obtain $\lambda_{\perp} \approx 5-10$ μm which fulfill the conditions $w \leqslant \lambda_{\perp}$ and d

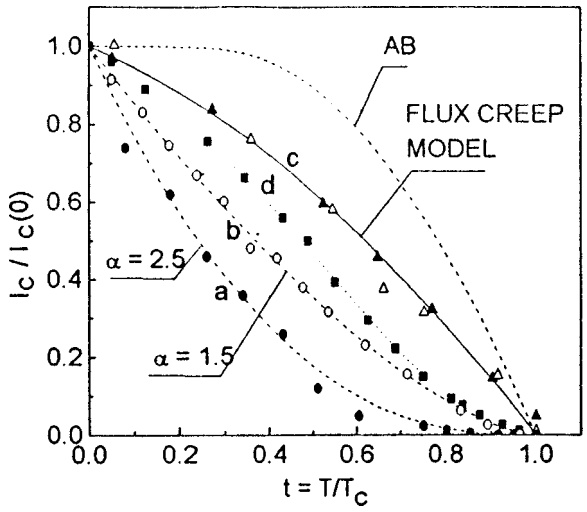

FIG. 1. Temperature dependence of the critical current density of YBCO thin film strips of different quality (see text).

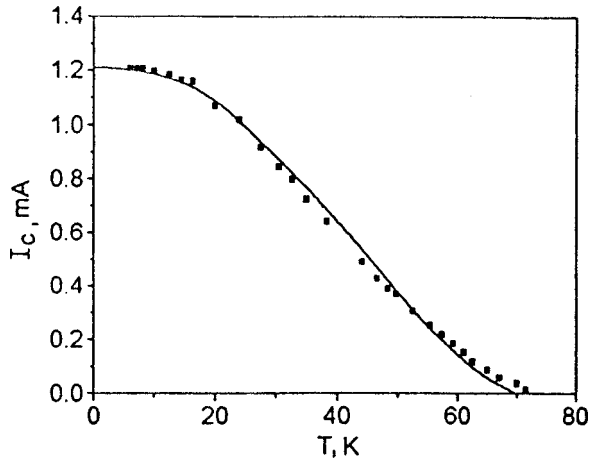

FIG. 3. The dependence of critical current I_c vs temperature of a bicrystal grain boundary Josephson junction. Full line: modified Usadel equation for $L/\xi_N = 0.6-4.2$.

$\ll\lambda_\perp$ [$\lambda(0)=200$ nm and $d=50$ nm were used in Eq. (2)], i.e., homogeneous cross-sectional distribution of transport current in the strip. In Fig. 2 the experimental $j_c(t)$ dependence (solid squares) is compared with GL depairing current density (full line)

$$j_d(t)=j_d(0)(1-t)^{3/2}, \tag{3}$$

where $j_d(0)=[\Phi_0/3\sqrt{3}\mu_0\pi\lambda^2(0)\xi(0)]$is the depairing current density at $T=0$; Φ_0 is magnetic flux quantum and $\xi(0)$ is coherence length. The value $j_d(0)\approx 2\times 10^7$ A/cm^2 extrapolated from experimental dependence is in reasonable agreement with the value computed from Eq. (3): $j_d(0)\approx 8\times 10^7$ A/cm^2 for $\lambda(0)\approx 200$ nm and $\xi(0)\approx 3$ nm. These experimental results have shown that $j_c(t)$ close to T_c may approach the GL depairing current as a limiting mechanism.

In the low temperature range (the dependence d in Fig. 1, $t<0.6$) where $w>\lambda_\perp$ (wide strip) another CCLM takes place. Due to current concentration at the strip edges, the edge barrier to vortex entry is lowered, and dissipation process in microstrip starts at the current value[8]

$$I_{c1}\approx(\Phi_0/\mu_0\lambda_\perp)\ln(d/4\xi), \tag{4}$$

the ''lower'' critical current. The depression of $j_c(t)$ more than one order of magnitude [for wide strips $w>\lambda_\perp(t)$], in comparison to $j_d(t)$, can be explained by the entering of Abrikosov vortices into the superconductor and their motion across the strip.[6]

Phase-slip phenomena (PSP) in the one-dimensional superconducting strips[9] as well as in wide strips (moving phase-slip centers or phase-slip lines), may occur as CCLM.[1] In this case the temperature dependence of the critical current density is described by the relation $j_c(t)=j_c(0)\times(1-t)^{3/2}$, predicted by GL theory [Eq. (3), but $j_c(0)<j_d(0)$], and the dissipation process is characterized by ''quantized'' increases of differential resistance in the *I-V* characteristic. We observed properties similar to PSP in 10-μm wide and 100 μm long granular YBCO strips.[10] The estimated quasi-particle diffusion length (≈ 25 μm) and temperature dependence of current at voltage steps (i.e., differential resistance increases) are in accordance with the PSP theory. We have concluded that grain boundaries and quality of the strip edges play very important roles in the PSP, and in the critical current limitation in wide as well as narrow YBCO strips.

We also investigated the $I_c(T)$dependencies of YBCO grain boundary Josephson junctions of bicrystal type.[11] The most adequate fit (full line in Fig. 3) to the experimental $I_c(T)$ dependence (solid squares) we explained by the model of the temperature dependent ratio L/ξ_N, where L is the length of a normal region in the YBCO strip at a bicrystal boundary in the direction of current flow and ξ_N is the coherence length of the normal region. In this case the temperature dependent transparency of the junction normal region for superconducting carriers is the main factor of

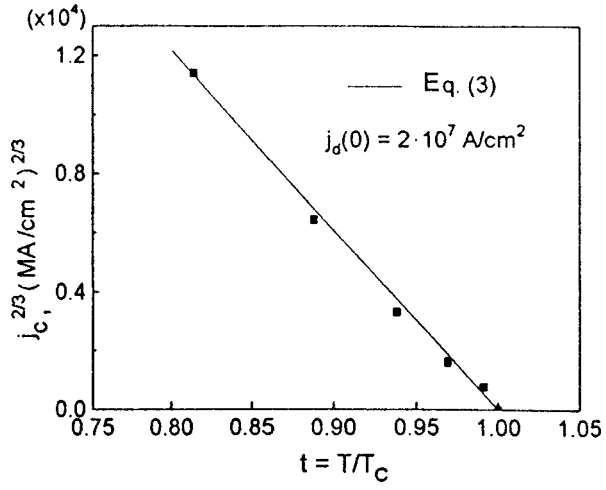

FIG. 2. Ginzburg–Landau depairing critical current density limitation (full line) for ''narrow'' YBCO strips close to the critical temperature.

CCLM. The Ambegaokar–Baratoff[12] $I_c(t)$ dependence (AB in Fig. 1) in our studies is not suitable for approximation of any one dependence for YBCO strips, sandwich YBCO/PrBaCuO/YBCO[13] or bicrystal grain boundary SNS junctions.

3. SUMMARY

In this contribution we reviewed various mechanisms of critical current limitation in high T_c superconducting YBCO thin film strips and structures. We analyzed these mechanisms on the base of the temperature dependence of the critical current and corresponding models that are valid for low T_c superconductors. The weak links, mainly of SNS and ScS types, flux-creep, Ginzburg–Landau depairing current, phase slip phenomena and temperature dependent ''transparency'' of the bicrystal junction for transport superconducting current are responsible for critical current limitation in high temperature superconducting thin film samples.

The authors are obliged to Professor I. M. Dmitrenko for a great many fruitful working discussions and human contacts in Bratislava and Kharkov, and they wish dear I.M. even better years of productive work, health, and further close contacts with the group in Bratislava.

*E-mail: elekbena@savba.sk

[1] I. M. Dmitrenko, Fiz. Nizk. Temp. **22**, 849 (1996) [Low Temp. Phys. **22**, 648 (1996)].
[2] V. Štrbik, Š. Beňačka, Š. Gaži, Š. Chromik, J. Levarsky, and J. Sith, Mod. Phys. Lett. B **3**, 729 (1989).
[3] N. Savvides, Physica C **165**, 371 (1990).
[4] J. Mannhart, P. Chaudhari, O. Dimos, C. C. Tsnei, and T. R. McGuire, Phys. Rev. Lett. **61**, 2476 (1988).
[5] V. Štrbik, R. Adam, Š. Beňačka, and Š. Chromik, in *Proceedings of the Intern. Workshop on Critical Current Limitations in High Temperature Superconductors*, Zaborow (Poland) (1991), p. 366.
[6] V. Štrbik, Š. Beňačka, Š. Chromik, R. Adam, P. Tomaš, E. Pinčik, and V. Šmatko, *presented on International Conference: Critical Currents in High T_c Superconductors*, Vienna (1992).
[7] K. K. Likharev, Zh. Éksp. Teor. Fiz. **61**, 1700 (1971) [Sov. Phys. JETP **34**, 906 (1972)].
[8] K. K. Likharev, Radiofizika **14**, 919 (1971).
[9] W. J. Skocpol, M. R. Beasley, and M. Tinkham, J. Low Temp. Phys. **16**, 145 (1974).
[10] V. Štrbik, R. Adam, and Š. Beňačka, in *Proceedings of Weak Superconductivity Symposium*, Smolenice (Slovak Republic) (1989), p. 75.
[11] V. Štrbik, O. Harnack, Š. Chromik, M. Darula, and Š. Beňačka, Appl. Supercond. (1997); in *Proceedings of EU-CAS'97*, H. Rogalla and D. H. A. Blank (Eds.), Inst. of Physics, Conf. Series No. 158, p. 503.
[12] V. Ambegaokar and A. Baratoff, Phys. Rev. Lett. **10**, 486 (1963).
[13] Unpublished results of authors.

This article was published in English in the original Russian journal. It was edited by R. T. Beyer.

Frequency and temperature dependences of impedance of HTSC ceramics

V. M. Dmitriev,*,** L. A. Ishchenko, and N. N. Prentslau

B. Verkin Institute for Low Temperature Physics and Engineering, National Academy of Sciences of the Ukraine, 310164 Kharkov, Ukraine

(Submitted August 12, 1997; revised March 10, 1998)
Fiz. Nizk. Temp. **24**, 624–626 (July 1998)

Anomalies in ohmic losses in HTSC ceramics are considered in the low- and radio-frequency ranges. It is found experimentally that the width of the $N-S$ transition in the ceramics ($YBa_2Cu_3O_7+1\%$ ^{57}Fe), $SmBa_2Cu_3O_7$, and $YBa_2Cu_{3-x}Sc_xO_7$ in a weak magnetic field (up to 50 Oe) becomes smaller in the frequency interval between f_c and f_F at which the resistance does not depend on temperature. It is shown that, for some types of HTSC and for different samples of the same type, the frequency f_c does not correlate with the superconducting transition temperature T_c. © *1998 American Institute of Physics.* [S1063-777X(98)00307-7]

INTRODUCTION

In our previous publications,[1–4] we reported on the peculiarities in ohmic losses R for high-temperature superconductors (HTSC) in the low- and radio-frequency ranges ($0-10^8$ Hz) where the magnitude and sign of the temperature derivative $\partial R/\partial T$ are complex functions of frequency. Among other things, we proved that the derivative $\partial R/\partial T$ changes sign in a certain frequency range $\Delta f=f_F-f_c$, and hence ohmic losses at frequencies f_F and $f_c<f_F$ do not depend on temperature ($\partial R/\partial T=0$).[2,3] This property of resistance R, which has been observed for most types of HTSC in the normal state,[3] can be explained qualitatively in the two-band model of a superconductor with narrow and wide electron bands.[2]

According to Ref. 4, the frequency f_c and the temperature derivative of the dc resistivity ρ reduced to ρ_0 ($S=(\partial\rho/\partial T)/\rho_0$) are interrelated. (Here ρ_0 is the resistivity on the initial segment of the linear dependence $\rho(T)$ at low temperatures.)

In the frequency range Δf, the temperature-, frequency-, and magnetic-field dependence of the resistance R display singularities in the superconducting state of HTSC also. For example, the effect of the magnetic field H on R in the range Δf is observed not at the superconducting transition temperature T_c measured in direct current or at frequencies outside the range Δf, but at a temperature T_{c1} which can be lower than T_c by several kelvins (up to ten). (Here T_c is the temperature at which the resistance changes under the effect of a weak magnetostatic field during the $N-S$ transition.) In the temperature range $\Delta T=T_c-T_{c1}$, ohmic losses R are virtually independent of temperature.

Thus, the properties typical of a superconductor ($\partial R/\partial T>0$ and $\partial R/\partial H>0$) start being manifested at $T<T_{c1}$ in the frequency range Δf and at $T<T_c$ outside this frequency interval.

These peculiarities of R in the range Δf are observed virtually for all samples being investigated and for all types of HTSC except ceramics with ferromagnetic impurities ($YBa_2Cu_3O_7+1\%$ ^{57}Fe) or with paramagnetic properties (PMP) $SmBa_2Cu_3O_7$[3] and $YBa_2Cu_{3-x}Sc_xO_7$.[3,5]

By way of an example, it was proved[3] that a weak magnetic field $YBa_2Cu_3O_7+1\%$ ^{57}Fe ceramic at $T<T_c$ partially reduces ohmic losses in the rf range Δf, while outside this range the field enhances the losses.

Here we report on the results of further investigations of this effect at $T<T_c$ in HTSC ceramics with a low value of f_c and consider the interrelation between T_c and f_c.

DISCUSSION OF RESULTS

We measured the $R(T,H,f)$ dependences at $T<T_c$ in the HTSC ceramic $YBa_2Cu_{2.95}Sc_{0.05}O_7$ with the following parameters: $T_c=92$ K, $T_{c1}=91.8$ K, $f_c=3\times10^3$ Hz, and $f_F=10^5$ Hz.

Figure 1 shows temperature dependences of the resistance R reduced to $R(92\text{ K})$ and measured at frequencies 10^3 Hz (curves *1* and *2*), 5×10^3 Hz (curves *3* and *4*), and 10^7 Hz (curves *5* and *6*) in zero magnetic field (odd curves) and in a magnetostatic field of 50 Oe (even curves).

It can be seen from Fig. 1 that at frequencies below f_c (curves *1* and *2*) and above f_F (curves *5* and *6*), ohmic losses in the ceramic in the magnetostatic field become higher, and the effect of magnetic field on the resistance R starts being manifested at the temperature $T_c(92\text{ K})$. Thus, the ceramics under investigation at these two frequencies exhibits ordinary properties of a superconductor.

A different situation is observed at frequencies in the interval Δf. In a certain temperature range $\Delta T=T_c-T_{c1}$, the resistance R is independent of temperature as in HTSC without ferromagnetic impurities or PMP. The resistance decreases at $T<T_{c1}$ and attains instrumental zero at $T=79$ K. However, the effect of a magnetic field on ohmic losses R starts being manifested in this case not at T_{c1} as in HTSC without ferromagnetic impurities or PMP, but at T_c. In this case, $\partial R/\partial T|_{H>0}>\partial R/\partial T|_{H=0}$, and hence the resistance R in a magnetic field attains instrumental zero even at 84 K.

Thus, the width of the $N-S$ transition in a HTSC with PMP or ferromagnetic impurities in a weak magnetic field H in the frequency range Δf becomes narrower than in zero magnetic field.

Since ohmic losses R are manifested in HTSC in the

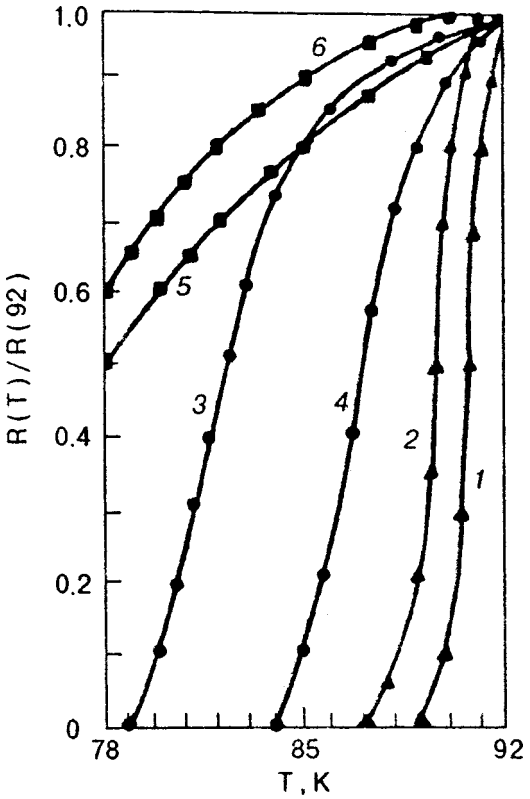

FIG. 1. Temperature dependence of ohmic losses in $YBa_2Cu_{2.95}Sc_{0.05}O_7$ ceramics, which are reduced to $T=92$ K, at frequencies 10^3 Hz (curves *1, 2*), 5×10^3 Hz (curves *3, 4*), and 10^7 Hz (curves *5, 6*) in zero magnetic field (curves *1, 3, 5*) and in a magnetic field of 50 Oe (curves *2, 4, 6*).

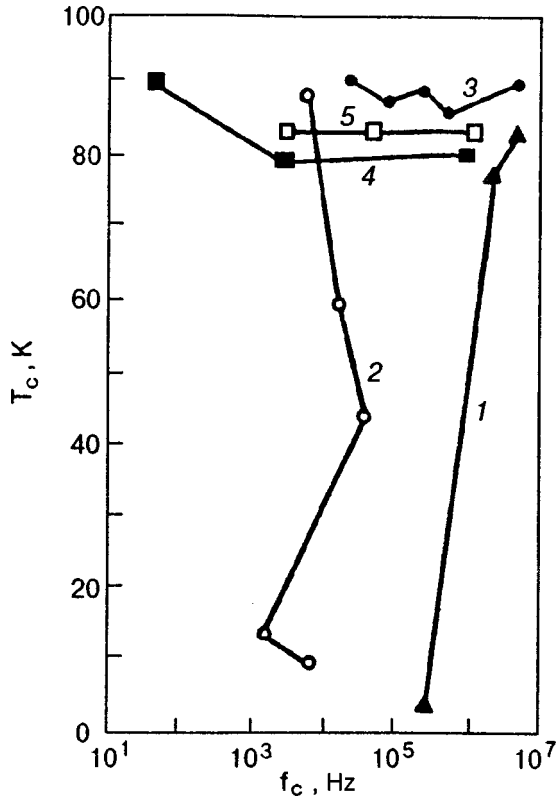

FIG. 2. The $T_c(f_c)$ curves for ceramics $SmBa_2Cu_3O_x$ (curve *1*), $YBa_2Cu_3O_x$ (curves *2, 3*, different samples), $YBa_2Cu_{2.95}Ti_{0.05}O_x$ (curve *4*), and $Bi_{2.16}Sr_{1.33}Ca_{0.566}CuO_x$ (curve *5*).

range Δf at temperatures above and below T_c, it would be interesting to find out whether T_c is connected with f_c.

In this connection, we investigated various HTSC materials and samples made of them. The samples were annealed repeatedly in oxygen, and the values of ρ_0, $\partial\rho/\partial T$, T_c, and f_c for these materials were measured after each annealing and heating–cooling cycle.

Figure 2 shows the $T_c(f_c)$ dependences for some samples of HTSC ceramics: $SmBa_2Cu_3O_x$ (*1*), $YBa_2Cu_3O_x$ (*2,3*), $YBa_2Cu_{2.95}Ti_{0.05}O_x$ (*4*) and $Bi_{2.16}Sr_{1.33}Ca_{0.566}CuO_x$ (*5*).

It can be seen that the shapes of the $T_c(f_c)$ curves for different HTSC type or sample are different. The strong (curve *1, 2*) and weak (curves *3, 4*) $T_c(f_c)$ dependences are observed, while in some cases the value of T_c is virtually independent of f_c (curve *5*). Different samples of the same HTSC material can exhibit different relations between T_c and f_c (curves *2* and *3*). At the same time, there exists a certain relation between f_c and S for all values of f_c, which was established in Ref. 4 and is presented in Fig. 2.

Thus, the entire body of the data described above indicate the absence of a correlation between the values of f_c and T_c measured in direct current.

CONCLUSION

It has been established experimentally that a weak magnetic field in HTSC ceramics with ferromagnetic impurities or paramagnetic properties reduces the width of $N-S$ transition in the frequency range Δf bounded by the frequencies f_c and f_F at which the resistance R is independent of temperature ($\partial R/\partial T=0$).

It is shown that the critical temperature T_c measured in direct current does not correlate with the frequency f_c.

The authors are grateful to the Editorial Board for the opportunity to congratulate Igor' Mikhailovich Dmitrenko on his jubilee. We were brought up in his department and cherish fond memories of our association with him. We wish him many more years of creative achievements.

Thanks are also due to Prof. V. D. Fil' for fruitful discussions.

*E-mail: dmitriev@ilt.kharkov.ua
**International Laboratory of High Magnetic Fields and Low Temperatures, 53-421 Wroclaw, Poland

[1] V. M. Dmitriev, M. N. Ofitserov, and N. N. Prentslau, Fiz. Nizk. Temp. **16**, 387 (1990) [Sov. J. Low Temp. Phys. **16**, 214 (1990)].
[2] V. P. Galaiko, V. M. Dmitriev, M. N. Ofitserov, and N. N. Prentslau, Fiz. Nizk. Temp. **19**, 135 (1993) [Low Temp. Phys. **19**, 96 (1993)].
[3] V. M. Dmitriev, M. N. Ofitserov, N. N. Prentslau *et al.*, Fiz. Nizk. Temp. **21**, 397 (1995) [Low Temp. Phys. **21**, 308 (1995)].
[4] V. M. Dmitriev, M. N. Ofitserov, N. N. Prentslau *et al.*, Fiz. Nizk. Temp. **21**, 906 (1995) [Low Temp. Phys. **21**, 698 (1995)].
[5] V. M. Dmitriev, A. P. Isakina, I. G. Korsunskaya *et al.*, Fiz. Nizk. Temp. **20**, 12 (1994) [Low Temp. Phys. **20**, 8 (1994)].

Translated by R. S. Wadhwa

LOW-TEMPERATURE MAGNETISM

Low-temperature properties of uniaxial paramagnets in a tilted magnetic field

O. B. Zaslavskii, V. V. Ulyanov, and Yu. V. Vasilevskaya

*Physics Department, Kharkov State University, 310077 Kharkov, Ukraine**

(Submitted February 12, 1998; revised March 11, 1998)
Fiz. Nizk. Temp. **24**, 627–634 (July 1998)

The behavior of uniaxial paramagnets in a tilted magnetic field is considered as a function of temperature. The structure of the energy spectrum as well as magnetization and susceptibility components are determined. Exact formulas for the spin $S=1/2$ are obtained. Thermodynamic parameters of the system are studied for arbitrary values of S in an easy-axis and easy-plane cases in different approximations (weak and strong magnetic fields, low and ultralow temperatures, etc.). It is shown that in the easy-plane case, the transverse magnetization and longitudinal susceptibility as functions of magnetic field at low temperatures exhibit peculiarities in the form of a series of sharp spikes, while the longitudinal components of these quantities in the easy-axis case display only a single spike. © *1998 American Institute of Physics.* [S1063-777X(98)00407-1]

1. INTRODUCTION

In various branches of physics,[1,2] one frequently encounters systems whose Hamiltonian is constructed from spin operators and which are therefore called ''spin systems.'' We shall consider a specific type of such systems with a spin Hamiltonian of the form

$$H=\alpha S_z^2-B_xS_x-B_zS_z, \tag{1}$$

appearing in the theory of magnetism and describing a uniaxial paramagnet in an arbitrarily directed magnetic field, where S_j is the spin component, B_j the magnetic field components, and α the anisotropy constant. When such systems are studied in conventional dimensionless variables (the dimensionless energy is introduced as the ratio of energy to the magnitude of anisotropy constant, which also leads to the corresponding dimensionless characteristic of the magnetic field B_j),[1,2] only the sign of α is actually important. For this reason, we shall henceforth consider that α assumes only two values: $\alpha=-1$ corresponds to the easy-axis type of anisotropy, while $\alpha=+1$ corresponds to the easy-plane anisotropy.

Some properties of the systems of the type (1) have already been investigated.[1–3] Special attention was paid to the case when the magnetic field is perpendicular to the anisotropy axis ($B_z=0$ and $\alpha=-1$). The other case with a longitudinal magnetic field ($B_x=0$ and $\alpha=+1$) was partly considered in Refs. 4 and 5. We shall consider here the general case of a tilted magnetic field for both types of anisotropy ($\alpha=\pm1$) and pay special attention to the thermodynamic properties of anisotropic paramagnets at low temperatures.

Turning to the origin of the problem, we must refer the reader to our earlier publication[1] in which the physical properties of uniaxial paramagnets were analyzed in detail purely from the standpoint of the quantum theory, though only in a transverse magnetic field at ultralow temperatures. In Ref. 1, an important method of effective potentials was developed. This method was subsequently used for studying various physical properties of uniaxial and biaxial paramagnets and to discover new classes of exact solutions of the Schrödinger equation.[2,3,6]

Some preliminary remarks are appropriate here. We shall study five main parameters of the system: two components of the magnetization vector (M_x and M_z) and three components of the magnetic susceptibility tensor χ_{xx}, χ_{xz}, and χ_{zz}. In stationary states marked by the subscript $n=0, 1, \ldots, 2S$, these quantities are connected with the relevant derivatives of energy levels E_n with respect to the magnetic field components B_x and B_z:

$$M_k^{(n)}=\langle S_k\rangle_n=-\langle(\partial H)/\partial B_k\rangle_n=-\frac{\partial E_n}{\partial B_k}, \tag{2}$$

$$\chi_{kl}^{(n)}=2\frac{\partial M_k^{(n)}}{\partial B_l}=-2\frac{\partial^2 E_n}{\partial B_k\partial B_l}\quad (k,l=x,z). \tag{3}$$

The factor 2 introduced for convenience in Ref. 1 will be preserved for matching the results.

It can be easily proved that thermodynamic quantities can be expressed in terms of corresponding mean values:

$$M_k^T=\overline{M}_k,\quad \chi_{kl}^T=\overline{\chi_{kl}}+\frac{1}{2T}(\overline{M_kM_l}-\overline{M}_k\overline{M}_l), \tag{4}$$

where the bar over a certain quantity f indicates averaging of the type

$$\overline{f}=\sum_{n=0}^{2S} f^{(n)}\exp(-E_n/T)\Big/\sum_{n=0}^{2S}\exp(-E_n/T). \tag{5}$$

Taking into account the fact that we are dealing with three extrinsic parameters (B_x,B_z,T) and two intrinsic

parameters (S,α), we must clearly pay special attention to certain selected quantities that reflect peculiarities typical of all other parameters most clearly and comprehensively.

2. EXACT RESULTS FOR SPIN $S=1/2$

This is a unique case, when two types of anisotropic paramagnets (easy-axis and easy plane) actually coincide (the energy spectra differ only by a constant that does not play any role in the characteristics $\mathbf{M}$ and $\hat{\chi}$ under investigation).

If the spin is equal to 1/2, we obtain two simple explicit formulas for the two available energy levels,

$$E_{0,1}=\alpha/4\mp B/2, \quad B=\sqrt{B_x^2+B_z^2},$$

so that the magnetization components are given by

$$M_k^{(0)}=-M_k^{(1)}=\frac{B_{k*}}{2B}, \quad \text{i.e.} \quad \mathbf{M}^{(0,1)}\|\mathbf{B},$$

while the magnetic susceptibility tensor components have the form

$$\chi_{zz}^{(0)}=-\chi_{zz}^{(1)}=B_x^2/B^3, \quad \chi_{xz}^{(0)}=-\chi_{xz}^{(1)}=-B_xB_z/B^3,$$
$$\chi_{xx}^{(0)}=-\chi_{xx}^{(1)}=B_z^2/B^3.$$

This leads to the following expressions for thermodynamic quantities:

$$M_k^T=\frac{1}{2}\frac{B_k}{B}\tanh\frac{B}{2T}, \quad \chi_{zz}^T=\frac{B_x^2\sinh(B/T)+B_z^2(B/T)}{2B^3\cosh^2(B/2T)},$$

$$\chi_{xz}^T=-B_xB_z\frac{\sinh(B/T)-(B/T)}{2B^3\cosh^2(B/2T)},$$

$$\chi_{xx}^T=\frac{B_z^2\sinh(B/T)+B_x^2(B/T)}{2B^3\cosh(B/2T)}.$$

For example, we have

$$\chi_{zz}^T=\frac{1}{2T\cosh^2(B_z/2T)}$$

for $B_x=0$,

$$\chi_{zz}^T=\frac{1}{|B_x|\tanh(|B_x|/2T)}, \quad \chi_{xx}^T=\frac{1}{2T\cosh^2(B_x/2T)}$$

for $B_z=0$, while for $B_x=B_z=0$, the nonzero components are $\chi_{zz}^T=\chi_{xx}^T=1/(2T)$.

The exact formulas for energy levels, magnetization, and susceptibility can also be obtained for $S=1$ and $S=3/2$, but these formulas are more cumbersome and will not be given in explicit form. We shall use them in graphic illustrations and as test examples.

3. THERMODYNAMIC PARAMETERS OF EASY-AXIS PARAMAGNETS

For $\alpha=-1$, the main parameters in the ground state can be obtained by using the formula for the ground energy level. The algorithm of the solution is split into two stages. First we consider a system in a purely transverse weak magnetic field ($B_z=0$, $|B_x|<1$). In this case, the structure of energy spectrum of a paramagnet is such that the energy levels are arranged in pairs (except the highest solitary energy level for integral S) as a result of splitting due to B_x in the case of double degeneracy in zero magnetic field. For the pair of energy levels under investigation, viz., the ground level and the first excited level, the following formulas hold for the shift that is common for this pair and the energy gap:

$$E_{0,1}^0=-S^2-\frac{S}{2(2S-1)}B_x^2+O(|B_x|^3), \quad S>1,$$

$$E_{0,1}^0=-1-B_x^2+O(B_x^4), \quad S=1, \tag{6}$$

$$\Delta(0)=\Delta|_{B_z=0}=E_1^0-E_0^0=\frac{S^2}{2^{2S-3}(2S)!}|B_x|^{2S}+O(|B_x|^{2S+2}). \tag{7}$$

The first of these results follows directly from the conventional perturbation theory, while the second is a finer effect which was obtained by using a special modification of perturbation theory, taking into account the specific form of the perturbation operator $V=-B_xS_x$ (see Ref. 2). We shall also write a more exact expression for the gap:

$$\Delta(0)=\frac{S^2}{2^{2S-3}(2S)!}|B_x|^{2S}\left[1-\frac{S+1}{2(2S-1)^2}B_x^2\right]. \tag{8}$$

Such a formula ensures a very high accuracy up to $|B_x|\sim\sqrt{S}$. For example, for $|B_x|=\sqrt{S/2}$, the relative error does not exceed 1%.

The second step involves taking into account the longitudinal component B_z of the magnetic field, which enhances the splitting of energy levels. This is done by using a special version of the perturbation theory for closely spaced energy levels.[7] If the Hamiltonian of the system is $H=H^0+V$, we have

$$E_{0,1}=\frac{1}{2}(E_0^0+E_1^0)\mp\frac{1}{2}\sqrt{(E_0^0-E_1^0)^2+4|V_{01}|^2}, \tag{9}$$

where we have taken into account the fact that the perturbation $V=-B_zS_z$ in our case has strictly zero diagonal matrix elements in the representation of the unperturbed Hamiltonian $H^0=-S_z^2-B_xS_x$, and the nondiagonal elements $V_{01}=-B_z\langle 0|S_z|1\rangle$ can also be obtained with the help of the perturbation theory:

$$|\langle 0|S_z|1\rangle|^2\approx S^2\left[1-\frac{1}{(2S-1)^2}B_x^2\right], \quad S>1/2. \tag{10}$$

Thus, for $|B_x|\ll 1$, relations (8), (9), and (10) lead to ''symmetric repulsion'' (Fig. 1) between the ground and first excited energy levels, which is important for further analysis:

$$E_{0,1}=-S^2-\frac{S}{2(2S-1)}B_x^2\mp\frac{\Delta}{2}, \quad S>1, \tag{11}$$

where the terms of higher order of smallness in B_x and B_z have been omitted, and the energy gap in the first approximation is given by

$$\Delta=\sqrt{\Delta(0)^2+4S^2B_z^2} \tag{12}$$

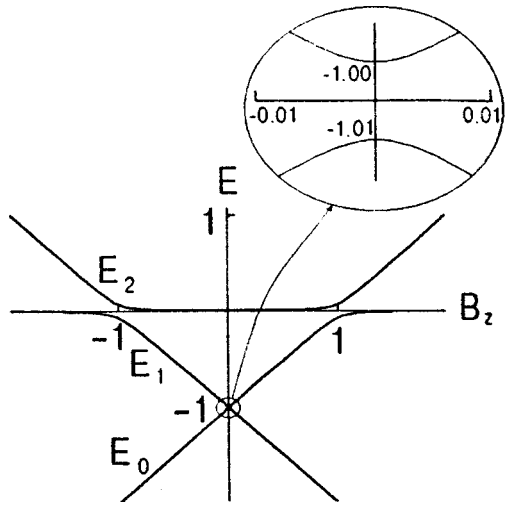

FIG. 1. Structure of energy spectrum of an easy-axis paramagnet for $B_x=0.1$ and $S=1$ (E_j are energy levels).

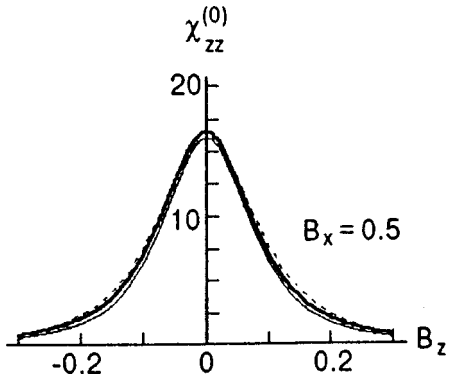

FIG. 2. Magnetic susceptibility $\chi_{zz}^{(0)}$ as a function of B_z for $B_x=0.5$ and $S=1$.

with $\Delta(0)$ from (7). A more exact equation for Δ can be obtained on the basis of (8) and by replacing the coefficient of $4B_z^2$ in (12) by $S^2-S^2B_x^2/(2S-1)^2$ in accordance with (10). It should be noted that in subsequent calculations we shall use explicitly for the sake of brevity formula (12), although it should be borne in mind that it can be refined by the above method. Going over to the magnetic parameters of the ground state, we obtain from (11) and (12) the magnetization

$$M_z^{(0)}(B_z)=\frac{2S^2B_z}{\sqrt{\Delta(0)^2+4S^2B_z^2}} \tag{13}$$

and the susceptibility

$$\chi_{zz}^{(0)}(B_z)=\frac{4S^2\Delta(0)^2}{[\Delta(0)^2+4S^2B_z^2]^{3/2}} \tag{14}$$

(other components are not written here). This leads to the following conclusions. First, for $S=1/2$ these results coincide with exact formulas. Second, the susceptibility component $\chi_{zz}^{(0)}$ has, like the function B_z, the form of the so-called two-dimensional Student distribution for all S. Third, for $B_z\to 0$, we can write, taking into account corrections,

$$\chi_{zz}^{(0)}(0)=\frac{2^{2S-1}(2S)!}{|B_x|^{2S}}\left[1+\frac{S-1}{2(2S-1)^2}\,B_x^2\right],\quad S>1/2.$$

A typical profile of this susceptibility component is shown in Fig. 2 for $B_x=0.5$ and $S=1$, where the exact solid curve, the approximate dashed curve obtained by formula (14), and the refined approximate thin curve illustrating the efficiency of the used approximation virtually coincide.

Going over to thermodynamic parameters, we note that the results obtained for the ground state correspond to ultralow temperatures $T\ll\Delta$ at which the contribution of excited states to all thermodynamic parameters is exponentially small. However, the role of these results is not exhausted by what has been said above since for $T\ll 2S-1$ a pair of lower energy levels is separated from the remaining levels, so that the contribution to all the thermodynamic parameters comes only from the ground and first excited states, while the second and next excited stated states give exponentially small corrections. Such temperatures will be referred to as low, and the corresponding approximation is called the two-level approximation.

Using formulas (11) for ''symmetric repulsion'' between the ground and first excited energy levels, we note that the quantities $M_z^{(1)}$, $\chi_{zz}^{(1)}$, and $\chi_{xz}^{(1)}$ in the first excited state differ from the corresponding quantities in the ground state only in sign. Consequently, it follows from formulas (2)–(4) that

$$M_z^T=M_z^{(0)}\tanh\frac{\Delta}{2T},$$

$$\chi_{zz}^T=\chi_{zz}^{(0)}\tanh\frac{\Delta}{2T}+\frac{(M_z^{(0)})^2}{2T\cosh^2(\Delta/2T)}. \tag{15}$$

Similar formulas can also be obtained for M_x^T, χ_{xz}^T, and χ_{xx}^T, the effect of temperature being similar to the effect of B_x. In both cases, sharp spikes of χ_{zz} are smoothed, becoming broader and lower at the center.

In order to have a comprehensive pattern of variation of $\chi_{zz}^{(0)}$ as a function of magnetic field, we must consider this quantity to be a function of the variables of B_x and B_z, i.e., as a surface over the plane (B_x,B_z). It will be more convenient, however, to consider the cross section $\chi_{zz}^{(0)}(B_z)$ of this surface for certain fixed values of B_x. In other words, we must consider variations of the longitudinal component B_z for a fixed transverse component B_x.

The obtained formulas and corresponding illustrations give a full idea of the behavior of the parameters under investigation in weak magnetic fields. In strong fields, however, the magnetization attains saturation, and susceptibilities decrease rapidly. Nevertheless, we consider the results of calculations in this case also, assuming that the first two terms in the Hamiltonian $H=-B_xS_x-B_zS_z-S_z^2$ are principal and taking into account the magnetic anisotropy term as a correction. It is convenient in this case to choose the coordinate axes so that one of them is directed along the magnetic field. In this case, the Hamiltonian assumes the form $H=-BS_z'-\cos^2\varphi S_z'^2+\cos\varphi\sin\varphi(S_x'S_z'+S_z'S_x')-\sin^2\varphi S_x'^2$, where $\cos\varphi=B_z/B$; $\sin\varphi=B_x/B$; $B=(B_x^2+B_z^2)^{1/2}$. The first term is principal, while the remaining terms are perturba-

tions. Taking into account quadratic corrections for the ground energy level in perturbation theory, we obtain

$$E_0 = -BS - S^2\cos^2\varphi - \frac{S}{2}\sin_2\varphi + O(B-1)$$

$$= -S\sqrt{B_x^2+B_z^2} - S^2 + S\left(S-\frac{1}{2}\right)\frac{B_x^2}{B_x^2+B_z^2} + O(B^{-1}).$$

Using these expressions for calculating the magnetic moment

$$M_z^{(0)} = \frac{SB_z}{(B_x^2+B_z^2)^{1/2}} + S(2S-1)\frac{B_x^2B_z}{(B_x^2+B_z^2)^2} + O\left(\frac{1}{B^2}\right),$$

$$M_x^{(0)} = \frac{SB_x}{(B_x^2+B_z^2)^{1/2}} - S(2S-1)\frac{B_z^2B_x}{(B_x^2+B_z^2)^2} + O\left(\frac{1}{B^2}\right),$$

we obtain the magnetic susceptibility component

$$\chi_{zz}^{(0)} = \frac{2SB_x^2}{(B_x^2+B_z^2)^{3/2}} + 2S(2S-1)\frac{B_x^2(B_x^2-3B_z^2)}{(B_x^2+B_z^2)^3} + O\left(\frac{1}{B^3}\right),$$

in particular,

$$\chi_{zz}^{(0)}|_{B_z=0} = \frac{2S}{|B_x|} + \frac{2S(2S-1)}{B_x^2} + O\left(\frac{1}{|B_x|^3}\right).$$

The other susceptibility tensor component is given by

$$\chi_{xx}^{(0)} = \frac{2SB_z^2}{(B_x^2+B_z^2)^{3/2}} - 2S(2S-1)\frac{B_z^2(B_z^2-3B_x^2)}{(B_x^2+B_z^2)^3} + O\left(\frac{1}{B^3}\right),$$

so that

$$\chi_{xx}^{(0)}|_{B_z=0} = O\left(\frac{1}{|B_x|^3}\right).$$

Moreover,

$$\chi_{xx}^{(0)}|_{B_x=0} = \frac{2S}{|B_z|} - \frac{2S(2S-1)}{B_z^2} + O\left(\frac{1}{|B_z|^3}\right).$$

Finally,

$$\chi_{xz}^{(0)} = -\frac{2SB_xB_z}{(B_x^2+B_z^2)^{3/2}} - 4S(2S-1)B_xB_z\frac{B_x^2-B_z^2}{(B_x^2+B_z^2)^3} + O\left(\frac{1}{B^3}\right).$$

Similar results can also be obtained for easy-plane paramagnets in a strong magnetic field (see below), the only difference being the sign of the corrections.

4. THERMODYNAMIC PARAMETERS IN EASY-PLANE PARAMAGNETS

As in the case of easy-axis paramagnets, the results obtained for easy-plane paramagnetic ($\alpha=+1$) are also based on the formula for symmetric splitting of energy levels of the ground state. However, we now have a sequence of points on the B_z axis, for which junctions in the energy spectrum are formed, for $B_x=0$.

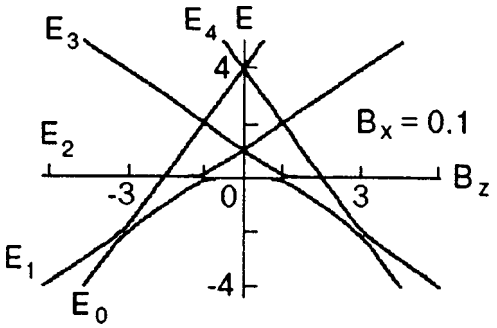

FIG. 3. Typical structure of the energy spectrum of an easy-plane paramagnet in a tilted magnetic field ($S=2$).

The eigenvalues of the Hamiltonian for the unperturbed problem in a purely longitudinal magnetic field $H_0=S_z^2-B_zS_z$ can be classified according to the representation of S_z, which leads to a broken–reticular form of the energy spectrum.[4] For small values of the transverse magnetic field component $|B_x|\ll 1$, the network of energy levels is slightly deformed so that gaps are formed in regions of broken junctions with double degeneracy (this is illustrated by Fig. 3 for $S=2$ and $|B_x|=0.1$). These gaps are correctly described by perturbation theory for double degeneracy (at the points of junctions) or for closely spaced energy levels (in the neighborhood of these points).

The junction points for the ground and first excited energy levels correspond to values of $B_z=B_m$, for which

$$B_m = 2m-1, \quad c_m=(S+m)(S-m+1),$$
$$m=-S+1, -S+2, ..., S-1, S \tag{16}$$

for integral S and

$$B_m = 2m, \quad c_m=(S+1/2)^2-m^2,$$
$$m=-S+1/2, -S+3/2, ..., S-3/2, S-1/2 \tag{17}$$

for half-integral S. Using the result obtained in the perturbation theory for double degeneracy or close energy levels, we obtain the following local formulas in the vicinity of each point B_m:

$$E_{0,1} = m^2-m+1/2-(m-1/2)B_z \mp \frac{1}{2}\sqrt{c_mB_x^2+(B_z-B_m)^2} \tag{18}$$

for integer S and

$$E_{0,1} = m^2-1/4-mB_z \mp \frac{1}{2}\sqrt{c_mB_x^2+(B_z-B_m)^2} \tag{19}$$

for half-integer S.

It is important to emphasize that the root term in (18) and (19) plays a leading role in the subsequent application of the obtained formulas to lower-lying energy levels. In this connection, we shall refer to results (18) and (19) as symmetric splitting. It should also be added that results (18) and

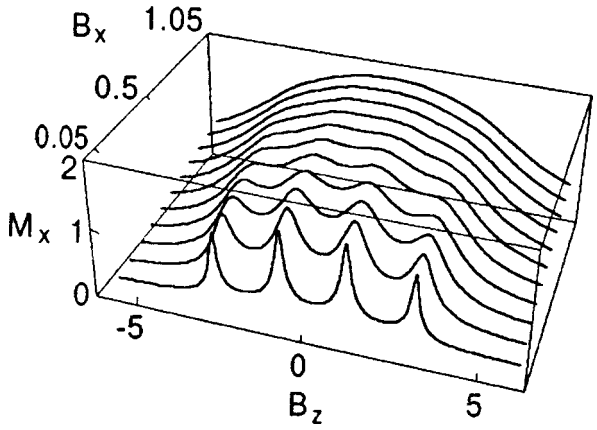

FIG. 4. Magnetization of an easy-plane paramagnet as a function of magnetic field for $S=1$.

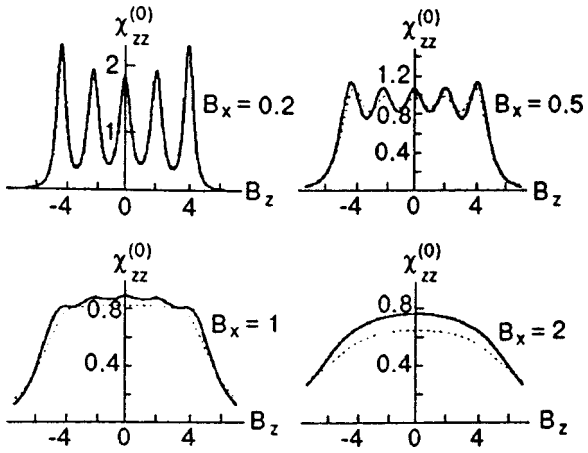

FIG. 5. Susceptibility of an easy-plane paramagnet as a function of the transverse magnetic field component B_x for $S=5/2$ (the dashed curve corresponds to the symmetric splitting approximation).

(19) are of independent interest in connection with the problem of spin tunneling,[8,9] where the splitting of energy levels forms the main subject of investigation.

Let us consider the magnetization $M_x^{(0)}$ in the ground state as a function of the longitudinal magnetic field B_z for various values of the transverse component B_x. In accordance with formulas (18) and (19) of symmetric splitting, the required quantity $M_x^{(0)}=-\partial E_0/\partial B_x$ for the ground energy level for small values of $|B_x|\ll 1$ in the vicinity of values $B_z=B_m$ with junctions between this energy level and the first excited level given by

$$M_x^{(0)}(B_z)=\frac{1}{2}\,\frac{c_m B_x}{[c_m B_x^2+(B_z-B_m)^2]^{1/2}},\quad |B_z-B_m|<1, \tag{20}$$

where B_m and c_m are defined by (16) and (17).

The number of spikes of $M_x^{(0)}$ on the entire B_z axis is equal to $2S$. Each peak has a typical sharpened shape with a maximum value of $\sqrt{c_m}/2$ at the points $B_z=B_m$ and a width $\sim\sqrt{c_m}|B_x|$ so that the central spikes are slightly higher and wider than the peripheral spikes. For example, in the case of half-integral S, the height of the tallest (central) peak is $(S+1/2)/2$, while the height of the lowest peak is $\sqrt{S/2}$ (in the case if integral S, we accordingly have $1/2\sqrt{S(S+1)}$ and $\sqrt{S/2}$). Since the separation between the peaks on the B_z axis is equal to 2, these peaks have a tendency (with increasing $|B_x|$) to overlapping and merging into one to form a ''crown'' which acquires the shape of a bell upon a further increase in $|B_x|$. This is illustrated clearly by a series of curves presented in Fig. 4 for the spin $S=2$.

The second example is the magnetic susceptibility component $\chi_{zz}^{(0)}$ as a function of B_z for various values of B_x. In analogy with $M_x^{(0)}$, this quantity can also be obtained from the formula for symmetric splitting. Being connected with the energy through the formula $\chi_{zz}^{(0)}=-2\partial^2 E_0/\partial B_z^2$, the susceptibility in the vicinity of broken junctions is given by

$$\chi_{zz}^{(0)}(B_z)=\frac{c_m B_x^2}{[c_m B_x^2+(B_z-B_m)^2]^{3/2}},\quad |B_z-B_m|<1, \tag{21}$$

where the quantities B_m and the coefficients c_m are the same as in formula (20).

In many respects, the properties of magnetic susceptibility are similar to those of magnetization, although in some respects they differ significantly. For example, the spikes are sharper in view of a more rapid decrease with increasing distance from the kink points B_m (following the two-dimensional Student's distribution), and the approximation (21) covers successfully not only the neighborhoods of kinks B_m, but also the regions between these points in which the spikes overlap. In this case, we can use a ''global'' representation of $\chi_{zz}^{(0)}$ in the form of the summation formula

$$\chi_{zz}^{(0)}(B_2)=\sum_{m=m_1}^{m_2}\frac{c_m B_x^2}{[c_m B_x^2+(B_z-B_m)^2]^{3/2}},$$

where $m_1=-S+1$, $m_2=S$ for integer S and $m_1=-S+1/2$, $m_2=S-1/2$ for half-integer S. For $\chi_{zz}^{(0)}$, the height $1/(\sqrt{c_m}|B_x|)$ of spikes decreases with increasing $|B_x|$ (the width $\sqrt{c_m}|B_x|$ remaining unchanged), and higher peaks are located at the center and not at the periphery. The corresponding illustrations are presented in Fig. 5. The effect of temperature is the same as in the easy-axis case, and is described by formulas of the type (15) and illustrated by the curves in Figs. 6 and 7.

5. CONCLUSION

The variety of quantities and special cases still allows us to draw some generalizing conclusions concerning the behavior of the systems under investigation on the whole. The main thing is that all peculiarities in the physical parameters mentioned above are observed in the range of small values of transverse magnetic field component, where the energy spectrum experiences a considerable rearrangement. Conversely, for large values of magnetic field, the magnetization attains saturation, while the susceptibility becomes negligibly small.

The type of magnetic anisotropy, i.e., the sign of the constant α, plays a significant role. In the language of susceptibility, we have solitary spikes for $\alpha=-1$ and a system

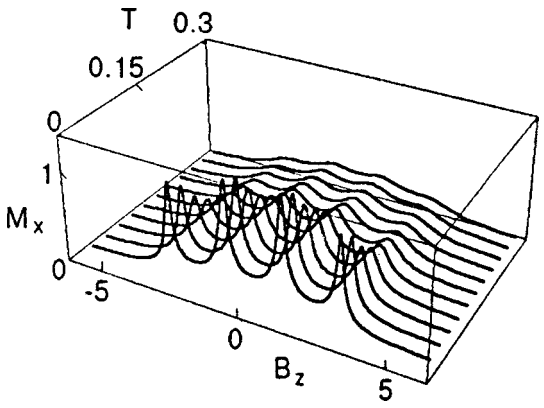

FIG. 6. Effect of temperature on the behavior of magnetization of an easy-plane paramagnet for $B_x=0.1$ and $S=2$.

of $2S$ spikes for $\alpha=+1$. This variety is generalized by universal formulas, e.g., in the form of the two-dimensional Student's distribution for χ_{zz}.

The effect of temperature is reduced to a certain smoothing or blurring of peaks. In the case of purely longitudinal field, point-like singularities of susceptibility in the form of δ-function are replaced by spikes of finite height and width. Similarly, the susceptibility χ_{xx} in a transverse magnetic field for $S=1/2$ becomes nonzero at a finite temperature. It should also be noted that a tilted magnetic field, i.e., the field with a B_x component, affects the shape of χ_{zz} in the same way as temperature.

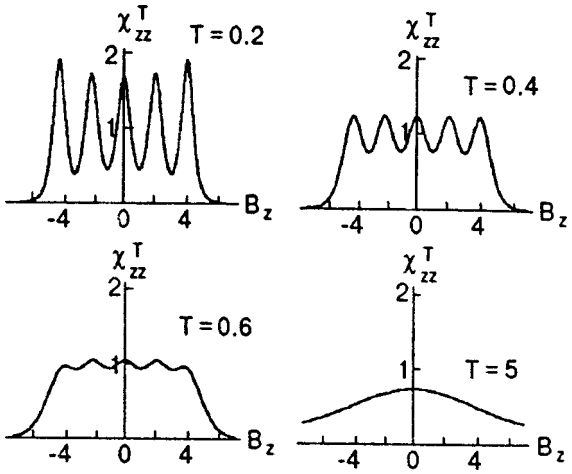

FIG. 7. Effect of temperature on magnetic susceptibility spikes for an easy-plane paramagnet for $B_x=0.2$ and $S=5/2$.

It should be emphasized once again that, in order to describe low-temperature properties of anisotropic paramagnets under investigation in the most interesting range of magnetic fields, it is sufficient to know the behavior of the ground energy level.

For brevity, only main results are given, and cumbersome formulas are omitted. Whenever it is possible, we compensate this omission by graphic illustrations.

It is also appropriate to make certain remarks concerning the method of calculations. The analysis of physical properties of uniaxial paramagnets was based, first, on exact analytic and various approximate calculations, and second, on analytic and numerical computations as well as on graphic illustrations. These approaches are mutually controlled and supplemented. It is the graphical method, which is an analog of a physical experiment, that often stimulates analytic calculations.

The authors express their deep gratitude to V. M. Tsukernik with whom they made their first calculations in the theory of spin systems.

This research is dedicated to A. M. Kosevich who is held as an example of devotion to science by us.

*E-mail: olegzasl@aptm.kharkov.ua;
valdimir.v.ulyanov@univer.kharkov.ua

[1] O. B. Zaslavskii, V. V. Ulyanov, and V. M. Tsukernik, Fiz. Nizk. Temp. **9**, 511 (1983) [Sov. J. Low Temp. Phys. **9**, 259 (1983)].
[2] V. V. Ulyanov and O. B. Zaslavskii, Phys. Rep. **216**, 179 (1992).
[3] V. V. Ulyanov, O. B. Zaslavskii, and Yu. V. Vasilevskaya, Fiz. Nizk. Temp. **23**, 110 (1997) [Low Temp. Phys. **23**, 82 (1997)].
[4] L. D. Filatova and V. M. Tsukernik, Zh. Éksp. Teor. Fiz. **56**, 1290 (1969) [Sov. Phys. JETP **29**, 694 (1969)].
[5] E. V. Rozenfeld, Pis'ma Zh. Éksp. Teor. Fiz. **24**, 60 (1976) [JETP Lett. **24**, 50 (1976)].
[6] O. V. Zaslavskii and V. V. Ulyanov, Zh. Éksp. Teor. Fiz. **87**, 1724 (1984) [Sov. Phys. JETP **60**, 991 (1984)]; Teor. Mat. Fiz. **71**, 260 (1987)].
[7] A. S. Davydov, *Quantum Mechanics*, Pergamon, Oxford, 1976.
[8] A. J. Leggett, S. Chakravarty, A. T. Dorsey *et al.*, Rev. Mod. Phys. **59**, 1 (1987).
[9] C. P. Bean and J. D. Livingston, J. Appl. Phys. **30**, 120S (1959).

Translated by R. S. Wadhwa

Resonance properties of domain walls in ferromagnets with a weak exchange interaction

M. V. Gvozdikova

Kharkov State University, 310077 Kharkov, Ukraine

A. S. Kovalev

*B. Verkin Institute for Low Temperature Physics and Engineering, National Academy of Sciences of the Ukraine, 310164 Kharkov, Ukraine**

Yuri S. Kivshar

*Optical Sciences Center, Research School of Physical Sciences and Engineering, Australian National University, ACT 0200, Canberra, Australia***

(Submitted February 13, 1998; revised March 16, 1998)
Fiz. Nizk. Temp. **24**, 635–640 (July 1998)

The spin dynamics of a domain wall is studied in an infinite ferromagnetic chain with an easy-axis anisotropy as well as in a chain of finite size. The dependence of the intrinsic mode frequency of the domain wall on the exchange interaction is studied for all admissible values of the latter. It is shown that this dependence is considerably modified in the region of transition of the domain wall from collinear structure to canted form. © *1998 American Institute of Physics.* [S1063-777X(98)00507-6]

In this communication, we report on the investigation of nonlinear dynamics of spin systems. Magnetic solitons were first studied in Kharkov more than 25 years ago, and Prof. A. M. Kosevich was one of the pioneers in this field. The authors are indebted to him for introducing them to this interesting field of physical research at different times.

Nonlinear excitations of magnetically ordered media (domain walls, magnetic solitons) have been studied extensively for traditional magnets both from theoretical and experimental points of view.[1,2] As a rule, the theoretical studies of these objects are carried out by using differential equations in the longwave approximation. However, it has been reported in a number of recent publications[3–5] that magnets with a weak exchange interaction (in which the exchange integral J becomes of the order of, or smaller than, the single-ion anisotropy constant β) undergo qualitative variations in structure and domain wall dynamics, and the results obtained from a longwave description of such systems become inapplicable.

This problem has attained significance in recent years following the synthesis of new magnetic materials which satisfy the condition $J \sim \beta$. Examples of such materials are the quasi-one-dimensional magnets $(CH_3)_3NH]NiCl_32H_2O$, $(C_9H_7NH)NiCl_3 \cdot 1{,}5H_2O$,[6] and layered antiferromagnets with a ratio $J/\beta \sim 10^{-2}$, e.g., $(CH_2)_n(NH_3)_2MnCl_4$, $(C_nH_{2n+1}NH_3)_2MnCl_4$,[7–11] and most of the high-temperature superconductors and their isostructural analogs. Significantly, it is possible to change in the above layered antiferromagnets the number n of organic molecules intercalating the magnetic layers, thus opening the possibility of experimental investigation of the dependence of the structure and dynamic properties of such magnets on the value of the exchange integral J.

Van den Broek and Zijlstra[3] were the first to show that for comparable values of the exchange interaction constant and the anisotropy constant, a domain wall ''collapses'' into a collinear structure of the size of atomic spacing with parallel and antiparallel spin orientations. Stepanov and Yablonskii[12] studied experimentally the resonance properties of layered antiferromagnets and observed an additional absorption band in the magnon spectral gap. The authors attributed this band to the emergence of an intrinsic mode in domain walls. Since such modes do not exist in the longwave description of a magnet, their emergence is associated with the discreetness of the magnetic medium and the transformation of domain walls to collinear form. Goncharuk *et al.*[4] actually established theoretically the existence of an intrinsic mode in a domain wall for values of the exchange integral J below the critical value corresponding to collapse of the wall.

In the present work, we demonstrate the existence of an intrinsic mode in a noncollinear domain wall for exchange interaction exceeding the critical value, and describe the variation of this mode in the vicinity of the critical value of J. This question is of importance not only for the investigation of magnetically ordered media, but also for the general development of ''nonlinear physics'' where the interest has been shifting in recent years towards essentially discrete systems.

The magnetization dynamics is studied in the framework of Heisenberg's classical one-dimensional discrete model for an easy-axis ferromagnet, i.e., by using the Landau–Lifshitz discrete equation without damping. The total energy of a spin chain can be represented in the form

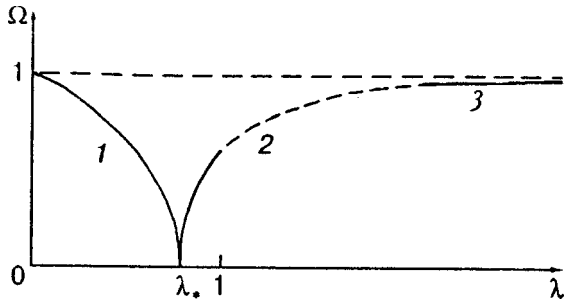

FIG. 1. Dependence of the intrinsic mode frequency Ω of a domain wall on the discreetness parameter $\lambda = J/(\beta a^2)$ of an infinite ferromagnetic chain for collinear (curve *1*) and canted (curve *2*) forms of the DW.

$$E = \sum_n \left[-\frac{J}{a^2}\,\mathbf{S}_n\mathbf{S}_{n+1} - \frac{\beta}{2}\,(\mathbf{S}_n\mathbf{e}_z)^2 \right], \tag{1}$$

where $\mathbf{S}_n$ is the spin of a lattice site ($|\mathbf{S}_n|^2 = 1$), J is the exchange interaction constant ($J>0$ for a ferromagnet), and β the single-ion anisotropy constant ($\beta>0$ for an easy-axis ferromagnet with the easy axis along the $\mathbf{e}_z$-axis. In this case, the Landau–Lifshitz equation can be written in the form[2]

$$\frac{1}{\omega_0}\frac{d\mathbf{S}_n}{dt} + \left(\frac{l_0}{a}\right)^2 [\mathbf{S}_n, (\mathbf{S}_{n+1} + \mathbf{S}_{n-1})] + [\mathbf{S}_n e_z](\mathbf{S}_n \cdot \mathbf{e}_z) = 0, \tag{2}$$

where $\omega_0 = 2\beta\mu_0 S_0/\hbar$ is the frequency of a uniform ferromagnetic resonance (μ_0 is the Bohr magneton, S_0 the nominal magnetization, and $l_0 = \sqrt{J/\beta}$ the characteristic scale of spatial inhomogeneity of magnetization in a domain wall (''magnetic length''). It is convenient to go over to the complex quantity $\Psi_n = S_n^x + iS_n^y$ (the classical analog of the magnon creation operator) and spin projection onto the z-axis ($S_n^z \equiv m_n$). In this case, if we measure time in units of ω_0^{-1} and introduce the parameter $\lambda = (l_0/a)^2$, we can write Eq. (2) in the form

$$i\,\frac{d\Psi_n}{dt} + \lambda(\Psi_n m_{n+1} - \Psi_{n+1} m_n + \Psi_n m_{n-1} - \Psi_{n-1} m_n) + \Psi_n m_n = 0. \tag{3}$$

It was shown in Refs. 3 and 4 that this equation has a static solution for a collinear domain wall with the following spin orientation:

$$m_n = 1 (n \leqslant 0), \quad m_n = -1 (n>0) \tag{4}$$

(the domain wall is located between spins with numbers 0 and 1) for values of the parameter λ smaller than the critical value $\lambda_* = 3/4$. Substituting into Eq. (3) the solution (4) and the function Ψ_n in the form $\Psi_n = \Psi_n \exp(i\Omega t)$, we can easily obtain the intrinsic mode[4] of the domain wall for $\lambda < \lambda_*$:

$$\Omega^2 = \frac{1}{6}\,[6 - 4\lambda - \lambda^2 - \lambda\sqrt{4 + 8\lambda + \lambda^2}]. \tag{5}$$

Curve *1* in Fig. 1 shows the dependence $\Omega(\lambda)$. For $\lambda \ll \lambda_*$, we obtain $\Omega \simeq 1 - \lambda/2$, while $\Omega \approx (8/\sqrt{39})(\lambda_* - \lambda)^{1/2}$ near the critical point.

Let us consider the possibility of the existence of an intrinsic mode in a domain wall for exchange interactions exceeding the critical value ($\lambda > \lambda_*$). In this range of values of λ, the collinear structure corresponding to the solution (4) becomes unstable and the spin distribution in the domain wall becomes noncollinear ($m_n \neq \pm 1$). Using the smallness of the parameter $(\lambda - \lambda_*)$, we can find this distribution in the vicinity of the critical value $\lambda = \lambda_*$. For a noncollinear structure, it is convenient to represent Eq. (3) in terms of the components S_n^i:

$$\frac{dS_n^x}{dt} + \lambda[S_n^y m_{n+1}^z - m_n^z S_{n+1}^y + S_n^y m_{n-1}^z - m_n^z S_{n-1}^y] + S_n^y m_n^z = 0, \tag{6}$$

$$\frac{dS_n^y}{dt} + \lambda[m_n^z S_{n+1}^x - S_n^x m_{n+1}^z + m_n^z S_{n-1}^x - S_n^x m_{n-1}^z] + S_n^x m_n^z = 0, \tag{7}$$

where $m_n^z = [1 - (S_n^x)^2 - (S_n^y)^2]^{1/2}$.

To begin with, let us determine the static configuration of the domain wall by putting $S_n^y = 0$ for the sake of definiteness. It follows from symmetry consideration that $m_n^z = -m_{1-n}^z$ and $S_n^x = S_{1-n}^x (n>0)$. In the main (linear) approximation, the system of equations (6) and (7) can be reduced to the system

$$\begin{aligned} &(1-\lambda)S_1^x - \lambda S_2^x = 0, \quad n=1, \\ &(2\lambda+1)S_n^x - \lambda(S_{n+1}^x + S_{n-1}^x) = 0, \quad n>1, \end{aligned} \tag{8}$$

whose solution has the simple form

$$S_n^x = \frac{A}{3^{n-1}}, \quad \lambda = \frac{3}{4}, \quad n \geqslant 1, \tag{9}$$

where the constant A is determined from the next approximation in perturbation theory. We introduce the small parameter of expansion

$$\varepsilon = \lambda - \lambda_* \tag{10}$$

and present the approximate solution in the form

$$S_n^x = \frac{A}{3^{n-1}} + Z_n, \tag{11}$$

where $A - \sqrt{\varepsilon}$ and $Z_n - \varepsilon^{3/2} \ll A$. Retaining terms of the order of $\varepsilon^{3/2}$ in the static equations (6) and (7), we obtain the following system of difference equations:

$$\begin{aligned} &-\frac{4}{3}\,\varepsilon A + \frac{1}{4}\,Z_1 - \frac{3}{4}\,Z_1 + \frac{1}{3}\,A^3 = 0, \quad n=1, \\ &-\frac{4}{9}\,\varepsilon A + \frac{5}{2}\,Z_2 - \frac{3}{4}\,(Z_1 + Z_3) - \frac{8}{81}\,A^3 = 0, \quad n=2, \\ &\cdots\cdots\cdots\cdots\cdots\cdots\cdots\cdots\cdots\cdots\cdots\cdots\cdots\cdots\cdots\cdots \\ &-\frac{4}{3^n}\,\varepsilon A + \frac{5}{2}\,Z_n - \frac{3}{4}\,(Z_{n-1} + Z_{n+1}) - \frac{8}{3^{2n+2}}\,A^3 = 0. \end{aligned} \tag{12}$$

It can be shown easily that the solution of this system can be chosen in the form $Z_1 = Z_2 = 0$, $Z_n (n \geqslant 3) \neq 0$. This corresponds to the following expression for the constant A:

$$A = 2\sqrt{\varepsilon} \tag{13}$$

(a different choice of the sequence Z_n leads only to an additional expansion of the approximate solution with a different value of the small parameter of the expansion.) The first terms in the sequence Z_n and the asymptotic form for large values of n are given by

$$Z_1=Z_2=0, \quad Z_3=-\frac{32}{3^5}\,\varepsilon^{3/2}\approx -0.126\varepsilon^{3/2},$$

$$Z_4=-\frac{1432}{3^7}\,\varepsilon^{3/2}\approx -0.644\varepsilon^{3/2},\ldots \tag{14}$$

$$\ldots Z_n\approx\frac{2n}{3^n}\,\varepsilon^{3/2}, \quad n\gg 1.$$

Thus, in the main approximation in the small parameter ε, the solution for the static configuration of a domain wall has the form

$$S_n^{y(0)}=0, \quad S_n^{x(0)}=S_{1-n}^{x(0)}=\frac{2\sqrt{\varepsilon}}{3^{n-1}}, \quad n\geqslant 1. \tag{15}$$

It can be easily verified that this solution satisfies the system of static equations in which the nonlinear terms (cubic in $S_1^x, S_0^x, S_2^x, S_{-1}^x$) are considered only in two equations for spins in the vicinity of the center of the domain wall, while all the remaining equations are linearized in spin deviations S_n^x:

$$\left(\frac{1}{4}-\varepsilon\right)S_1^x-\left(\frac{3}{4}+\varepsilon\right)S_2^x+\frac{1}{4}\,(S_1^x)^3+\frac{3}{8}\,(S_1^x)^2S_2^x$$
$$-\frac{3}{8}\,(S_1^x)(S_2^x)^2=0, \quad n=1, \tag{16}$$

$$\frac{5}{2}\,S_n^x-\frac{3}{4}\,(S_{n+1}^x+S_{n-1}^x)=0, \quad n>1.$$

Solving the dynamic problem in the same approximation and with the same accuracy, we retain nonlinear terms only with numbers $n=0,1$ in the dynamic equations (6) and (7), and linearize them subsequently in small corrections to the static solution (15):

$$S_n^x=S_n^{x(0)}+\sqrt{2}W_n(t), \quad S_n^y=\sqrt{2}V_n(t), \tag{17}$$

where $W_n, V_n \ll S_n^{x(0)}$.

Substituting a solution in the form

$$V_n=v_n\cos\Omega t, \quad W_n=w_n\sin\Omega t \tag{18}$$

into the obtained system of equations, we arrive at the final form of the system of linear differential equations for v_n and w_n:

$$\frac{5}{2}\,w_n-\frac{3}{4}\,(w_{n+1}+w_{n-1})\pm\Omega v_n=0, \tag{19}$$

$$\frac{5}{2}\,v_n-\frac{3}{4}\,(v_{n+1}+v_{n-1})\pm\Omega w_n=0 \tag{20}$$

and

$$\left(1-\frac{2}{3}\,\varepsilon\right)w_1-\frac{3}{4}\left(1-\frac{14}{3}\,\varepsilon\right)w_0-\frac{3}{4}\left(1+\frac{2}{3}\,\varepsilon\right)w_2$$
$$+\Omega v_1=0,$$
$$\left(1-\frac{2}{3}\,\varepsilon\right)w_0-\frac{3}{4}\left(1-\frac{14}{3}\,\varepsilon\right)w_1-\frac{3}{4}\left(1+\frac{2}{3}\,\varepsilon\right)w_{-1}$$
$$-\Omega v_0=0, \tag{21}$$
$$\left(1-\frac{2}{3}\,\varepsilon\right)v_1-\frac{3}{4}\left(1-\frac{2}{3}\,\varepsilon\right)v_0-\frac{3}{4}\left(1-\frac{2}{3}\,\varepsilon\right)v_2$$
$$+\Omega w_1=0,$$
$$\left(1-\frac{2}{3}\,\varepsilon\right)v_0-\frac{3}{4}\left(1-\frac{2}{3}\,\varepsilon\right)v_1-\frac{3}{4}\left(1-\frac{2}{3}\,\varepsilon\right)v_{-1}$$
$$-\Omega w_0=0,$$

where the signs ''plus'' and ''minus'' in Eqs. (19) and (20) correspond to numbers $n>1$ and $n<0$, respectively, and Eqs. (21) describe the dynamics of spins with numbers $n=1$ and 0 adjoining the center of the domain wall. The intrinsic mode of the domain wall localized near its center corresponds to the following solutions of Eqs. (19)–(21):

$$w_n=A\,\exp[-\xi_1(n-1)]+B\,\exp[-\xi_2(n-1)], \quad n\geqslant 1,$$
$$v_n=A\,\exp[-\xi_1(n-1)]-B\,\exp[-\xi_2(n-1)], \quad n\geqslant 1, \tag{22}$$
$$w_n=C\,\exp(\xi_1 n)+D\,\exp(\xi_2 n), \quad n\leqslant 0,$$
$$v_n=-C\,\exp(\xi_1 n)+D\,\exp(\xi_2 n), \quad n\leqslant 0,$$

where

$$\exp(-\xi_{1,2})=\frac{1}{3}\left[5\pm 2\Omega-4\left(1\pm\frac{5\Omega}{4}+\frac{\Omega^2}{4}\right)^{1/2}\right]. \tag{23}$$

Substituting the solutions (22) and (23) into the system of equations (21), we arrive at the final expression for the dependence of the intrinsic mode frequency on the discreteness parameter λ of the spin chain. In the main approximation in the small parameter ε, this dependence has the form

$$\Omega\approx\frac{32}{3\sqrt{39}}\,\sqrt{\lambda-\lambda^*}. \tag{24}$$

Segment *2* of the dependence $\Omega(\lambda)$ in Fig. 2 shows this dependence. Segment *3* of the same dependence shows the asymptotic form of the frequency dependence of the intrinsic mode obtained numerically by Bogdan *et al.*[13] for large values of the parameter λ.

Thus, we have shown that the domain wall in an easy-axis ferromagnet has an intrinsic mode over the entire range of values of the discreteness parameter J/β, and the frequency dependence of this mode changes sharply in the vicinity of the critical value of this parameter corresponding to a transition of the domain wall from collinear to canted structure.

Unfortunately, the domain wall dynamics in an infinite spin chain with exchange interaction exceeding the critical

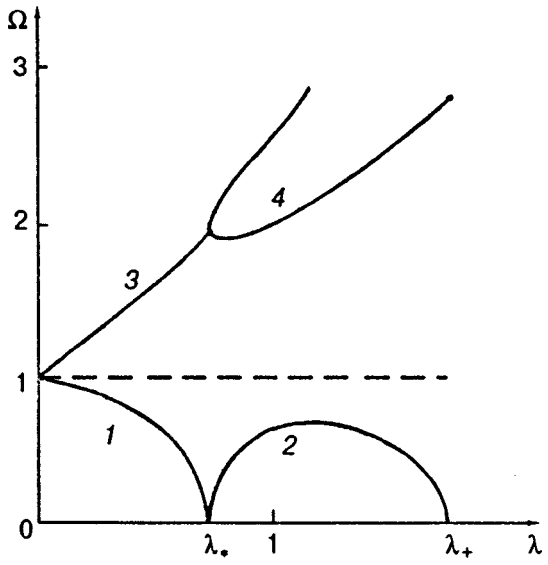

FIG. 2. Eigenfrequency spectrum of a finite spin chain containing a DW.

value can be studied only in a narrow range of values of J near the critical value by making a number of simplifying assumptions. Hence it should be interesting to study the spin dynamics of such a system by using a simplified model containing a finite number of spins. Since the width of a domain-wall for small values of the exchange integral is close to the atomic spacing and the value of spin deviation decreases rapidly with increasing distance from its center, the intrinsic dynamics of the wall is determined actually by a small number of spins near the center.

Let us consider a chain formed by four spins in the ''domain wall'' configuration. In other words, we shall assume that, for small values of the exchange integral, the spin system has a collinear structure of the type (4): $m_1=m_2=-1$, $m_0=m_{-1}=1$. In the collinear phase, the system of equations (3) can be split into four linear equations for solutions of the type $\Psi_n=\psi_n \exp(i\Omega t)$:

$$\begin{aligned}
&(\Omega-1)\psi_1+\lambda(\psi_2+\psi_0)=0,\\
&(-\Omega-1)\psi_0+\lambda(\psi_1+\psi_{-1})=0,\\
&(\Omega-1-\lambda)\psi_2+\lambda\psi_1=0,\\
&(-\Omega-1-\lambda)\psi_{-1}+\lambda\psi_0=0.
\end{aligned} \tag{25}$$

These equations describe the frequency spectrum of the given system with a finite number of degrees of freedom and its dependence on the discreteness parameter λ, as well as the critical value λ_* at which the domain wall goes over from collinear to canted form. The eigenfrequency spectrum is symmetric in the sign of Ω and contains four values. The dependence $\Omega(\lambda)$ has the form

$$\Omega^2=\lambda^2+\lambda+1\pm\lambda\sqrt{\lambda^2+6\lambda+5}, \tag{26}$$

where the minus sign corresponds to the intrinsic mode of the domain wall. By putting its frequency equal to zero, we get the value of the critical parameter $\lambda_*=1/\sqrt{2}\simeq 0.71$ which is quite close to the corresponding value of the parameter $\lambda_*=0.75$ for an infinite chain. Curve *1* in Fig. 2 shows the dependence (26) for the intrinsic mode. This dependence is identical to the function (5) for an infinite spin chain. The plus sign in formula (26) corresponds to a nonlocalized mode with $\psi_2\simeq-1.6\psi_1$. In the limit of an infinite chain, this state passes into antiphase spin vibrations of the upper boundary of the spin wave spectrum. Curve *3* in Fig. 2 shows the dependence $\Omega(\lambda)$ for this mode.

In the region $\lambda>\lambda_*$, the problem for a four-spin complex is solved exactly (in contrast to an infinite chain) even for a domain wall of canted form. It can be shown that its static configuration is described by the following solutions of the system of equations (6) and (7):

$$\begin{aligned}
&m_1=-m_0=-[1\pm(1/2)\sqrt{1+z/(2\lambda-1)^2}]^{1/2},\\
&S_1^x=S_0^x=[1\mp(1/2)\sqrt{1+z/(2\lambda-1)^2}]^{1/2},\\
&m_2=-m_{-1}=-[1\pm(1/2)\sqrt{(1+z)}]^{1/2},\\
&S_2^x=S_{-1}^x=[1\mp\sqrt{(1+z)}]^{1/2},
\end{aligned} \tag{27}$$

where

$$z(\lambda)=\frac{4\lambda^2(2\lambda^2-1)(2\lambda^2-4\lambda+1)}{(2\lambda-1)(4\lambda^2+2\lambda-1)}. \tag{28}$$

In the above formulas, we must take the upper signs for the region $\lambda_*<\lambda<\lambda_1$, upper (for $n=2,-1$) and lower signs (for $n=0,1$) in the interval $\lambda_1<\lambda<\lambda_2$, and lower signs for all n in the interval $\lambda_2<\lambda<\lambda_+$, where $\lambda_1\simeq 0.84$ is the root of the equation $z(\lambda)+(2\lambda-1)^2=1$, while $\lambda_2\simeq 1.24$ is the root of the equation $z(\lambda)+1=0$. The points λ_1 and λ_2 are not critical points, and all dependences at these points are smooth. (At these points, the rotation angles for spins with $n=1$ and 2 pass through the value $\pi/4$.) At the second critical point $\lambda=\lambda_+=1+1/\sqrt{2}$, the ''domain wall'' type configuration disappears, and all spins turn in a direction perpendicular to the easy axis. In this unstable configuration, the intrinsic mode frequency again becomes equal to zero and the spin complex goes over to the homogeneous ground state. However, the description of a domain wall in the framework of a four-spin complex becomes physically invalid for values of the parameter λ close to λ_+.

In order to describe the transformation of a spectrum in the region $\lambda>\lambda_*$, we linearize the dynamic equations (6) and (7) in the vicinity of the static configuration (27) (for the system with a finite number of spins under consideration, we must put in Eqs. (6) and (7) $S_n^x=S_n^y=m_n=0$ for all $n\geqslant 3$ and $n\leqslant -2$):

$$\begin{aligned}
&S_n^x=S_n^{x(0)}+W_n(t),\quad S_n^y=V_n(t),\\
&m_n=m_n^{(0)}-S_n^{x(0)}W_n/m_n^{(0)},
\end{aligned} \tag{29}$$

where the quantities $m_n^{(0)}$ and $S_n^{x(0)}$ are defined by (27) and $W_n, V_n \ll m_n^{(0)}$ and $S_n^{x(0)}$. As in the case of an infinite chain, we seek the solution of the linearized equations in the form $W_n=w_n \sin\Omega t$, $V_n=v_n\cos\Omega t$ and obtain a system of eight linear equations for the quantities w_n and v_n. Putting the determinant of this system equal to zero, we arrive at the final equation for determining the dependence of frequencies $\Omega(\lambda)$ for modes in the canted phase of the domain wall.

Nontrivial solutions for $\Omega^2(\lambda)$ (with $\Omega \neq 0$) satisfy cubic equations with a complex dependence of the coefficients on the parameter λ. We shall not write this equation here sinceit is quite cumbersome. However, we calculated the asymptotic dependences $\Omega(\lambda)$ near the critical values $\lambda = \lambda_*$ and $\lambda = \lambda_+$, and numerically plotted these dependences in the entire admissible range of values of λ (curves *2* and *4* in Fig. 2). The functions $\Omega(\lambda)$ have a root dependence near $\lambda = \lambda_*$. This is the bifurcation point for the high-frequency mode whose degeneracy is removed due to violation of symmetry in the domain wall. For the ''intrinsic mode,'' curve *2* in Fig. 2 is quite close to the corresponding dependence for an infinite chain: $\Omega^2 \simeq 3.09(\lambda - \lambda_*)$. (For an infinite chain, it follows from (24) that $\Omega^2 \simeq 2.92(\lambda - \lambda_*)$.) For not too large values of λ, curve *2* in Fig. 2 is also quite close to the corresponding dependence *2* in Fig. 1.

Thus, it can be seen that the model of spin chains of finite length can correctly describe the dynamics of a domain wall in the region of its transition from collinear to canted configuration. This is also confirmed by the correctness of all assumptions and approximations used in the analysis of an infinite spin chain containing a domain wall.

Two of the authors (A. S. Kovalev and Yu. S. Kivshar) thank the Australian Ministry of Industry, Science and Tourism for awarding a grant to support this research.

*E-mail: kovalev@ilt.kharkov.ua
**E-mail: ysk124@rsphysse.anu.edu.au

[1] A. Hubert, *Theorie der Domänenwände in Geordneten Medien*, Springer, Heidelberg (1974).
[2] A. M. Kosevich, B. A. Ivanov, and A. S. Kovalev, *Nonlinear Magnetization Waves. Dynamic and Topological Solitons* [in Russian], Naukova Dumka, Kiev (1988).
[3] J. J. Van den Broek and H. Zijlstra, IEEE Trans. Magn. **V. Mag.-7**, 226 (1971)
[4] A. N. Goncharuk, A. A. Stepanov, and D. A. Yablonskii, Fiz. Tverd. Tela (Leningrad) **31**, 132 (1989) [Sov. Phys. Solid State **31**, 2099 (1989)].
[5] B. Rumpf, Phys. Lett. A **221**, 197 (1996)
[6] A. A. Anders, V. G. Borisenko, and S. V. Volotskii, Fiz. Nizk. Temp. **15**, 39 (1989) [Sov. J. Low Temp. Phys. **15**, 21 (1989)].
[7] M. I. Kobets, A. A. Stepanov, and A. I. Zvyagin, Fiz. Nizk. Temp. **7**, 1473 (1981) [Sov. J. Low Temp. Phys. **7**, 716 (1981)].
[8] A. I. Zvyagin, M. I. Kobets, V. N. Krivoruchko *et al.*, Zh. Éksp. Teor. Fiz. **89**, 2298 (1985) [Sov. Phys. JETP **62**, 1328 (1985)].
[9] A. I. Zvyagin, V. N. Krivoruchko, V. A. Pashchenko *et al.*, Zh. Eksp. Teor. Fiz. **92**, 311 (1987) [Sov. Phys. JETP **65**, 177 (1987)].
[10] A. A. Stepanov, V. A. Pashchenko, and N. M. Kobets, Fiz. Nizk. Temp. **14**, 550 (1988) [Sov. J. Low Temp. Phys. **14**, 304 (1988)].
[11] A. A. Stepanov, V. A. Pashchenko, and N. M. Kobets, Fiz. Nizk. Temp. **14**, 1212 (1988) [Sov. J. Low Temp. Phys. **14**, 669 (1988)].
[12] A. A. Stepanov and D. A. Yablonskii, Fiz. Nizk. Temp. **15**, 215 (1989) [Sov. J. Low Temp. Phys. **15**, 122 (1989)].
[13] M. M. Bogdan, A. M. Kosevich, and V. P. Voronov, in *Solitons and Applications*, World Scientific, Singapore (1990).

Translated by R. S. Wadhwa

Bose gas with nontrivial particle interaction and semiclassical interpretation of exotic solitons

A. S. Kovalev

*B. Verkin Institute for Low Temperature Physics and Engineering, National Academy of Sciences of the Ukraine, 310164 Kharkov, Ukraine**

M. V. Gvozdikova

Kharkov State University, 310077 Kharkov, Ukraine

(Submitted February 13, 1998; revised March 16, 1998)
Fiz. Nizk. Temp. **24**, 641–646 (July 1998)

Many-particle bound states in a Bose gas with a complex pair interaction between particles are considered. It is shown that the combination of attraction and repulsion between particles leads to the emergence of bound states with peculiar physical properties. In the limit of a large number of bound states in the Hartree approximation, these states are close in the structure and properties to exotic solitons (compactons and peakons) in classical systems with weak spatial dispersion. Examples of exotic solitons of various types in magnetically ordered media are considered. © *1998 American Institute of Physics.* [S1063-777X(98)00607-0]

At the end of the sixties, comprehensive studies of soliton dynamics of nonlinear evolutionary systems acquired considerable significance. The investigation of this problem in Kharkov was started virtually at this time, Prof. A. M. Kosevich being a pioneer in this field. In 1990, Kosevich *et al*. published a review[1] in which they proposed new types of solitons, viz., magnetic compactons. This article is devoted to the study of compactons and their semiclassical interpretation.

The reason behind the existence of dynamic spatially localized excitations of nonlinear evolutionary systems (dynamic solitons) is the action and competition of two physical factors: the nonlinearity and spatial dispersion of the system.[1] The form of the energy–momentum relation $\omega=\omega(k)$ of linear waves affects considerably the properties of soliton states. Their structure differs significantly in systems with strong dispersion, when the dispersion $D=\partial^2\omega/\partial k^2$ remains finite in the long-wave limit $k\to 0$ and in weakly dispersive media for which $D\to 0$ for $k\to 0$. It has been established that even in the case of zero dispersion of linear waves, soliton solutions may exist due to so-called nonlinear dispersion, but solitons acquire peculiar ''exotic'' form. This was noted for the first time in the review by Kosevich *et al.*[2] in the description of Ising ferromagnets.

In the case of a one-dimensional Heisenberg ferromagnet with uniaxial exchange and one-ion anisotropy, the energy of the system has the form

$$E=\frac{\alpha}{2}\left(\frac{\partial \mathbf{m}}{\partial x}\right)^2+\frac{\alpha_1}{2}\left(\frac{\partial m_z}{\partial x}\right)^2-\frac{\beta}{2}\,m_z^2, \tag{1}$$

where $\mathbf{m}$ is the magnetization vector and $\beta>0$ for an easy-axis ferromagnet. If we measure time in the units of $1/\omega_0$, where $\omega_0=2\beta\mu_0 M_0/\hbar$ is the frequency of uniform ferromagnetic resonance, and introduce dynamic variables $\psi=m_x+im_y$ and $m=m_z=(1-|\psi|^2)^{1/2}$, the equations of magnetization dynamics (Landau–Lifshitz equations) acquire the following simple form[1]:

$$i\,\frac{\partial\psi}{\partial t}-l^2 m\,\frac{\partial^2\psi}{\partial x^2}+L^2\psi\,\frac{\partial^2 m}{\partial x^2}+m\psi=0, \tag{2}$$

where two ''magnetic lengths'' are denoted by $l=(\alpha/\beta)^{1/2}$ and $L=[(\alpha+\alpha_1)/\beta]^{1/2}$.

In the simplest case of stationary envelope soliton with $\psi=(1-m^2(x))^{1/2}\exp(i\omega t)$, we can write Eq. (2) after the first integration in the form

$$\left(\frac{\partial u}{\partial x}\right)^2=u^2\,\frac{(1-\omega)-u^2}{4(L^2-l^2)u^2+l^2/(1-u^2)}, \tag{3}$$

where we have introduced a new variable $u=\sqrt{(1-m)/2}$.

In the limit of an Ising ferromagnet with $l=0$, the soliton solution of Eq. (3) (Fig. 1a) has the form

$$u=\sqrt{1-\omega}\,\cos(x/2L),\quad |x|<\pi L,$$
$$u=0,\quad |x|>\pi L. \tag{4}$$

Since the field in the given case differs from zero only in a finite region of space, such solutions were later called compactons. The frequency dependence of the amplitudes for compactons is the same as for envelope solitons, but the region of localization is not connected with frequency and is determined only by material constants. It is important to note that Eq. (2) linearized in ψ in the Ising limit has zero dispersion, and $\omega(k)\equiv 1$. In magnets close to Ising magnets with $l\ll L$, Eq. (3) in the small-amplitude limit $(1-\omega\ll 1)$ can be reduced to a simpler equation

$$\left(\frac{\partial u}{\partial x}\right)^2=u^2\,\frac{(1-\omega)-u^2}{l^2+4L^2u^2}. \tag{5}$$

The interest in compactons was stimulated by the publication of articles by Rosenau,[3,4] who proposed a new version

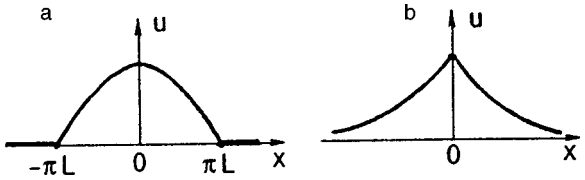

FIG. 1. Profiles of the compacton (a) and peakon (b) solutions.

of the well-known Korteweg–de Vries (KdV) equation with a nonlinear dispersion term and proved that this version has a compact soliton solution with a stationary profile, an amplitude proportional to the velocity, and with a localization region independent of the velocity.

At the same time, Kosevich[5,6] considered compact envelope solitons for antiphase high-frequency oscillations in an anharmonic chain taking into account nonlinear dispersion terms. In this case, the dynamic equation for atomic displacements $v(x)$ has the form

$$\frac{\partial^2 v}{\partial t^2}+\varepsilon\,\frac{\partial^2 v}{\partial x^2}+v+v^3+\lambda v\,\frac{\partial^2(v^2)}{\partial x^2}=0. \tag{6}$$

For $\lambda>0$, the solution of Eq. (6) in the resonance approximation $v\approx W(x)\sin(\omega t)$ disregarding linear dispersion ($\varepsilon=0$) has the form of a compacton close to expression (4). Holm and Kamassa proposed in 1994 their own modification of the KdV equation which assumes the existence of a localized wave of a stationary profile of the form $A\exp(-B|x-V_0t|)$ with definite values of the constants A and B for a certain value of velocity (see Fig. 1b). This new type of exotic solitons was called peakon. In analogy with this type of solitons, we can also find the envelope solitons of the peakon type which also exist only for a certain critical value of frequency of the solution.

If we take into account weak linear dispersion ($\varepsilon\neq 0$) in the anharmonic chain considered above and change the sign of the nonlinear dispersion term ($\lambda<0$), the wave amplitude $W(x)$ in the resonance approximation satisfies the equation

$$\left(\frac{\partial W}{\partial x}\right)^2=W^2\,\frac{(\omega-1)-3W^2/8}{\varepsilon-3|\lambda|W^2/2}. \tag{7}$$

It can be easily seen that the solution of Eq. (7) for the critical value of frequency $\omega=\sqrt{1+\varepsilon/4|\lambda|}$ assumes the form of a peakon:

$$W=\left(\frac{2\varepsilon}{3|\lambda|}\right)^{1/2}\exp(-|x|/(2\sqrt{\lambda})). \tag{8}$$

It should be noted that, for solutions of Eq. (6) of the type of standing waves $v=W\sin(kx)\sin(\omega t)$, the nonlinear energy–momentum relation has the form $\omega^2=1-\varepsilon k^2+9W^2/16+3|\lambda|k^2W^2/2$. Thus, the dispersion $D=\partial^2\omega/\partial k^2$ vanishes for the selected amplitude $W=\sqrt{2\varepsilon/3|\lambda|}$ coinciding with the amplitude of the peakon (8).

Equations (5) and (7) are typical of problems in which solitons close to compactons and peakons are formed. In connection with a peculiar field distribution in exotic solitons, it would be interesting to consider quantum systems in which states with analogous properties can exist. It is well known that classical nonlinear evolutionary equations can be put in correspondence with certain quantum systems of interacting particles.[7–12] For example, soliton excitations in weakly nonlinear systems are normally described on the basis of the nonlinear Schrödinger equation (NSE)[1]

$$i\,\frac{\partial\psi}{\partial t}-\frac{\partial^2\psi}{\partial x^2}+\psi-g|\psi|^2\psi=0, \tag{9}$$

whose solution for dynamic solitons is well known and has the standard form

$$\psi=\sqrt{2/g}\,\varepsilon\ \mathrm{sech}(\varepsilon x)\exp(-i\omega t),\quad \varepsilon=\sqrt{1-\omega}. \tag{10}$$

The properties of these solitons are similar in many respects to the properties of coupled many-boson stationary states in a quantum one-dimensional Bose gas with a δ-shaped attraction between particles.[1] The wave function $\Phi(x_1,x_2,\ldots,x_N)$ of such states satisfies the following Schrödinger equation:

$$-\sum_i\ \frac{d^2\Phi}{dx_i^2}+N\Phi+\sum_{i<j}U_{ij}\Phi=E\Phi,$$

$$U_{ij}=-g\,\delta(x_i-x_j). \tag{11}$$

(We put $\hbar=1$ and $m=1/2$.) The classical nonlinear Schrödinger equation can be integrated completely by the method of the inverse scattering problem, while the quantum Schrödinger equation with a δ-shaped interaction can be integrated completely by the Bethe ansatz method.[13,14] The energy spectrum of the bound many-boson complex has the form $E=N-g^2N(N^2-1)/48$ and coincides with the result of semiclassical quantization of the soliton solution (9) taking into account the dependence $\varepsilon(N)=gN/4$. The boson density distribution in the bound state coincides with the envelope of the function $|\psi|^2$ for soliton (9) in the limit of a large number of particles $N\gg 1$.

However, the description of soliton dynamics in terms of the NSE is justified only in the small-amplitude limit (small N) and leads to soliton collapse in the limit $N\to\infty$. Limitations imposed on the increase of the amplitude for large N are usually taken into account by introducing into Eq. (9) additional terms with a higher degree of nonlinearity (''saturated nonlinearity''). In this case, the NSE is modified as follows[1,15]:

$$i\,\frac{\partial\psi}{\partial t}-\frac{\partial^2\psi}{\partial x^2}+\psi-g|\psi^2|\psi+\delta|\psi|^4\psi=0. \tag{12}$$

The soliton solution of this equation has the form of a function with a ''plateau'' and corresponds to a ''drop'' in the condensed state. A semiclassical analog of the ''NSE with saturation'' (12) is a one-dimensional Bose gas with paired and three-particle δ-type interaction,[15] in which the parameter 2δ characterizes the intensity of the three-particle interaction.

However, the soliton solution of (12) shows that the soliton amplitude $|\psi|$ and the spatial derivative $\partial/\partial x$ in the main approximation have the same order of smallness ($|\psi|,\partial/\partial x\sim\varepsilon$). For this reason, we must generally take into account in Eq. (12) cubic terms containing two spatial derivatives along

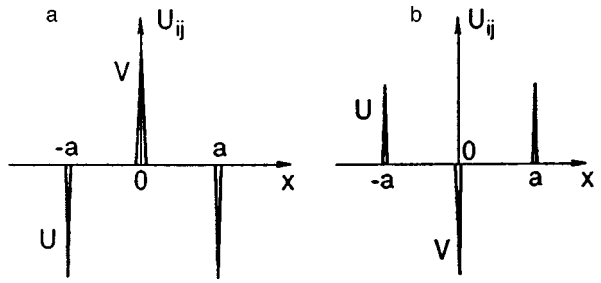

FIG. 2. Pair particle interaction potential leading to compacton (a) and peakon (b) solitons.

with nonlinear terms $\sim\psi^5$. For example, the Landau–Lifshitz equation (2) written to within ε^5 inclusively has the form

$$i\frac{\partial\psi}{\partial t}-l^2\frac{\partial^2\psi}{\partial x^2}+\psi-\frac{1}{2}|\psi|^2\psi=\frac{1}{8}|\psi|^4\psi-\frac{l^2}{2}|\psi|^2\frac{\partial^2\psi}{\partial x^2}+\frac{L^2}{2}\psi\frac{\partial^2(|\psi|^2)}{\partial x^2}. \tag{13}$$

Since $\psi\sim\varepsilon$ and $\partial/\partial x\sim\varepsilon/l$ in the main approximation, we must retain only the last terms on the right-hand side of (13) for ferromagnets close to Ising ferromagnets with $L\gg l$, writing it in a simpler form:

$$i\frac{\partial\psi}{\partial t}-l^2\frac{\partial^2\psi}{\partial x^2}+\psi-\frac{1}{2}|\psi|^2\psi-\frac{L^2}{2}\psi\frac{\partial^2(|\psi|^2)}{\partial x^2}=0. \tag{14}$$

This equation contains only cubic nonlinear terms, and hence this classical system must be put in correspondence to a quantum system with a paired particle interaction more complex than in (11).

We choose for the potential U_{ij} in (11) a more complex function including both the attraction and repulsion at different distances. Such a potential is usually employed in statistical physics in which the repelling core at small distances and weak attraction at large distances are normally taken into account. In our case, bound states of the soliton type exist when the total potential is attractive. For simplicity, we simulate the potential by a system of δ-functions. In this case, two versions (Fig. 2a and 2b) of such a potential are possible:

$$U_{ij}=2V\delta(x_i-x_j)-2U[\delta(x_i-x_j+a)+\delta(x_i-x_j-a)]. \tag{15}$$

In the first case (a), $V>0$, $U>0$, and $V-2U=-W>0$, while in the second case (b), $V<0$, $U<0$, and $V-2U=-W<0$ (see Figs. 2a and 2b, respectively). Equation (11) with potential (15) can be integrated by the Bethe ansatz method, but in view of the cumbersome calculations involved, we simplify the problem, replacing potential (15) by the point-like potential

$$U_{ij}=-2W\delta(x_i-x_j)-2Ua^2\frac{\partial^2}{\partial x_i^2}\delta(x_i-x_j). \tag{16}$$

It will be proved below that exotic solitons under investigation correspond to extremely large numbers N for which the Hartree approximation is applicable. In order to describe nonstationary states of a nonideal Bose gas, the time-dependent Hartree approximation (TDHA) proposed by Dirac is normally used. This approximation leads to an equation of the type (14) for the Hartree function. However, it is sufficient to analyze stationary soliton states by using the ordinary approximation in which the wave function $\Phi(x_1,x_2,\ldots,x_N)$ in (11) has the form of a product of one-particle functions: $\Phi=\Pi\varphi(x_i)$, where $\varphi(x)$ is the normalized Hartree function ($\int|\varphi|^2dx=1$). Substituting the expression for Φ into (11), multiplying both its sides by $\varphi^*(x_2)\ldots\varphi^*(x_N)$, and integrating with respect to $x_2,x_3,\ldots,x_N$, we can easily obtain the equation for the function $\varphi(x)$ in the case of potential (16):

$$\frac{d^2\varphi}{dx^2}-\varepsilon\varphi+2(N-1)W\varphi^3+2(N-1)Ua^2\varphi\frac{d^2(\varphi^2)}{dx^2}=0, \tag{17}$$

where the Hartree energy ε and the total energy E can be expressed in terms of the solution of Eq. (17) as follows:

$$\varepsilon=\int dx\left[-\left(\frac{d\varphi}{dx}\right)^2+2(N-1)W\varphi^4-2(N-1)Ua^2\varphi^2\left(\frac{d\varphi}{dx}\right)^2\right], \tag{18}$$

$$E=N+N\int dx\left[\left(\frac{d\varphi}{dx}\right)-(N-1)W\varphi^4+(N-1)Ua^2\varphi^2\left(\frac{d\varphi}{dx}\right)^2\right]. \tag{19}$$

(For stationary states, the function φ can be chosen as real-valued.) It can be seen that Eq. (17) has the same structure as Eq. (14) for an Ising ferromagnet.

The solution of Eq. (17) depends on ε and N as parameters. Substituting the solution into the normalization condition gives the dependence of the Hartree energy ε on the number of particles N. The dependence $E(N)$ can then be determined from Eq. (19).

The differential equations can be used in the case of small spatial derivatives d/dx. The last term in (17) should be taken into account only under the condition $Ua^2/W\gg1$, i.e., the total potential must be small, or the finiteness of the range a of paired interaction must be manifested clearly. If, however, we proceed from the potential energy (15), we can prove that a transition to the simplified potential (16) is possible when the additional inequality $WUa^2\ll1$ is satisfied. The fulfillment of both inequalities $W^2\ll UWa^2\ll1$ requires that the total potential be small: $W\ll1$.

After the first integration, Eq. (17) can be reduced to a form permitting an analysis in the phase plane $(\varphi,d\varphi/dx)$:

$$\left(\frac{d\varphi}{dx}\right)^2=\varphi^2\frac{\varepsilon-NW\varphi^2}{1+4NUa^2\varphi^2}, \tag{20}$$

where we assume that $N\gg1$.

In the case (a), Eq. (20) has qualitatively the same form as Eq. (5), permitting compact solutions in the limiting version. On the other hand, In the case (b), when $U<0$,

Eq. (20) coincides qualitatively with Eq. (7) having a peakon solution for the critical value of the parameter.

Equation (20) can be integrated, although its soliton solutions can be obtained only in an implicit form.

In the case (a) for $U>0$, this solution has the form

$$\frac{1}{\sqrt{A}}\ln\frac{\sqrt{A}-f}{\sqrt{A}+f}-\arcsin\frac{f^2-1}{f^2+1}=2x\,\frac{\sqrt{\varepsilon}}{\sqrt{A}}, \tag{21}$$

where $A=4Ua^2\varepsilon/W$ and $f=[(4Ua^2/W)\times(\varepsilon-WN\varphi^2)/(1+4Ua^2N\varphi^2)]^{1/2}$.

In the case (b) for $U<0$, the solution can also be written in an implicit form:

$$\frac{1}{\sqrt{B}}\ln\frac{F-\sqrt{B}}{F+\sqrt{B}}-2\ln\left[(1-F)\sqrt{1-4|U|Na^2\varphi^2}\right]=\left(\frac{W}{4|U|a^2}\right)^{1/2}x, \tag{22}$$

where $B=4|U|a^2\varepsilon/W$ and

$$F=[(4|U|a^2/W)\times(\varepsilon-WN\varphi^2)/(1-4|U|a^2N\varphi^2)]^{1/2}.$$

Solutions (21) and (22) contain the dependence $\varepsilon=\varepsilon(N)$ to be determined. It can be found by using the normalization condition and Eq. (20).

If we introduce the characteristic value of the Hartree energy $\varepsilon_*=W/4Ua^2$ and the characteristic number of particles $N_*=1/\sqrt{4WUa^2}$, the dependence $N=N(\varepsilon)$ in the case (a) has the form

$$\frac{N}{N_*}=\left(\frac{\varepsilon}{\varepsilon_*}\right)^{1/2}+\left(1+\frac{\varepsilon}{\varepsilon_*}\right)\arcsin\left(\frac{\varepsilon}{\varepsilon+\varepsilon_*}\right)^{1/2}. \tag{23}$$

Consequently, for small values of N $(N\ll N_*)$, the Hartree energy is proportional to the square of N: $\varepsilon\approx(NW/2)^2$, while for large $N\gg N_*$, this dependence is transformed into the linear dependence $\varepsilon\approx(NW/2\pi)\times(4W/Ua^2)^{1/2}$ (curve *1* in Fig. 3).

In the case (b), the dependence $N=N(\varepsilon)$ changes as follows:

$$\frac{N}{N_*}=\left(\frac{\varepsilon}{\varepsilon_*}\right)^{1/2}+\left(1-\frac{\varepsilon}{\varepsilon_*}\right)\ln\left(\frac{\sqrt{\varepsilon_*}+\sqrt{\varepsilon}}{\sqrt{\varepsilon_*}-\sqrt{\varepsilon}}\right)^{1/2}, \tag{24}$$

where we have made the substitution $U\to|U|$ in the definition of ε_* and N_*. For small N, the dependence $\varepsilon=\varepsilon(N)$ coincides with that for the case (a). However, in the case (b) the value of N is bounded from above by the value of N_* for which ε assumes the maximum value ε_* (curve *2* in Fig. 3).

For a small number $N\ll N_*$ of bound bosons, the solutions in the cases (a) and (b) virtually coincide and have the standard form

$$\varphi=\frac{\sqrt{NW}}{2}\,\mathrm{sech}\left(\frac{NW}{2}\,x\right). \tag{25}$$

It should be noted that the inequalities considered above imply that $N_*\gg1$. Consequently, solution (25) also exists for large values of N: $1\ll N\ll N_*$.

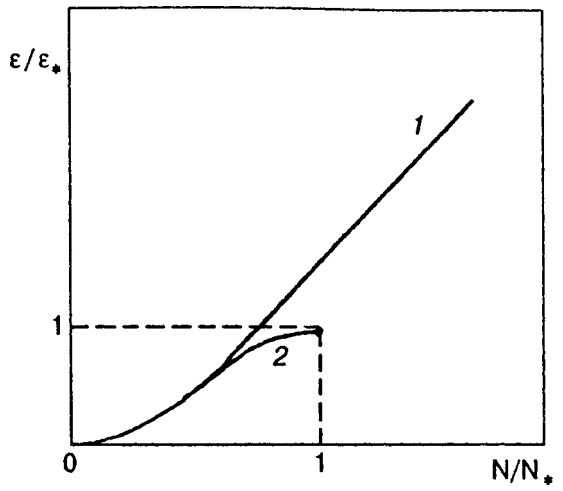

FIG. 3. Dependence of the Hartree energy of a bound many-boson complex on the number of bound particles in it in the case of potential (a) (curve *1*) and (b) (curve *2*).

In the opposite limit $N\gg N_*$, the soliton amplitude tends to a finite value $(W/\pi^2Ua^2)^{1/4}$, and the soliton is localized in a finite region of space $2\Delta=2/\sqrt{\varepsilon_*}$. For $N\to\infty$, we have

$$\varphi=\sqrt{2/\pi\Delta}\,\cos\frac{x}{\Delta},\quad |x|>\pi\Delta/2,$$

$$\varphi=0,\quad |x|<\pi\Delta/2, \tag{26}$$

i.e., the soliton has a typical compacton form [see (4)] shown in Fig. 1a. Although the boson density $\rho=N\varphi^2$ in the soliton increases with N to infinity, the soliton size remains finite, and its collapse differs from the collapse in a Bose gas with a conventional δ-function interaction.

Substituting the compacton solution (26) into the expression (19) for energy, we can easily verify that the dependence $E=E(N)$ for such solutions is also peculiar:

$$E=N(1+\varepsilon_*)-N^2\,\frac{11\varepsilon_*}{12\pi N_*}. \tag{27}$$

Thus, the eigenenergy of a particle in a compacton is renormalized, and the correction to energy nonlinear in N is proportional to N^2 and not to N^3 as in conventional solitons. It should be noted that the dependence $E=N\omega_0-\gamma N^2$ is typical of an anharmonic oscillator, i.e., a compacton possesses some features of a localized nonlinear oscillator due to its peculiar localization. The same result is also preserved for the magnetic compacton (4) in an Ising ferromagnet. Substituting solution (4) into the expression for energy (1) for $\alpha=0$ and for spin deviations $N=\int(1-m)dx=2\int u^2dx$, we arrive at the same dependence

$$E=N-N^2/8\pi L. \tag{28}$$

In conclusion, we consider the limit of a large number $N\to N_*$ of bound bosons in the case (b) with a negative parameter U. In this limit, Eq. (20) assumes the form

$$(\sqrt{\varepsilon_*}-\varphi^2)\left(\Delta^2\left(\frac{d\varphi}{dx}\right)^2-\varphi^2\right)=0, \tag{29}$$

and its soliton solution has the form of a peakon (see Fig. 1b):

$$\varphi = \frac{1}{\sqrt{\Delta}} \exp(-|x|/\Delta), \tag{30}$$

where $\Delta = 1/\sqrt{\varepsilon_*}$ as before. Solution (30) formally has a jump in the derivative at the junction point $(x=0)$. However, the soliton amplitude is not arbitrary at this point, but coincides with the homogeneous solution $\varphi^2 = \sqrt{\varepsilon_*}$ of the nonlinear equation (29). Substituting solution (30) into formula (19), we obtain the relation between the total energy and the number of bosons in a soliton: $E = N_*(1+3\varepsilon_*/8)$.

The energy of a peakon was found to be larger than the energy of N_* free particles, and the same states are probably unstable.

Thus, bound many-particle complexes in a one-dimensional quantum system of bosons with a complex pair interaction possess in the limit of a large number of bound particles the properties of classical exotic solitons (compactons and peakons) in the mean-field approximation and can be described by analogous nonlinear evolutionary equations with a small spatial anisotropy.

*E-mail: kovalev@ilt.kharkov.ua

[1] A. M. Kosevich, B. A. Ivanov, and A. S. Kovalev, Phys. Rep. **194**, 117 (1990).
[2] A. M. Kosevich and A. S. Kovalev, *Introduction to Nonlinear Physical Mechanics* [in Russian], Naukova Dumka, Kiev (1989).
[3] P. Rosenau and J. Hyman, Phys. Rev. Lett. **70**, 564 (1993).
[4] P. Rosenau, Phys. Rev. Lett. **73**, 1737 (1994).
[5] Yu. A. Kosevich, Phys. Lett. A **176**, 257 (1993).
[6] Yu. A. Kosevich, Phys. Rev. B **47**, 3138 (1993).
[7] L. D. Faddeev and V. E. Korepin, Phys. Rep. **42C**, 1 (1978).
[8] E. K. Sklyanin and L. D. Faddeev, Dokl. Akad. Nauk SSSR **243**, 1430 (1978) [Sov. Phys. Dokl. **23**, 902 (1978).
[9] E. K. Sklyanin, L. A. Takhtadzhan, and L. D. Faddeev, Teor. Mat. Fiz. **40**, 194 (1979).
[10] V. E. Zakharov and L. A. Takhtadzhan, Teor. Mat. Fiz. **38**, 26 (1979).
[11] G. R. W. Quispel and H. R. Capel, Physica A **117**, 1 (1983).
[12] H. B. Thacker, Rev. Mod. Phys. **53**, 253 (1981).
[13] E. H. Lieb and W. Lineger, Phys. Rev. **130**, 1605 (1963).
[14] J. B. McGuire, J. Math. Phys. **5**, 622 (1964).
[15] A. S. Kovalev and A. M. Kosevich, Fiz. Nizk. Temp. **2**, 913 (1976) [Sov. J. Low Temp. Phys. **2**, 449 (1976)].

Translated by R. S. Wadhwa

ELECTRONIC PROPERTIES OF METALS AND ALLOYS

Spin waves in a two-dimensional non-ferromagnetic electron liquid with electron impurity states in a magnetic field

N. V. Gleizer and A. M. Ermolaev

*Kharkov State University, 310077 Kharkov, Ukraine**
(Submitted February 5, 1998)
Fiz. Nizk. Temp. **24**, 647–653 (July 1998)

Spin waves in a non-ferromagnetic electron liquid in a magnetic field are studied in the random phase approximation. The electron bound states in the field of impurity atoms are considered. It is shown that electron localization facilitates the propagation of spin waves. New branches of wave spectrum are found in the frequency region where propagation of Silin's waves is not possible. The spectrum and damping decrement of waves are obtained. Intersection of the dispersion curve for a Silin wave with the resonance frequency of electron transitions between Landau levels and local levels results in a cross situation typical of coupled waves. The differential cross-section of magnetic scattering of neutrons by a two-dimensional electron liquid in a magnetic field is calculated. The energy spectrum of scattered neutrons contains additional peaks associated with one-particle excitations of localized electrons and spin waves. The positions and widths of these peaks provide information about the spectrum of electron impurity states as well as the spectrum and damping of spin waves.
 [S1063-777X(98)00707-5]

A cross situation is the intersection of curves describing the energy–momentum relation for two types of waves or elementary excitations...

A. M. Kosevich
Encyclopedic Dictionary of Solid State Physics
[in Russian], Naukova Dumka, Kiev (1996)

INTRODUCTION

The existence of spin waves in nonferrromagnetic metals in a magnetic field was predicted by Silin[1] who proceeded from Landau's Fermi-liquid theory.[2] Soon afterwards, such waves were detected experimentally in alkali metals.[3,4] These waves are associated with the spin resonance of conduction electrons forming a degenerate electron liquid in the metal. The spin branch of the spectrum of excitations in a system of interacting electrons corresponds to the dynamic spin susceptibility pole lying outside Stoner sectors.[1,4] The damping of spin waves at low temperatures is caused by collisions of electrons with impurity atoms and lattice defects, which are usually taken into account by introducing the collision frequency determined by the relaxation of electron momentum and spin.[4]

For a sample containing impurity atoms attracting electrons and in a magnetic field, other types of resonance electron transitions can also be induced by a varying magnetic field. Such transitions include those involving spin transfer between quasilocal levels,[5] as well as between magnetic impurity levels,[6] and Landau levels. New branches of spin wave spectra, called magnetic impurity branches, are situated in the vicinity of these transition frequencies.[7,8]

The existence of additional poles of dynamic spin susceptibility associated with the above-mentioned resonance transitions of electrons can be verified by using a simple approximation in the random phase approximation taking into account the electron– electron interaction.[4] This approximation takes into account the exchange energy of electrons, and their mutual scattering is considered in the ladder approximation.[4] The random phase approximation for describing spin waves in nonferromagnetic metals in a magnetic field was used by Edwards.[9] Moriya[10] has presented a review of works devoted to the effect of impurity atoms on the spin susceptibility dynamics without taking into account the electron impurity states.

The growing interest towards two-dimensional electron systems[11] has made it necessary to find the effect of impurity atoms on the properties of spin waves propagating in a two-dimensional electron liquid in a magnetic field. The importance of this problem is associated with the fact that in a two-dimensional system of electrons in a magnetic field, an impurity of even the lowest intensity removes degeneracy of the electron ''orbit'' center position under even the weakest electron–impurity interaction, and detaches local levels from each Landau level. The positions of these levels were determined by Kosevich and Tanatarov[12] who obtained the electron energy spectrum in a dislocation field and in a magnetic field. Bataka *et al.*[13] considered a strictly two-dimensional electron gas in the field of a special type of impurity potential in the presence of a magnetic field. In contrast to the three-dimensional case,[6] local levels exist in a two-

dimensional system in attractive as well as repulsive impurity atoms. Resonance transitions of electrons between local levels and Landau levels must be accompanied by the emergence of new branches in the wave spectrum.

In this work, we present the results of computations of the spectrum and attenuation of spin waves in a two-dimensional electron liquid taking into account the local electron states at impurity atoms in a magnetic field. The electron–electron interaction is taken into consideration in the random-phase approximation. Rare impurity atoms are assumed to be distributed randomly. Spin waves of different polarizations are considered in Secs. 1 and 2, while Sec. 3 is devoted to their detection in experiments with slow neutrons.

1. SPIN WAVES WITH ''NEGATIVE'' POLARIZATION

Let us consider a two-dimensional electron liquid in the plane $z=0$ with a constant magnetic field $\mathbf{H}$ at right angles to this plane. The energy-momentum relation for electrons is assumed to be isotropic and quadratic, while the potential of randomly distributed impurity atoms with a low concentration is assumed to be short-range potential. In the random-phase approximation, the dispersion equation for spin waves propagating in a two-dimensional electron liquid at right angles to the applied magnetic field has the form[9]

$$1-\frac{I}{2\mu^2}\,\chi_{\pm}(\mathbf{q},\omega)=0, \tag{1}$$

where μ is the spin magnetic moment of an electron, $\chi_{\pm}=\chi_{xx}\pm i\chi_{yx}$ are the circular components of the dynamic spin susceptibility tensor which depend on the wave vector $\mathbf{q}$ and the frequency ω, and I is the Fourier component of the electron–electron interaction energy taking into consideration only the s-wave part of the amplitude of mutual scattering of particles. The magnetic susceptibility of the medium into which the sheet $z=0$, occupied by electrons is immersed, is equal to unity. The quantity I in the semiclassical approximation is associated with the parameter B_0 figuring in the Fermi-liquid theory through the following relation

$$B_0=mI/(2\pi\hbar^2)$$

(m is the effective electron mass.) The constant B_0 is proportional to the zeroth-order term in the expansion of the spin component of the Landau interaction function in Legendre polynomials.[4] Its sign is opposite to that of the constant used by Platzman *et al.*[4]

We shall use the semiclassical longwave approximation for the components $\chi_{\pm}^{(0)}$ of the susceptibility of a pure sample:

$$\chi_{\pm}^{(0)}(q,\omega)=\chi_0\,\frac{\Omega_0}{\Omega_0\pm\omega}\left[1+\frac{1}{2}\left(\frac{qv_F}{\Omega_0\pm\omega}\right)^2\right], \tag{2}$$

where v_F is the Fermi velocity, $\Omega_0=2\mu H/\hbar$ is the EPR frequency, and $\chi_0=m\mu^2/\pi\hbar^2$ is the Pauli susceptibility of two-dimensional electrons. Substituting formula (2) into the dispersion equation (1), it can be verified that spin waves having a ''positive'' (+) polarization in (1) and (2) cannot propagate in the electron system. Waves with ''negative'' (−) polarization obey the following energy–momentum relation:

$$\omega(q)=\Omega_0(1-B_0)\left[1-\frac{1}{2B_0}\left(\frac{qv_F}{\Omega_0}\right)^2\right]. \tag{3}$$

This relation differs from the corresponding relation for a three-dimensional sample[1] only in the numerical factor before q^2. The damping decrement of waves with the spectrum (3) is equal to the frequency ν of electron collisions with impurity atoms associated with the relaxation of momentum and spin.[4]

In an earlier work,[14] we showed that, if local levels are taken into account in the energy spectrum of two-dimensional electrons, the tensors of high-frequency ($\omega\gg\nu$) susceptibility acquire resonance contributions $\delta\chi_{\pm}$. These contributions must be taken into account in the dispersion equation (1). Near the frequencies $\omega_s^{\pm}$ of resonant electron transitions between Landau levels and local levels, the circular components of spin susceptibility contain, in addition to (2), a term[14]

$$\delta\chi_{\pm}^{(s)}=\chi_0\alpha_s^{\pm}\,\frac{\omega_s^{\pm}}{\omega_s^{\pm}-\omega-i\nu_0}, \tag{4}$$

where $\alpha_s^{\pm}$ are the oscillator forces for resonance transitions, and $\hbar\nu_0$ is the local level width. The quantities $\alpha_s^{\pm}$ depend on the wave vector. This dependence is manifested in terms of the order of $(qR)^2$ (R is the cyclotron radius), which cause a weak renormalization of the group velocity of waves and will be disregarded in the subsequent analysis.

For electron transitions from a Landau level to a local level with a spin flip $\pm\to\mp$, the resonance frequencies are given by[14]

$$\omega_s^{\pm}=s\omega_c\mp\Omega_0-\omega_0, \tag{5}$$

where ω_c is the cyclotron frequency of an electron, $\hbar\omega_0$ is the separation between the Landau level and a local level detached from it, and s is the resonance number. In the present case, we have

$$\alpha_s^{\pm}=\frac{\omega_c n_i}{\hbar^2(s\omega_c-\omega_0)^2\omega_s^{\pm}}\sum_k r_k^{\mp}[f(\varepsilon_{(k-s)\pm})-f(\varepsilon_{k\mp}^l)], \tag{6}$$

where $\varepsilon_{n\sigma}$ and $\varepsilon_{k\sigma}^l$ are the positions of the nth Landau level and the kth local level with a spin projection $\sigma=\pm$, f is the Fermi function, $r_k^{\pm}$ is the residue of the electron–impurity scattering amplitude at the pole $\varepsilon_{k\pm}^l-i\hbar\nu_0$, and n_i the number density of impurity atoms. Summation in Eq. (6) is carried out over pairs of levels participating in transitions at the frequency $\omega_s^{\pm}$. The Fermi function difference obeys Pauli's exclusion principle. The number of terms in Eq. (6) depends on the position of the Fermi energy ε_F of degenerate electrons.

The frequencies of electron transitions from a local level to the Landau level with spin flip $\pm\to\mp$ are defined as

$$\omega_s^{\pm}=s\omega_c\mp\Omega_0+\omega_0. \tag{7}$$

The corresponding oscillator forces have the form[14]

$$\alpha_s^{\pm}=\frac{\omega_c n_i}{\hbar^2(s\omega_c+\omega_0)^2\omega_s^{\pm}}\sum_k r_k^{\pm}[f(\varepsilon_{k\pm}^l)-f(\varepsilon_{(k+s)\mp})]. \tag{8}$$

Let us consider the neighborhood of the frequency $\omega_0^- = \Omega_0-\omega_0$ of electron transitions from the Landau level ε_{N-} to the local level ε_{N+}^l. Since $\varepsilon_{N-}<\varepsilon_F<\varepsilon_{N+}^l$, the sum over k appearing in formula (6) retains only one term with $k=N$. Other transitions at the frequency ω_0^- are forbidden by Pauli's exclusion principle. It is assumed that $\Omega_0>\omega_0$. If, in addition, $\omega_0>B_0\Omega_0$, the resonance frequency ω_0^- will be lower than the boundary frequency $\Omega_0(1-B_0)$ of a wave whose spectrum is defined by (3). In this case the dispersion curve (3) for a Silin wave intersects with the straight line $\omega=\omega_0^-$ and a cross situation similar to the one observed in the spectrum of crystal lattice with quasilocal vibrations arises.[15] Taking into consideration the contributions from Eqs. (2) and (4), we can present the dispersion equation (1) for boundary frequencies ($q=0$) in the spin wave spectrum in the form

$$\frac{1-B_0-\omega/\Omega_0}{1-\omega/\Omega_0}=B_0\,\frac{\alpha}{1-\omega/\omega_r}, \tag{9}$$

where $\omega_r=\omega_0^-$, and

$$\alpha=\alpha_0^-=\frac{\omega_c r_N^+ n_i}{(\hbar\omega_0)^2\omega_0^-}. \tag{10}$$

This equation has two roots $\omega_{\pm}$ corresponding to the low- and high-frequency branches of the spin wave spectrum:

$$\omega_{\pm}=\frac{1}{2}\,\omega_r(1-\alpha B_0)+\frac{1}{2}\,\Omega_0(1-B_0)\pm\frac{1}{2}\,\{[\omega_r(1-\alpha B_0)-\Omega_0(1-B_0)]^2+4\Omega_0\omega_r\alpha B_0^2\}^{1/2}. \tag{11}$$

The boundary frequency ω_- lies below ω_r, while ω_+ lies in the interval $[\Omega_0(1-B_0),\Omega_0]$. The parameter α defines the splitting of branch (3) into two branches. As $\alpha\to 0$, the frequency ω_- approaches ω_r, and ω_+ approaches $\Omega_0(1-B_0)$. The spin wave spectrum contains a gap $[\omega_-,\omega_r]$ in which wave propagation is not possible. The width of this gap is defined as

$$\delta\omega=\Omega_0-\omega_0-\omega_-. \tag{12}$$

Curve (3) intersects the line $\omega=\omega_r$ at the point

$$q_0=\frac{\Omega_0}{v_F}\left[\frac{2B_0(\omega_0-B_0\Omega_0)}{\Omega_0(1-B_0)}\right]^{1/2}.$$

For $q\ll q_0$, we can confine the expansion of solutions of the dispersion equation (1) into a power series in q. In the long-wave approximation, the energy–momentum relation for the spin wave branches under consideration assumes the form

$$\omega_{\pm}(q)=\omega_{\pm}-\frac{1}{2}\,\frac{(qv_F)^2}{\Omega_0-\omega_{\pm}}\left[1+\alpha\,\frac{\omega_r}{\Omega_0}\left(\frac{\Omega_0-\omega_{\pm}}{\omega_r-\omega_{\pm}}\right)^2\right]^{-1}. \tag{13}$$

The dispersion of these waves is anomalous. They constitute a nonuniform precession of magnetization around the constant magnetic field direction, propagating in the plane $z=0$. In waves with spectrum (13), the ratio of the components of the spin magnetization vector **m** induced by a varying magnetic field is defined as

$$\frac{m_y}{m_x}=\frac{\chi_{yx}}{\chi_{xx}}=i\,\frac{\chi_--\chi_+}{\chi_-+\chi_+}.$$

The Cartesian components of the susceptibility tensor can be determined easily from (2) and (4).

The damping of spin waves propagating at right angles to the magnetic field is caused by collisions of electrons with impurity atoms. These collisions are taken into account through parameters ν and ν_0 characterizing the impurity broadening of Landau levels and local levels, respectively. Taking into account the small imaginary corrections in the expansions of (2) and (4), we can show that the solution of the dispersion equation (1) has the form $\omega=\omega_{\pm}(q)-i\gamma_{\pm}(q)$, where $\omega_{\pm}(q)$ is the energy–momentum relation (13) for waves, and $\gamma_{\pm}$ is the damping decrement defined as

$$\gamma_{\pm}=\left[\nu+\nu_0\alpha\,\frac{\omega_r}{\Omega_0}\left(\frac{\Omega_0-\omega_{\pm}}{\omega_r-\omega_{\pm}}\right)^2\right]\times\left[1+\alpha\,\frac{\omega_r}{\Omega_0}\left(\frac{\Omega_0-\omega_{\pm}}{\omega_r-\omega_{\pm}}\right)^2\right]^{-1}. \tag{14}$$

The small quantities ν and ν_0 ensure that the inequality $\gamma_{\pm}\ll\omega_{\pm}$ is satisfied. For $\alpha\to 0$, formulas (13) and (14) lead to the spectrum and damping decrement of spin waves in the absence of electron localization.

The dispersion equation has two roots (13) for $\omega_0<B_0\Omega_0$ also. In this case, however,

$$\omega_-<\Omega_0(1-B_0),\quad \omega_0^-<\omega_+<\Omega_0.$$

Let us consider electron transitions from the local level ε_{N-}^l to the Landau level ε_{N+}. The transition frequency is defined as $\omega_r=\Omega_0+\omega_0$, while the oscillator force is defined as

$$\alpha=\frac{\omega_c r_N^- n_i}{(\hbar\omega_0)^2(\Omega_0+\omega_0)}. \tag{15}$$

In the present case, the dispersion equation for boundary frequencies has the same form (9), except that we now have $\omega_r=\Omega_0+\omega_0$ and the oscillator force α is defined by (15). The limiting frequencies are confined in the intervals

$$\omega_-<\Omega_0(1-B_0),\quad \Omega_0<\omega_+<\omega_r.$$

The low-frequency spectral branch overlaps with the Silin wave band (3). The high-frequency branch lies in the frequency range where Silin's semiclassical waves cannot propagate. The solutions of the dispersion equation differ from (11), (13) and (14) in the resonance frequency and oscillator force have different values. The spin waves with the energy–momentum relation $\omega_+(q)$ attenuate weakly in a transparency band $[\omega_+,\omega_r]$ of width

$$\Delta\omega=\Omega_0+\omega_0-\omega_+. \tag{16}$$

2. WAVES WITH A "POSITIVE" POLARIZATION

It can be seen from formula (2) that in the absence of localization of electrons, a weakly attenuating solution of Eq. (1) for spin waves with a "positive" polarization can exist only for $B_0>1$. However, the electron liquid becomes unstable in this case.[4] For a positive contribution (4) from local levels to the real part of spin susceptibility in the region $\omega<\omega_s^+$, the propagation of such waves becomes possible. This situation is reminiscent of antihelicons in an electron gas,[16] whose propagation becomes possible owing to the existence of a subsystem of localized electrons, the direction of whose rotation is defined not only by the magnetic field, but also by the impurity center.

The resonance frequency of electron transitions from the Landau level $\varepsilon_{(N-1)+}$ to the local level ε_{N-}^l with a spin-flip $+\to-$ is defined as $\omega_1^+=\omega_c-\Omega_0-\omega_0$. The oscillator force is defined as

$$\alpha_1^+=\frac{\omega_c r_N^- n_i}{\hbar^2(\omega_c-\omega_0)^2\omega_1^+}\,[f(\varepsilon_{(N-1)+})-f(\varepsilon_{N-}^l)]. \tag{17}$$

In this case, the dispersion equation for boundary frequencies of spin waves has the form

$$\frac{\omega+\Omega_0(1-B_0)}{\omega+\Omega_0}=\alpha B_0\,\frac{\omega_r}{\omega_r-\omega}, \tag{18}$$

where $\omega_r=\omega_1^+$ and $\alpha=\alpha_1^+$. In the interval $\omega<\omega_r$, this equation has two roots:

$$\omega_\pm=\frac{1}{2}\,\omega_r(1-\alpha B_0)-\frac{1}{2}\,\Omega_0(1-B_0)\pm\frac{1}{2}\,\{[\omega_r(1+\alpha B_0)+\Omega_0(1-\beta_0)]^2-4\alpha B_0\omega_r(\omega_r+\Omega_0)\}^{1/2}. \tag{19}$$

As $\alpha\to0$, the upper branch of (19) approaches the resonance frequency ω_r, while the root ω_- becomes negative.

In the longwave approximation, the solutions of Eq. (1) can be defined for the case under consideration as

$$\omega_\pm(q)=\omega_\pm+\frac{1}{2}\,\frac{(qv_F)^2}{\Omega_0+\omega_\pm}\left[1-\alpha\,\frac{\omega_r}{\Omega_0}\left(\frac{\Omega_0+\omega_\pm}{\omega_r-\omega_\pm}\right)^2\right]^{-1}, \tag{20}$$

where $\omega\pm$ are the boundary frequencies (19). These waves have a normal dispersion. They attenuate weakly as a result of electron collisions with impurity atoms in the transparency bands between boundary frequencies (19) and the resonance frequency ω_1^+.

The frequency of transitions of electrons from the local level ε_{N+}^l to the Landau level $\varepsilon_{(N+1)-}$ is equal to $\omega_r=\omega_c-\Omega_0+\omega_0$, while the oscillator force is defined as

$$\alpha=\frac{\omega_c r_N^+ n_i}{\hbar^2(\omega_c+\omega_0)^2\omega_r}\,[f(\varepsilon_{N+}^l)-f(\varepsilon_{(N+1)-})]. \tag{21}$$

In this case, two branches of the spin wave spectrum lie in the interval $(0,\omega_r)$. The solutions of the dispersion equation are given by formulas (19) and (20) in which $\omega_r=\omega_c-\Omega_0+\omega_0$ and the oscillator force is defined by formula (21).

3. MAGNETIC SCATTERING OF NEUTRONS BY SPIN WAVES

The spin waves considered in Secs. 1 and 2 may be observed in experiments with slow neutrons. The differential cross section of magnetic scattering of neutrons by a two-dimensional electron liquid per unit area is defined as[17]

$$\frac{d^2\sigma}{dO'd\varepsilon'}=\frac{1}{4\pi}\left(\frac{\gamma r_0}{\mu}\right)^2\frac{k'}{k}\,(n_\omega+1)\times\sum_{ik}\,(\delta_{ik}-e_ie_k)\,\mathrm{Im}\,\chi_{ik}^s(\mathbf{q},\omega), \tag{22}$$

where χ_{ik}^s is the symmetrized spin susceptibility tensor, $r_0=e^2/mc^2$ the classical electron radius, $\gamma=1.91$ the gyromagnetic ratio for neutrons, $\mathbf{q}=\mathbf{k}-\mathbf{k}'$ and $\hbar\omega=\varepsilon-\varepsilon'$ the change in the electron wave vector and neutron energy for scattering in a solid angle dO', n_ω is the Planck's distribution function, and $\mathbf{e}=\mathbf{q}/q$. Since the scattering vector $\mathbf{q}$ is perpendicular to the magnetic field, the sum appearing in (22) is defined as

$$\frac{1}{2}\,(\chi_++\chi_-)+\chi_{zz}, \tag{23}$$

where the spin susceptibility tensor components are calculated in the random phase approximation. In the absence of electron–electron interaction, the contribution from local levels to the longitudinal component of dynamic spin susceptibility is given by

$$\delta\chi_{zz}(\omega)=\frac{1}{2}\,\chi_0\hbar\omega_c n_i\sum_{nk\sigma}\,\frac{r_k^\sigma}{(\varepsilon_n-\varepsilon_k^l)^2}\,[f(\varepsilon_{k\sigma}^l)-f(\varepsilon_{n\sigma})]\times\left(\frac{1}{\varepsilon_n-\varepsilon_k^l+\hbar\omega+io}+\frac{1}{\varepsilon_n-\varepsilon_k^l-\hbar\omega-io}\right).$$

This function has resonance singularities at frequencies $|\varepsilon_n-\varepsilon_k^l|/\hbar$ of electron transitions between Landau levels and local levels without spin flip.

The contribution of one-particle excitations of electrons localized at the impurity atoms in inelastic magnetic scattering cross section of neutrons can easily be obtained from formula (22). Terms with $\chi_\pm$ in (23) contribute to scattering cross section with spin flip $\pm\to\mp$, while terms with χ_{zz} contribute to scattering cross section without spin flip. In particular, the cross section of scattering accompanied by electron transitions from a local level to a Landau level with spin flip $\pm\to\mp$ is defined in the vicinity of $\omega=\omega_s^\pm$ (7) as

$$\frac{d^2\sigma_\pm}{dO'd\varepsilon'}=\frac{1}{8\pi}\left(\frac{\gamma r_0}{\mu}\right)^2\frac{k'}{k}\,\chi_0\omega_s^\pm\alpha_s^\pm\,\frac{\nu_0}{(\omega-\omega_s^\pm)^2+\nu_0^2}. \tag{24}$$

Here, it is assumed that the temperature is low in comparison with the transition energy. The energy spectrum of scattered neutrons contains symmetric peaks (24) associated with one-particle excitations of localized electrons. Similar peaks formed as a result of electron transitions from Landau levels to local levels must also be observed at $\omega=\omega_s^\pm$ (5). Note that

such peaks are asymmetric in the three-dimensional case.[18] This is due to the asymmetry of electron density of states at Landau levels.

In addition to the peaks described by formula (24), the spectrum of scattered neutrons also contains a series of Lorentz peaks formed as a result of scattering by spin waves with a spectrum (13) and (20). The cross section of scattering with the emission of a spin wave quantum with the energy–momentum relation ω_q is defined as

$$\frac{d^2\sigma_s}{dO'd\varepsilon'} = \frac{1}{2m\Omega_0}\left(\frac{\hbar\gamma r_0}{I}\right)^2 \frac{k'}{k}(\omega_q-\Omega_0)^2 \times\left[1+\alpha\frac{\omega_r}{\Omega_0}\left(\frac{\omega_q-\Omega_0}{\omega_q-\omega_r}\right)^2\right]^{-1} \frac{\gamma_q}{(\omega-\omega_q)^2+\gamma_q^2}, \tag{25}$$

where ω_r is the resonance frequency (5) or (7), α is the oscillator force (6) or (8), and γ_q is the damping decrement of the waves. For $\alpha\to 0$, formula (25) leads to the cross section of neutron scattering by spin waves with a spectrum (3).[19]

So far, we have not discussed specifically the characteristics of local electron states (positions and widths of local levels, residues of amplitude of electron scattering by an impurity atom). We have only used the fact that electron–impurity scattering amplitude has poles. These characteristics may be obtained by comparing theory with experiment, or calculated by using a certain model for the impurity potential. In particular, the scattering amplitude residue for the short-range potential of an impurity atom and a weak splitting of local level from the Landau level ($\omega_0 \ll \omega_c$) can be represented in the form[14]

$$r = 2\pi\hbar^3\omega_0^2/m\omega_c .$$

In order to estimate the magnitude of peaks of differential cross section of neutron scattering obtained in this section, we use the values of parameters typical of thin semimetal films and inversion layer at silicon–silicon dioxide interface:[11] $m=10^{-31}$ g, the number density of a two-dimensional electron liquid $n_e=10^{16}$ m^{-2}, $n_i/n_e=0.01$, $\omega_0/\Omega_0=0.2$, $B_0=0.1$, $\nu=\nu_0$. Hence we obtain $\Omega_0=1.9\times10^{12}$ s^{-1} in a magnetic field with induction 10 T, and the ratios of the maximum values of cross-sections (24) and (25) to the peak of cross section of scattering by a Silin wave are equal to 0.23 and 0.12, respectively. In this case, the ratio of widths of the gap (12) and transparency band (16) to Ω_0 are 0.74 and 0.02, respectively.

CONCLUSIONS

In two-dimensional systems, impurity atoms exert a considerable influence on the energy spectrum of quasiparticles. In such systems, an impurity can form a local electron level at the edge of the conduction band for an indefinitely weak electron–impurity interaction. In a quantizing magnetic field perpendicular to the plane in which the electrons move, the local levels get ''multiplied.'' They are split upwards or downwards from each Landau level depending on the sign of the impurity potential. Such a structure of the spectrum of a two-dimensional electron system in a magnetic field affects its high-frequency characteristics. Among other things, the dynamic spin susceptibility has resonance singularities at frequencies of electron transitions accompanied by a spin flip between Landau levels and local levels. New branches of spin wave spectra are formed at these singularities in a nonferromagnetic two-dimensional electron liquid.

We have shown in this work that localization of electrons at impurity atoms competes with dissipative processes and facilitates the propagation of spin waves. New spectral branches of collective vibrations of spin magnetization exist in frequency regions where Silin waves cannot propagate. The spectrum and damping decrement of such waves are calculated.

If the frequency of a Silin wave coincides with the frequency of resonance transitions of electrons between Landau levels and local levels, the spin wave spectrum undergoes rearrangement due to a coupling of spin wave magnetization vibrations with vibrations at resonance. The dispersion curve for a Silin wave in a two-dimensional electron liquid is split into a low-frequency branch and a high-frequency branch. These branches are separated by a gap in which waves cannot propagate.

The spin waves considered here can be detected in experiments on measurement of differential cross-section of inelastic magnetic scattering of neutrons by the spin magnetization current of two-dimensional electrons. The energy spectrum of scattered neutrons contains peaks associated with one-particle excitations of electrons localized at impurities, as well as with spin waves. The symmetric peaks resulting from one-particle excitations are formed at resonance frequencies of electron transitions between Landau levels and local levels. The width of these peaks is determined by the width of levels participating in transitions. The positions of Lorentz peaks in the cross-section of scattering by spin waves can be used to obtain the wave spectrum, while their width gives the damping decrement.

The results presented in this communication can be used for studying two-dimensional metals, inversion layers at a semiconductor–insulator interface, layered systems, and thin films of metals in which the electrons are at the lower energy level formed as a result of size quantization.

*E-mail: alexander.m.ermolaev@univer.kharkov.ua

[1] V. P. Silin, Zh. Éksp. Teor. Fiz. **35**, 1243 (1959) [Sov. Phys. JETP **8**, 870 (1959)].
[2] L. D. Landau, Zh. Éksp. Teor. Fiz. **30**, 1058 (1956) [Sov. Phys. JETP **3**, 920 (1956)].
[3] S. Schultz and G. Dunifer, Phys. Rev. Lett. **18**, 283 (1967).
[4] P. Platzman and P. Wolf, *Waves and Interactions in Solid State Plasmas*, Academic Press, New York (1973).
[5] I. M. Lifshitz, S. A. Gredeskul, and L. A. Pastur, *Introduction to the Theory of Disordered Systems*, Wiley, New York, 1988.
[6] A. M. Ermolaev and M. I. Kaganov, JETP Lett. **6**, 395 (1967).
[7] A. M. Ermolaev, Fiz. Tverd. Tela (Leningrad) **30**, 1065 (1988) [Sov. Phys. Solid State **30**, 618 (1988)].
[8] A. M. Ermolaev and N. V. Ul'yanov, Fiz. Nizk. Temp. **18**, 1375 (1992) [Sov. J. Low Temp. Phys. **18**, 960 (1992)].
[9] D. M. Edwards, J. Phys. C **2**, 84 (1969).
[10] T. Moriya, *Spin Fluctuations in Itinerant Electron Magnetism*, Springer, Heidelberg (1985).

[11] T. Ando, A. Fowler, and F. Stern, *Electronic Properties of Two-dimensional Systems*, American Physical Society, New York (1982).
[12] A. M. Kosevich and L. V. Tanatarov, Fiz. Tverd. Tela (Leningrad) **6**, 3423 (1964) [Sov. Phys. Solid State **6**, 2738 (1964)].
[13] E. P. Bataka and A. M. Ermolaev, Izv. Vuzov. Fizika No. 1, 111 (1983).
[14] N. V. Gleizer, A. M. Ermolaev, and A. D. Rudnev, Fiz. Nizk. Temp. **23**, 1092 (1997) [Low Temp. Phys. **23**, 820 (1997)].
[15] A. M. Kosevich, *Theory of Crystal Lattice* [in Russian], Vishcha Shkola, Kharkov (1988).
[16] E. A. Kaner and A. M. Ermolaev, Zh. Éksp. Teor. Fiz. **92**, 2245 (1987) [Sov. Phys. JETP **65**, 1266 (1987)].
[17] Yu. A. Izyumov and R. P. Ozerov, *Magnetic Neutron Spectroscopy* [in Russian], Nauka, Moscow (1966).
[18] A. M. Ermolaev and N. V. Ul'yanov, Fiz. Tverd. Tela (Leningrad) **34**, 1676 (1992) [Sov. Phys. Solid State **34**, 891 (1992)].
[19] E. A. Pamyatnykh, V. P. Silin, and A. Z. Solontsov, Zh. Éksp. Teor. Fiz. **70**, 2286 (1976) [Sov. Phys. JETP **43**, 1193 (1976)].

Translated by R. S. Wadhwa

Size-effect of Kondo scattering in point contacts (revisited)

I. K. Yanson, V. V. Fisun, and N. L. Bobrov

*B. Verkin Institute for Low Temperature Physics and Engineering, 47, Lenin Ave., 310164 Kharkov, Ukraine**

J. A. Mydosh and J. M. van Ruitenbeek

Kamerlingh Onnes Laboratorium, Leiden University, P.O. Box 9506, 2300 RA Leiden, The Netherlands
(Submitted February 11, 1998)
Fiz. Nizk. Temp. **24**, 654–660 (July 1998)

The size-effect of Kondo-scattering in nanometer-sized metallic point contacts is measured with the simplified, mechanically-controlled break–junction technique for CuMn alloy of different Mn concentrations: 0.017; 0.035; and 0.18 (± 0.017) at.%. The results are compared with our previous publication on nominally 0.1 at. % CuMn alloy.[1,2] The increase of width of the Kondo resonance and enhanced ratio of Kondo-peak intensity to electron–phonon scattering intensity is observed for contacts with sizes smaller than 10 nm. From the comparison of electron–phonon scattering intensity for the pressure-type contacts, which correspond to the clean orifice model, we conclude that the size effect is observed in *clean* contacts with the shape of a *channel* (nanowire).
[S1063-777X(98)00807-X]

1. INTRODUCTION

Recently the size-effect of Kondo scattering has been observed in point contacts.[1,2] This appears to be opposite to the suppression of the Kondo effect in thin films and wires.[3] The effect was observed in ballistic contacts of nanometer-size and explained as being due to the strong enhancement of Kondo temperature by fluctuations of local electron density of states. These fluctuations are the result of the lateral electron resonances in the narrow part of the metallic bridge connecting bulk electrodes.[4] In the present work we have found additional confirmation of the model, proposed in Ref. 4.

Initially, it was noticed that the estimates of the Kondo-temperature made by the quasi-classical theory[1,2,5,6] is too large compared to the bulk value. Unfortunately, the experimental conditions do not satisfy the weak coupling limit in Kondo scattering which is assumed in the theory. Another problem is an unknown geometry and electron mean free path in a constriction, which are often encountered in the point-contact study and which force one to use the idealized clean-orifice model.[7] Roughly speaking, due to this model any dependence of a normalized Kondo-peak intensity at zero bias $\delta R_K/R_0$ (Fig. 1) on a contact diameter d slower than proportional to d would result in the increase of the apparent Kondo temperature according to the formulas[1]

$$k_B T_K = E_F \exp(-2E_F/3J), \tag{1}$$

$$\frac{J}{E_F} = -0.044\left[\frac{1}{c\sqrt{R_0}}\frac{dR_K}{d(\log_{10} V)}\right]^{1/3}, \tag{2}$$

since $\delta(\log eV)$ are approximately constant and $d \propto R_0^{-1/2}$. Here E_F and c are the Fermi energy and impurity concentrations, respectively. There are many reasons for the exponent n in $\delta R_K/R_0 \propto d^n$ to be smaller than one. One of them is the finite electron mean path,[8] the other is changing the contact shape while studying the d-dependence. The theory[6] is valid in the limit when the average distance between magnetic impurities r_0 is much smaller than the contact size d which is not the case for the smallest contacts. Hence, the application of formula (2) can't be justified.

Fortunately, for $r_0 \ll d$ the ratio of size-dependent phonon and Kondo scatterings does not depend on the geometry and mean free path in the contact, and can be taken as a reliable evidence of different behavior of these two types of scatterers. Another important experimental feature is the widening of the Kondo peak while decreasing the contact size d[1,2] which also qualitatively points to an increase of the Kondo temperature.

In the present work we use these properties to show qualitatively that the Kondo temperature indeed greatly increases for nanometer-sized contacts in the form of a clean channel (wire). We prove that the clean channel (wire) model is essential for clear observation of the effect. In the previous publication[9] we have noted this feature, but only in the present work (based on a great amount of experimental data) we do find it to be the necessary condition for observing the size effect. The effect is shown for different known concentrations, and this enables us to correct our previous results for CuMn with nominal concentration 0.1 at.%,[1,2] which corresponds to the measured concentration of 0.028 at.% (uncertainty ± 0.017 at.%). The size-effect is maximal when the wire diameter is of the order or less than the average distance between impurity, and decreases with shortening of the electron mean free path. These conclusions correspond pretty well to the Zarand–Udvardi theory.[4]

A more direct way of showing the enhanced Kondo temperature is to study nanosize contacts in magnetic fields. It

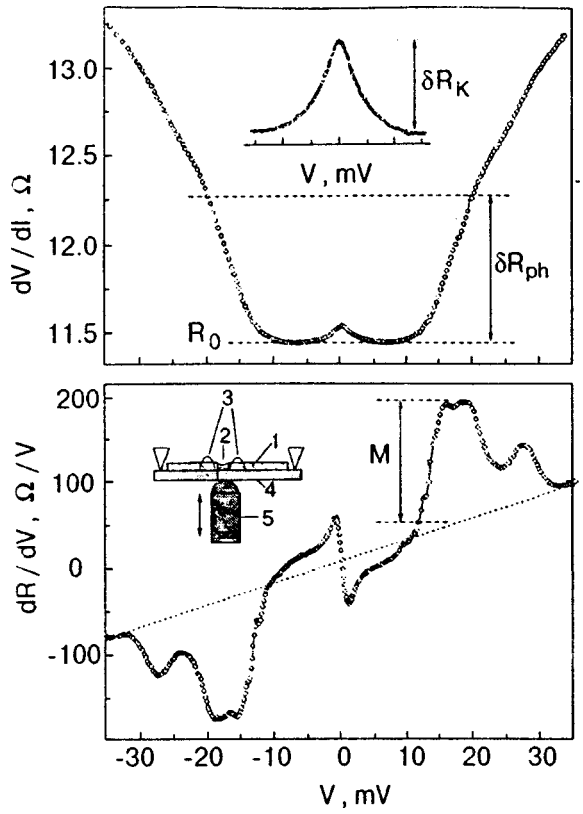

FIG. 1. Upper panel: differential resistance of MCB junction of CuMn (0.18 at.%). In the inset the magnified Kondo peak is shown. R_0 is a resistance connected with contact diameter d via Sharvin formula (Eq. (4)). $\delta R_{\rm ph}$ is the increase of resistance due to the phonon backscattering at $V=20$ mV. δR_K is Kondo-peak height. Lower panel: the second derivative of current–voltage characteristic of the same contact. M is the maximum intensity of electron–phonon interaction background subtracted, according to formula (Eq. (3). In the inset: the schematic view of mechanically-controlled break junction: *1*—the CuMn alloy; *2*—notch; *3*—Staycast glue; *4*—bending beam; *5*—push-pulling rod, $T=1.6$ K.

was shown that Kondo resonance becomes less sensitive to the field for decreased sizes.[1,2,10,11] Despite the experimental difficulties of preserving high resistance contacts during magnetic field measurements, these experiments would give not only qualitative but also the quantitative information. These remain for future studies.

2. EXPERIMENTAL

We study CuMn dilute alloys of three concentrations determined by x-ray analysis: 0.18; 0.035; and 0.017 at.%. In addition, we repeat the measurements for our previous alloy which was nominally about 0.1 at.%[1,2] but appears to be 0.028 at.% by x-ray. The accuracy of concentration determination is about 0.017 at.%. Thus, the alloys with concentration of 0.017; 0.028; and 0.035 at.% give the same results in the limits of data-point scattering.

The measurements were carried out on the break junctions shown schematically in the inset of Fig. 1 (lower panel). The sample (*1*) is a wire with diameter 0.2 mm notched (*2*) at the center by a sharp knife, then etched and annealed at 700 °C during 2.5 h with spontaneously cooling down. The annealing seems to be important for obtaining elongated neck while breaking the notch. The sample is glued to the substrate (*4*) with Staycast (*3*). The rod (*5*) is pushed mechanically to bend the substrate (*4*). The whole system is immersed in superfluid He at a temperature of 1.6 K. This improves the sample cooling and greatly simplifies the measurements which enable us to collect a huge amount of experimental data.

After breaking the neck the contact is readjusted for the initial resistance of the order of 1 Ω. The continuous pulling off the electrodes (1) enable us to obtain the successive series of resistances up to several hundreds Ohm until the neck is completely broken. Each series containing about 10 contacts is repeated several times. Sometimes the contact resistance inside the same series jumps to unwanted high values. Then it was readjusted back by pushing the electrodes slightly. After a number of breakings, the metal in the contact region becomes so defective that the making of an elongated clean neck appears to be difficult. These series show a suppressed Kondo size-effect.

For each contact three successive recordings are taken, each of about 5–10 minutes long. These are the $d^2V/dI^2(V)$ and $dV/dI(V)$ characteristics taken in the range of phonon energies -35–35 mV, and $dV/dI(V)$ taken at about -8–8 mV near zero bias for Kondo-peak recorded separately (see Fig. 1). Usually, the non-linearities of $V(I)$ characteristics due to phonons and Kondo-effect are the same on different recordings, showing that the contact is stable during the measurements. Sometimes, especially for low impurity concentration and small size contacts, the intensity of Kondo peak changes due to the electromigration of impurities. For these cases we use either the maximum intensity (which is observed for the previous recording), or the average of two, since we assume that the maximum current density in the center of the contact forces the impurities to move from the center to the periphery.[12]

Care is taken to have the temperature and modulation smearing[13] less than the changes of the measurable quantities discussed below.

3. RESULTS

Typical first and second derivatives of current–voltage characteristic are shown in Fig. 1. The Kondo peak at zero bias is seen on the $dV/dI(V)$-characteristic. The phonon backscattering sharply increases the resistance at about ± 20 mV. In the ballistic limit the $dR/dV(V)$ characteristic is directly proportional to the electron-phonon interaction (EPI) function $g_{PC}(eV)$ through the relation[7]

$$\frac{1}{R}\frac{dR}{dV}(V)=\frac{8}{3}\frac{ed}{\hbar v_F}g_{PC}(eV), \quad (T\simeq 0). \tag{3}$$

The Sharvin resistance R_0 which we identify with shallow minima in $dV/dI(V)$ is connected in copper with contact diameter d through the formula

$$d\approx\frac{30}{\sqrt{R_0[\Omega]}}\,[\text{nm}]. \tag{4}$$

This formula is valid both for the model of orifice and for long wire only in the case of specular reflections from

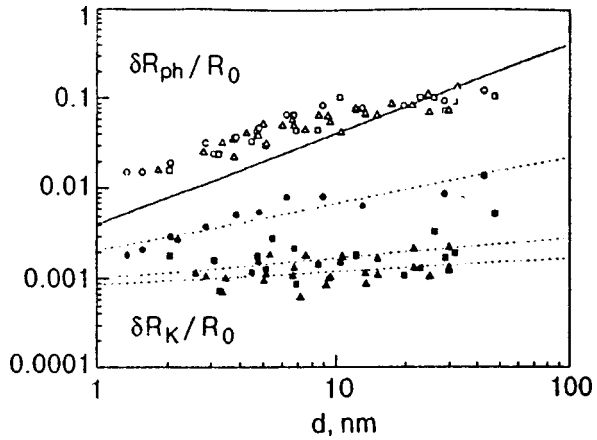

FIG. 2. Normalized increase of differential resistances due to phonon (open data points) and Kondo (solid data points) scatterings. Triangles, squares and circles stand for CuMn alloys of 0.026; 0.028; and 0.18 at.%, respectively. The solid straight line stands for the clean-orifice phonon-scattering intensity. Dotted straight lines are the apparent linear fits for Kondo scattering of three concentrations.

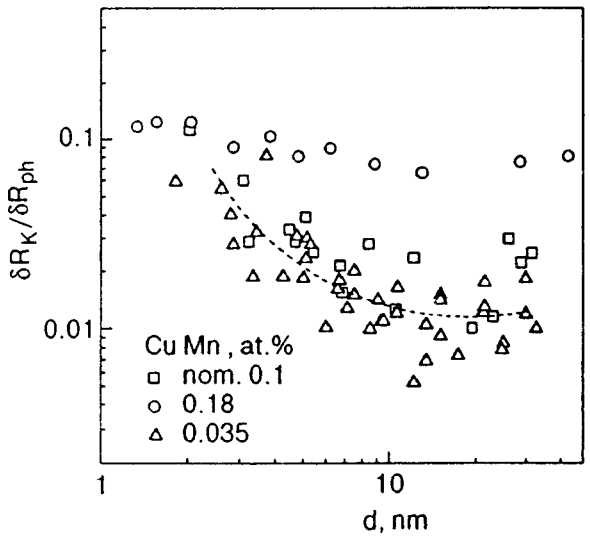

FIG. 3. The ratio of resistance increase due to Kondo and phonon scattering as a function of diameter. Squares, triangles, and circles stand for CuMn alloys of 0.028; 0.026; and 0.18 at.%, respectively. The dashed line serves as the guide to the eye for 0.026 at.%.

inner boundaries. We shall use d as a parameter characterizing the contact diameter although it should be remembered that it is model dependent in the general case. We recall that the true experimental parameter is the contact resistance R_0 which can be restored through Eq. (4).

As the quantitative estimates of phonon and Kondo scattering intensity we choose the increase of differential resistance from R_0 to the value at $V=\pm 20$ mV ($\delta R_{\rm ph}$) and the height of Kondo peak (δR_K) shown in Fig. 1, upper panel, respectively. One more parameter proportional to the phonon scattering is the intensity of maximum M in $dR/dV(V)$ spectra which can be connected with the maximum of EPI function through Eq. (3). This quantity has an advantage that the background [approximated by a straight line (shown in the lower panel of Fig. 1)] can be subtracted.

3.1. Contact-size dependence of phonon and Kondo scatterings

Figure 2 shows the cumulative results of our measurements. The phonon (open) data points follow the same trend for all concentrations, namely, at small sizes they are proportional to d while for large diameters they are flattened. These new data correspond well to our previous results cited in Refs. 1, 2 and 9. The pure copper follows the same dependence (not shown). The solid straight line denotes the $\delta R_{\rm ph}/R_0$ vs. d for a clean orifice model according to tabulated experimental $g_{PC}(eV)$ function in Ref. 7:

$$\left(\frac{\delta R_{\rm ph}}{R_0}\right)_{V=20{\rm mV}} = \frac{8}{3}\frac{ed}{\hbar v_F}\int_0^{20{\rm mV}} g_{PC}(\omega)\,d\omega = 4.05\times 10^{-3} d[{\rm nm}]. \quad (5)$$

It is important that the experimental points lie above the clean orifice line for sizes smaller than 10 nm. For larger diameters the experimental points coincide with and lie below this line since the elastic electron mean free path becomes smaller than the contact diameter.

In general, the Kondo data points rise less steeply with increasing d than to the phonons; this is especially clear for lower concentrations. The apparent linear fits for $\delta R_K/R_0$ vs. d amounts

(a) $\log Y = 0.51(0.06)\log X - 2.68(0.05)$ for 0.18%,
(b) $\log Y = 0.21(0.11)\log X - 2.99(0.12)$ for 0.028%,
(c) $\log Y = 0.14(0.08)\log X - 3.05(0.08)$ for 0.026%,

which are shown in Fig. 2 with the straight dotted lines. Here $X=d$ [nm], $Y=\delta R_K/R_0$ and in brackets we denote the standard deviation. We join the experimental data for concentrations of 0.035 and 0.017 at.% in one set with an averages concentration 0.026 at.%, since they are indistinguishable in view of large uncertainty (0.017 at.%).

The scattering of data points is rather high which is due to the dispersion between different series. The scattering inside each series is much less. Thus, we can conclude that the property of the metal differs from sample to sample, and from the series to series for the same alloy.

The alloy with nominal concentrations of 0.1 at.% which we have studied in previous works[1,2,9] yields quite a similar exponent b) (in the limits of errors) dependence[9,14] in the present study despite the quite different experimental conditions ($T=1.6$ K instead of 0.5 K, an environment of liquid helium instead of high vacuum).

For pure copper the zero-bias Kondo peak $\delta R_K/R_0$ is of the order of $1e-4$ which corresponds to the purity of our Cu metal. Previous studies in the analogous break-junction devices[15,16] also have not revealed the zero-bias Kondo peaks in pure copper. The ratio between Kondo and phonon intensities are plotted in Fig. 3. As we have noted above this ratio does not depend upon the constriction geometry and elastic mean free path. It is seen that $\delta R_K/\delta R_{\rm ph}$ increases by almost an order of magnitude for diameters smaller than 10 nm. For higher concentration (0.18 at.%) this dependence is masked. Here we want to notice that, while 0.017; 0.028; and

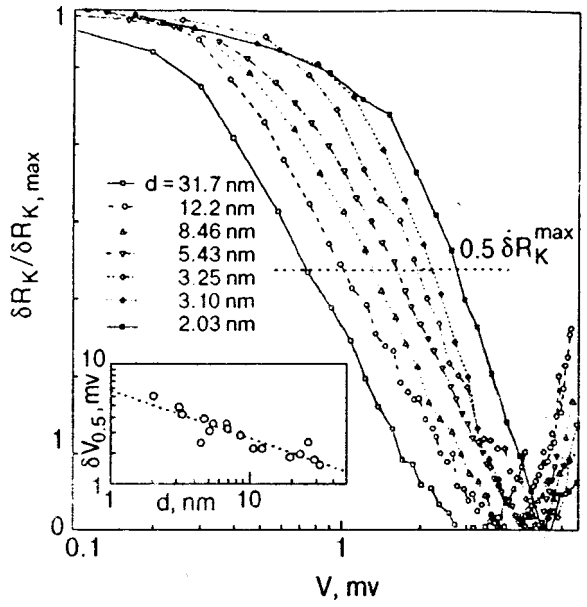

FIG. 4. The normalized Kondo maximum for CuMn (0.028 at.%) for different contact diameters. In the inset: the width of the maximum at the half height (see the horizontal dotted line in the main panel) is shown as a function of diameter.

0.035 at.% correspond to different series and samples (and this is a cause of big scattering of data points) the results for 0.18 at.%, represent only a single series and are more continuous.

3.2. Energy dependence of Kondo scattering

The energy dependence for the normalized Kondo resistance is shown as a function of contact diameter for 0.028 at.% alloy in Fig. 4. For other concentrations these dependences look similar. The new measurements are practically the same as already reported (see Fig. 2(b) in Ref. 10 and Fig. 5(b) in Ref. 11), but are more detailed since the simplified experimental technique enables us to collect more data. The logarithmic voltage dependences of $\delta R_K/\delta R_{K,\max}$ are quite evident for all curves. In the inset to Fig. 4 the voltage width at the half-maximum height vs. diameter is plotted as shown with the dotted horizontal line in the main panel. More data points are plotted in the inset since not the all curves are shown in the main panel. The observed scattering is due to the data points from different series.

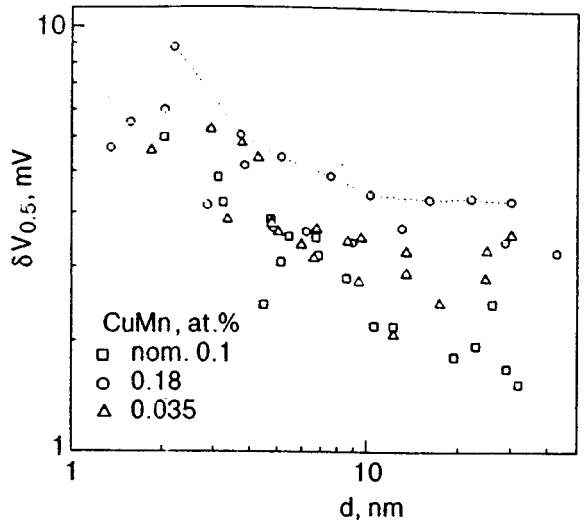

FIG. 5. The width of the Kondo maximum as a function of contact diameter. Squares, triangles, and circles stand for CuMn alloys of 0.028; 0.026; and 0.18 at.%, respectively. The dashed line connects data-points of single series.

The widths of the Kondo-resistance-peaks are shown for different concentrations as a function of contact diameter in Fig. 5. In spite of the large data scattering, the increase of $\delta V_{0.5}(d)$ for diameters smaller than 10 nm is clearly seen. This increase can be observed for each concentration, including 0.18 at.%. It proves that even for this alloy we did observe increased energy-scale for Kondo-effect, although it may not be so evident from Fig. 3. It is important to note that the increase of Kondo-peak width was not observed in Cu(Fe)-contacts[10,11] with comparable and higher resistances. The difference between Mn and Fe impurities proves that the widening of Kondo-peak is not due to extrinsic effects (like quantum diffraction of electron wave functions at small constrictions) but is connected with the Kondo-mechanism itself. Note also, that at the *large* diameters the width of the Kondo-peak increases at the increasing Mn concentrations in the row 0.028; 0.035, and 0.18 at.%, as expected due to the spin-glass effects. Indeed, for low-resistance contacts with $c=0.0018$ we observe the splitting of Kondo-peak due to the internal field (not shown here).

4. DISCUSSION

The PC EPI spectral functions are summarized for pressure-type point contacts in Refs. 7 and 17. These are made either by pressing together the sharp needle to the flat surface (other version: by pressing together the sharp edges of metallic electrodes) or by electrical microwelding by a current pulse. In all these cases the probability of formation of the metallic contact with a length much smaller than its width (diameter) is high enough. These contacts are satisfactorily modelled as an orifice in an infinitely thin partition. Indeed, the experimentally observed maximum intensity of PC EPI spectra are saturated at a constant value. For copper this value is about $g_{PC}^{\max}=0.24$ (linear background being subtracted). Theoretical calculation for the simplest metal—sodium—gives a value coinciding with the experiment, that can be taken as a quantitative proof of observing the clean orifice.[17] With invention of nanofabricated thin film junctions,[18] STM,[19] and mechanically-controllable break (MCB) junctions[20] a new possibility appears. The shape of a contact can be fabricated as a channel (wire) whose length is equal or greater than a diameter. According to Ref. 21, the shape of a contact for STM (and evidently, for MCB[22]) depends on the fabrication procedure, and can be made similar to both orifice and channel for different prehistories. It was shown in Ref. 21 for gold STM junctions that the gentle touch of a needle to the flat surface leads to observing the contact whose shape was close to the orifice, while the more deep intrusion results in producing a long wire. Something like this one could expect also for the MCB junctions.

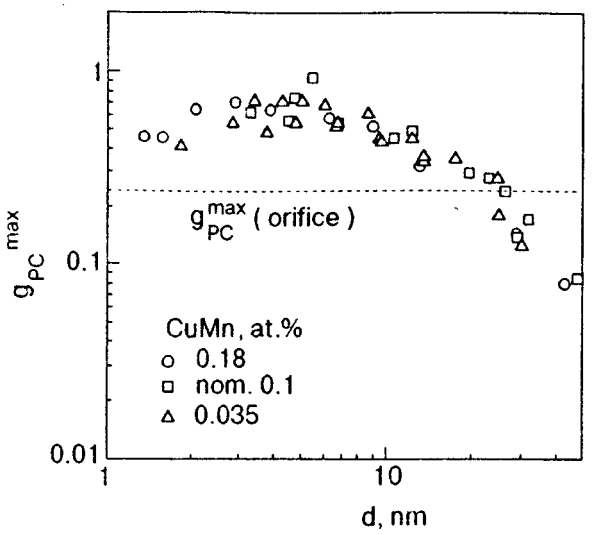

FIG. 6. Maximum of the electron-phonon interaction spectral function as a function of contact diameter. Squares, triangles, and circles stand for CuMn alloys of 0.028; 0.026; and 0.18 at.%, respectively. Horizontal dotted line shows the maximum g_{PC} of clean orifice value.

We show the $g_{PC}^{\max}$ for our contacts of different concentration in Fig. 6. It is seen that the maximum intensities exceed the orifice value by 2–3 times. This was never observed for pressure-type contacts. If we assume a linear interpolation between theoretical limits for clean orifice and channel[7]

$$\frac{1}{R}\frac{dR}{dV}(V)=\frac{8}{3}\frac{e\left(d+\frac{3\pi}{4}L\right)}{\hbar v_F}g_{PC}(eV), \quad (T\simeq 0), \qquad (6)$$

then this means that the length of the ''wire'' (or channel) is approximately equal to its diameter.

Correspondingly, the experimental data points for $\delta R_{\rm ph}/R_0$ in Fig. 2 lie about twice as high than the straight solid line which stands for the clean orifice model according to the Eq. (5). Thus, we can state that our contacts with diameter smaller than $\simeq$10 nm are similar to nanosized wire (channel). More about the length, shape, and purity of this wire can be said from the *d*-dependence of phonon intensity but this lies beyond the scope of this work.

Figure 7 shows schematically what may happen. After the first breaking there are presumably hillocks seeing each other (a) and separating by the least distance. First, the pressure type contact gives the shape more like an orifice (b). These correspond to contact diameter greaters than 20 nm. The more pressure—the more defects are introduced, and this leads to a decrease in the phonon intensity below the clean orifice value (Fig. 6) for the largest diameters. Pulling off the electrodes results to a shape similar to a wire (channel), but the greater the separation distance the more defects are introduced to the thinner wire, and this probably leads to a decrease in the intensity at the least contact diameters. Other causes may be quantum diffraction effects for electron and phonon, since their wavelengths become comparable to the wire diameter.[23]

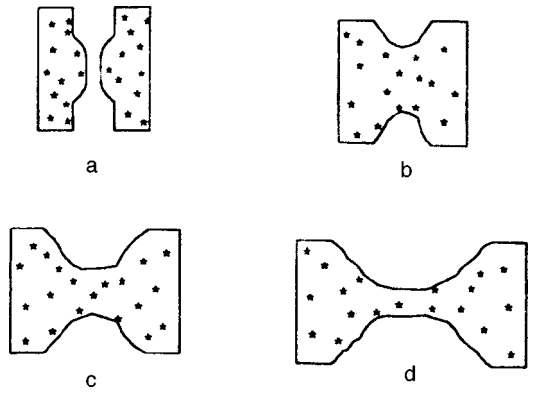

FIG. 7. Schematic view of MCB junction: before touching (a); first touch starting from the low resistance contact (b); successively forming the neck while pulling the electrodes off (c and d). Small stars denote the magnetic impurities.

Recently, Kolesnichenko *et al.*[24] have predicted a classical mesoscopic size effect for impurities whose average interimpurity distance is comparable or greater than the contact diameter. This effect is a version of the classical correlation phenomena in point contacts considered by Gal'perin and Kozub in Ref. 25. Due to the scattering probability which is proportional to the solid angle by which an orifice is seen from the impurity location, the maximum scattering probability has the impurity located at the interface of the orifice model. It is easy to see that the number of these impurities increases if the shape of the contact deviates from an orifice to a wire (Fig. 7). Qualitatively, this effect can explain nonlinear in *d* dependence of Kondo scattering (with increase at small size contacts), but it hardly can be responsible neither for the increase of width of the Kondo peak (Fig. 5), nor for the loss of sensitivity to external magnetic field for ultra small contacts.

5. CONCLUSION

The results of the present work proves the correspondence of Zarand–Udvardi model[4] to the experiments. This model ascribes the enhancement of the Kondo temperature of magnetic impurities in metallic point contacts due to fluctuations of the local electron density of states. There are no fluctuations for a pure orifice since lateral quantization of electron wave function is smeared out.[26] On the other hand, for dirty channels (wires) quantization is destroyed by scatterings, especially if they involve spin flip. Note, that for large biases (of the order of phonon characteristic frequencies) Kondo scatterings with spin flip are negligible. Thus, we conclude that the size effect can be observed in clean enough nanosized wires, in accordance with Ref. 4. The necessary conditions for observing the Kondo size effect in point contacts are that the phonon intensity should be noticeably greater than that of a clean orifice model.[7]

We are indebted to A. I. Yanson who settled the automatic data recording in our lab, which enabled us to carry out this work. Our thanks are to V. V. Demirski for making the quantitative analysis of alloys. I. K. Y. and N. L. B.

appreciate the financial support of Soros Foundation. I. K. Y. is grateful to Alexander von Humboldt Foundation and to the Physikalishes Institute of Karlsruhe University for hospitality in the frame of Humboldt-Forschungspreisträger Program.

The Kharkov authors are delighted to dedicate this paper to Academician I. M. Dmitrenko on the occasion of his 70th birthday.

*E-mail: yanson@ilt.kharkov.ua

[1] I. K. Yanson, V. V. Fisun, R. Hesper, A. V. Khotkevich, J. M. Krans, J. A. Mydosh, and J. M. van Ruitenbeek, Phys. Rev. Lett. **74**, 302 (1995).
[2] I. K. Yanson, V. V. Fisun, A. V. Khotkevich, R. Hesper, J. M. Krans, J. A. Mydosh, and J. M. van Ruitenbeek, Fiz. Nizk. Temp **20**, 1062 (1994) [Low Temp. Phys. **20**, 836 (1994)].
[3] M. A. Blachly and N. Giordano, Phys. Rev. B **51**, 12537 (1995).
[4] G. Zarand and L. Udvardi, Phys. Rev. B **54**, 7606 (1996).
[5] A. G. M. Jansen, A. P. van Gelder, P. Wyder, and S. Strässler, J. Phys. F: Metal Phys. **11**, L15-21 (1981).
[6] A. N. Omel'yanchuk and I. G. Tuluzov, Fiz. Nizk. Temp. **11**, 388 (1985) [Sov. J. Low Temp. Phys. **11**, 211 (1985)].
[7] A. V. Khotkevich, I. K. Yanson, in *Atlas of Point Contact Spectra of Electron-Phonon Interactions in Metals*, Kluwer Academic, New York (1995).
[8] In the limit of dirty contact $n=0$ [Ref. 7].
[9] I. K. Yanson, V. V. Fisun, R. Hesper, A. V. Khotkevich, J. M. Krans, J. A. Mydosh, N. van der Post, and J. M. van Ruitenbeek, Physica B **218**, 77 (1996).
[10] N. van der Post, F. L. Mettes, J. A. Mydosh, J. M. van Ruitenbeek, and I. K. Yanson, Phys. Rev. B **53**, R476 (1996).
[11] N. van der Post, F. L. Mettes, J. A. Mydosh, J. M. van Ruitenbeek, and I. K. Yanson, Fiz. Nizk. Temp. **22**, 313 [Low Temp. Phys. **22**, 245 (1996)].
[12] K. S. Ralls, D. C. Ralph, and R. A. Buhrman, Phys. Rev. B **40**, 11561 (1989).
[13] The smearing of the first and second derivatives are equal to $\delta(eV_1)=[(2.45eV_1)^2+(3.53k_BT)^2]^{1/2}$ and $\delta(eV_2)=[(1.72eV_1)^2+(5.44k_BT)^2]^{1/2}$, respectively, according to[7,27] V_1, T are the effective values of modulation voltage and temperature, respectively.
[14] Equation cited in Ref. 9 reads: $\log Y=0.16(0.05)\log X-2.62(0.05)$.
[15] N. van der Post, Thesis, Leiden University (1997).
[16] F. Roche, Diplomarbeit, Max-Planck-Institut für Festkörperforschung, Centre National de la Recherche Scientifique, High Magnetic Field Laboratory, Grenoble.
[17] I. K. Yanson, Fiz. Nizk. Temp. **9**, 676 (1983) [Sov. J. Low Temp. Phys. **9**, 343 (1983)].
[18] K. S. Ralls, R. A. Buhrman, and R. C. Tiberio, Appl. Phys. Lett. **55**, 2459 (1989).
[19] N. Agraït, J. G. Rodrigo, S. Vieira, Phys. Rev. B **47**, 12345 (1993).
[20] C. J. Muller, J. M. van Ruitenbeek, and L. J. de Jongh, Phys. Rev. Lett. **69**, 140 (1992).
[21] C. Untiedt, G. Rubio, S. Vieira, and N. Agraït, Phys. Rev. B **56**, 2154 (1997).
[22] A. M. Bratkovsky, A. P. Sutton, and T. N. Todorov, Phys. Rev. B **52**, 5036 (1995).
[23] I. F. Itskovich and R. I. Shekhter, Fiz. Nizk. Temp. **11**, 373 (1985) [Sov. J. Low Temp. Phys. **11**, 202 (1985)].
[24] Yu. A. Kolesnichenko, A. N. Omel'yanchuk, and I. G. Tuluzov, Fiz. Nizk. Temp. **21**, 851 (1995) [Low Temp. Phys. **21**, 655 (1995)]; Yu. A. Kolesnichenko, A. N. Omelyanchouk, N. van der Post, and A. I. Yanson, Czech. J. Phys. **46**, Suppl. S4, 2383 (1996), *Proc. of the LT-21*; Fiz. Nizk. Temp. **23**, 1309 (1997) [Low Temp. Phys. **23**, 983 (1997)].
[25] Yu. M. Gal'perin and V. I. Kozub, Fiz. Nizk. Temp. **18**, 494 (1992) [Sov. J. Low Temp. Phys. **18**, 336 (1992)].
[26] J. A. Torres, J. I. Pascual, and J. J. Saenz, Phys. Rev. B **49**, 16581 (1994).
[27] A. M. Duif, Doctoraalscriptie, Nov. 1983, KUN Nijmegen, The Netherlands.

This article was published in English in the original Russian journal. It was edited by R. T. Beyer.

New size effects in the conductivity of metal–insulator–metal tunnel junctions

V. M. Svistunov, A. I. Khachaturov, and O. I. Chernyak

*A. Galkin Institute of Physics and Technology, National Academy of Sciences of the Ukraine, 340114 Donetsk, Ukraine**

R. Aoki

College of Industrial Technology, Amagasaki, Nishi-Koya, Japan
(Submitted March 2, 1998)
Fiz. Nizk. Temp. **24**, 661–667 (July 1998)

A simple theory that makes it possible to calculate the characteristics of metal–insulator–thin metal film tunnel junctions is developed. Along with the well-known oscillations in the voltage dependence $\sigma(V)$ of tunneling conductance due to commensurate states, it predicts a number of new effects. For example, even in the case of a symmetric tunnel junction formed by the identical materials with a rectangular potential barrier, the $\sigma(V)$ curve displays a noticeable asymmetry. The branch of the $\sigma(V)$ curve corresponding to tunneling to the thin-film electrode contains a structure consisting of conductance dips. © *1998 American Institute of Physics.* [S1063-777X(98)00907-4]

1. INTRODUCTION

The possibility of observing standing waves in thin metal films by using the electron tunneling method was predicted at the beginning of the sixties (''golden age'' of tunneling spectroscopy),[1] but their experimental studies was started only after a decade.[2] The main factor hampering experimental studies was the extremely high sensitivity of the effect to the thickness of the film under investigation, which makes its observation in real films difficult. Jaklevic and Lambe[2] took into account the fact that the thickness L of a polycrystalline film can change by only a discrete value multiple to the lattice constant a, and hence the film has the so-called commensurate states with the transverse wave vector component

$$k_z = \frac{S}{Q}\,\frac{\pi}{d} \tag{1}$$

(S/Q is an irreducible fraction and d the barrier thickness), whose energies $E_{nz} = (\hbar \pi n)^2/2mL^2$ are independent of thickness. The size quantization effect has been observed in various materials (Pb, Au, Ag, Bi)[3,4] by using the tunneling method and can be regarded as a well studied phenomenon. It can be applied for determining the positions of some special points of the band structure as well as the slope of energy–momentum curves $\varepsilon(k)$ near these points. The effect of external agencies on the quantum size effect has also been studied. For example, the effect of high hydrostatic pressures ($\sim$10 kbar) was studied in Refs. 5 and 6.

In all publications mentioned above, however, peculiarities emerging in tunneling parameters were considered for finite bias voltages V across the junction. The present research aims at studying the effect of standing waves on the behavior of the tunneling conductivity $\sigma(V) = dI/dV$ in a wide voltage range (of the order of a volt).

2. FORMULATION OF MODEL AND ANALYSIS OF OBTAINED RESULTS

Let us consider a metal–insulator–thin metal film tunnel junction. We assume that both electrodes are made of the same metal with a quadratic energy–momentum relation. The Fermi energies of these electrodes have the same value $E_{F1} = E_{F2} = E_F$. We also assume that the first electrode has a geometrical size such that its electron spectrum can be regarded as continuous, while the thickness L of the second electrode is small enough for the quantum size effect to be observed. Spatial quantization leads to a quasi-continuous energy spectrum. The energy band splits into two-dimensional subbands

$$\varepsilon_n(k_\parallel) = \frac{(\hbar k_\parallel)^2}{2m} + \frac{(\pi\hbar)^2}{2mL^2}\,n^2, \quad n = 1,2,3..., \tag{2}$$

where $k_\parallel$ is the wave vector component parallel to the tunnel barrier plane.

Since we are interested primarily in large-scale voltage effects, it is convenient to assume that the measuring temperature T is equal to zero. At $T = 0$, the occupied states for the nth subband of the thin-film electrode lie in the circle whose radius is $k_1 = \sqrt{2m(E_F - E_{nz})}/\hbar$ (all energies are measured from the bottom of the conduction band of the initial electrode). We supply the bias voltage V to the thin-film electrode and calculate the contribution to the tunneling current due to the nth subband. For a finite negative bias voltage V across the thin-film electrode, all the electrons whose states lie within the ring (see Fig. 1a) defined by the radii k_1 and $k_2 = \sqrt{2m(E_F - E_{nz} - eV)}/\hbar$, can take part in tunneling since all of them have a corresponding free state at the opposite bank of the junction. Dividing the area S of the disk by the two-dimensional density of states $(2\pi)^2$, we obtain the number of electrons N participating in tunneling. Multiplying this number by the charge e and the transverse

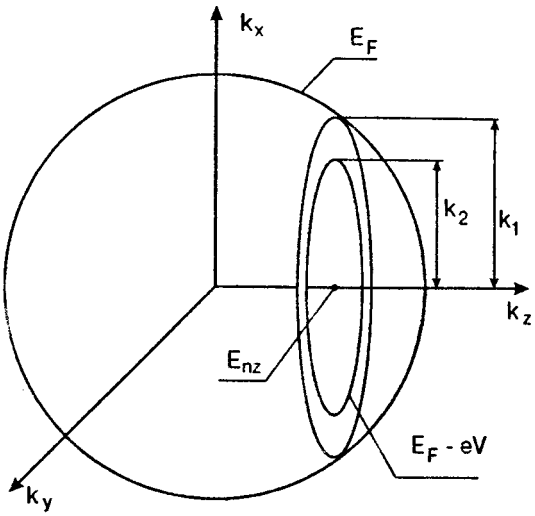

a

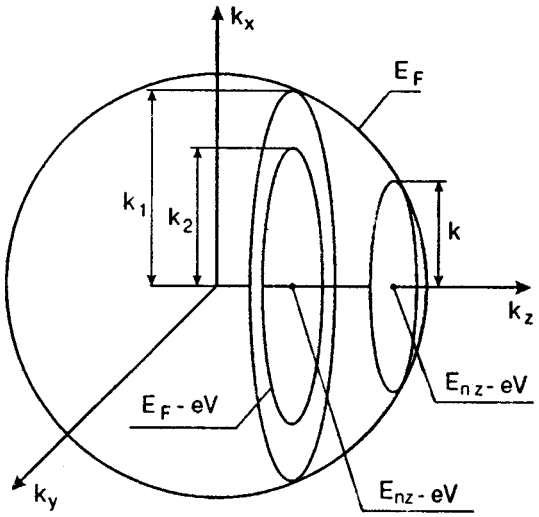

b

FIG. 1. (a) Reciprocal space for a quantized film. The Fermi level of the film is shifted upwards by V relative to that of an ordinary metal electrode. Electrons from the nth subband participating in tunneling lie in the ring of area $2\pi meV/\hbar$. (b) Reciprocal space for an ordinary metal electrode with the Fermi level shifted upwards by the bias voltage V relative to the Fermi level of the film. For tunneling planes lying below the Fermi level ($E_{nz}<E_F$) for $V=0$, electrons participating in tunneling lie in the ring. For tunneling planes lying above the Fermi level ($E_{nz}\geqslant E_F$) for $V=0$, electrons participating in tunneling lie on the disc.

velocity component v_{nz}, we obtain the contribution from one subband to the current incident on the plane of the junction:

$$J_{\text{in}}(E_{nz},V)=2ev_{nz}N=2e\,\frac{S}{(2\pi)^2}\,v_{nz}=\frac{m}{\pi\hbar^2}\,e^2Vv_{nz},$$

$$eV<E_F-E_{nz}. \tag{3}$$

(The factor 2 in this formula appeared due to the inclusion of the electron spin.) In the one-band model, all the electrons lying in the plane perpendicular to the z-axis have the same tunneling probability $P(E_{nz},V)$. Consequently, the calculation of the tunneling current does not require integration:

$$J(E_{nz},V)=\frac{e^2}{\pi\hbar^2}\,V\sqrt{2mE_{nz}}P(E_{nz},V),$$

$$eV<E_F-E_{nz}. \tag{4}$$

The tunneling probability $P(E_{nz},V)$ for a trapezoidal barrier with heights φ_1 and φ_2 and thickness d appearing in (4) in the WKB approximation has a relatively simple form[7]

$$P(E_{nz},V)=\exp\left\{-\frac{A_d}{\varphi_2-eV-\varphi_1}\right.$$

$$\left.\times[(\varphi_2-eV-E_{nz})^{3/2}-(\varphi_1-E_{nz})^{3/2}]\right\}, \tag{5}$$

where $A_d=4\sqrt{2m}d/3\hbar$ (for simplicity, we assume that the effective electron mass m in the forbidden band of the insulator and in the metallic electrodes is equal to the mass of a free electron). If $eV>E_F-E_{nz}$, it can easily be seen from Fig. 1a that a further increase in voltage does not lead to an increase in the number of electrons participating in tunneling since the subband is open completely, and all its electrons lying in the circle of the area $2\pi m(E_F-E_{nz})/\hbar^2$ are already involved in the tunneling process. The contribution to the tunneling current from a solitary subband in this case is given by

$$J_n(V)=\frac{e(E_F-E_{nz})}{\pi\hbar^2}\,\sqrt{2mE_{nz}}P(E_{nz},V),$$

$$eV>E_F-E_{nz}. \tag{6}$$

The current $J_n(V)$ for small bias voltages ($eV<E_F-E_{nz}$) is determined by two factors: the increase in the number of electrons participating in tunneling and the change in the tunneling probability $P(E_{nz},V)$, while for large bias voltages ($eV>E_F-E_{nz}$) its variation is associated only with the latter factor.

Differentiating the total current

$$J(V)=\Sigma_{E_{nz}<E_F}J(E_{nz},V)$$

with respect to voltage V, we obtain the following expression for the tunneling conductivity:

$$\sigma(V)=\sum_{E_{nz}<E_F}\sigma(E_{nz},V), \tag{7}$$

where

$$\sigma(E_{nz},V)$$

$$=\begin{cases}\dfrac{e^2}{\pi\hbar^2}\,\sqrt{2mE_{nz}}[P(E_{nz},V)+VP'(E_{nz},V)], \\ \qquad\qquad eV<E_F-E_{nz} \\ \dfrac{e}{\pi\hbar^2}\,\sqrt{2mE_{nz}}(E_F-E_{nz})P'(E_{nz},V), \\ \qquad\qquad eV>E_F-E_{nz}\end{cases}. \tag{8}$$

The derivative $P'(E_{nz},V)=dP(E_{nz},V)/dV$ of the tunneling probability with respect to bias voltage can be calculated analytically:

$$P'(E_{nz},V) = \frac{eA_d[(\varphi_2-3\varphi_1-eV+2E_{nz})\sqrt{\varphi_2-eV-E_{nz}}+2\sqrt{(\varphi_1-E_{nz})^3}]}{2(\varphi_2-eV-\varphi_1)^2} \times P(E_{nz},V). \quad (9)$$

Thus, we can expect the emergence of kinks in the voltage dependence of the tunneling current $J(V)$ at voltages $eV=E_F-E_{nz}$ and the emergence of steps in the differential conductivity $\sigma(V)$.

Let us suppose that the bias voltage is supplied to an ordinary electrode. In spite of the fact that the energy spectrum of the initial electrode is continuous, only those electrons which can find in the final electrode (i) allowed and (ii) free states can take part in tunneling. In the case of specular and elastic tunneling, the first condition indicates that all the tunneling electrons must lie on the planes $E'_{nz}=E_{nz}-eV$. These planes will be henceforth referred to as tunneling planes. The total tunneling current can obviously be determined by summing up the contributions E'_{nz} from all the tunneling planes of the initial electrode or, which is the same, by carrying out summation over the corresponding subbands E_{nz} of the final electrode. Let us first consider tunneling planes for which the subbands E_{nz} lie above the Fermi level $E_{nz}>E_F$. In this case, the second condition is satisfied automatically since all final states are unoccupied. However, for $eV<E_{nz}-E_F$, the current from the nth tunneling plane is zero since this plane contains no occupied states. Such states are formed only when eV exceeds the energy difference between the tunneling plane under investigation and the Fermi surface. For $eV>E_{nz}-E_F$, all these states in the reciprocal space lie on a disk (see Fig. 1b), the transverse energy component of this disk decreasing continuously with voltage ($E'_{nz}=E_{nz}-eV$), while the radius k increases in proportion to $\sqrt{E_{nz}-E_F+eV}$. The contribution to the total tunneling current from the electrons under consideration is defined by the formula

$$J1(E'_{nz},V) = \begin{cases} 0, & eV<E_{nz}-E_F \\ \dfrac{e}{\pi\hbar^2}(E_F-E'_{nz})P(V,E'_{nz})\sqrt{2mE'_{nz}}, & eV>E_{nz}-E_F \end{cases}. \quad (10)$$

Let us consider the tunneling planes whose corresponding subbands lie below the Fermi level ($E_{nz}\leqslant E_F$). In this case, free states are available on the opposite bank of the junction only for electrons lying in a ring of radii k_1 and k_2 (see Fig. 1b. As the bias voltage increases, the area S of this ring increases in proportion to the bias voltage ($S=2\pi meV/\hbar$), and the ring moves along the z-axis towards the bottom of the band. For $eV>E_{nz}-E_F$, the initial electrodes has no states from which an electron could get in the subband under investigation by tunneling. The contribution to the total tunneling current made by a tunneling plane is given by

$$J2(E'_{nz},V) = \begin{cases} \dfrac{e^2}{\pi\hbar^2}V\sqrt{2mE'_{nz}}P(V,E'_{nz}), & eV\leqslant E_{nz} \\ 0, & eV>E_{nz} \end{cases}. \quad (11)$$

The total tunneling current is the sum of the contributions from all the tunneling planes of individual subbands:

$$J(V)=\sum_{E_{nz}<E_F} J1(E'_{nz},V)+\sum_{E_F<E_{nz}<E_F+eV} J2(E'_{nz},V). \quad (12)$$

Differentiating this expression with respect to voltage, we obtain the formula

$$\sigma(V)=\sum_{E_{nz}<E_F}\sigma 1(E_{nz},V)+\sum_{E_F<E_{nz}<E_F+eV}\sigma 2(E_{nz},V), \quad (13)$$

for tunneling conductivity, where

$$\sigma 1(V) = \begin{cases} \dfrac{e\sqrt{2m}}{\pi\hbar^2}\left\{[(E_F-E_{nz}+eV)P1'(V,E_n)+eP1(V,E_{nz})] \times\sqrt{E_{nz}-eV}-\dfrac{e}{2}\dfrac{E_F-E_{nz}+eV}{\sqrt{E_{nz}-eV}}P1(V,E_{nz})\right\}, & eV\leqslant E_{nz}-E_F \\ 0, & eV>E_{nz}-E_F; \end{cases} \quad (14)$$

and

$$\sigma 2(V) = \begin{cases} \dfrac{e^2\sqrt{2m}}{\pi\hbar^2}\left\{[VP1'(V,E_{nz})+P1(V,E_{nz})] \times\sqrt{E_{nz}-eV}-\dfrac{e}{2}\dfrac{V}{\sqrt{E_{nz}-eV}}P1(V,E_{nz})\right\}, & eV\leqslant E_{nz} \\ 0, & eV<E_{nz} \end{cases}. \quad (15)$$

The tunneling probability $P1(V,E_{nz}$ and its derivative $P1'(V,E_{nz})$ in this case are defined by the formulas

$$P1(E_{nz},V)=\exp\left\{-\frac{A_d}{\varphi_2-eV-\varphi_1} \times[(\varphi_2-E_{nz})^{3/2}-(\varphi_1-E_{nz}+eV)^{3/2}]\right\}, \quad (16)$$

$$P1'(V,E_{nz})=A_dP1(V,E_{nz})e\left[\frac{\sqrt[3]{\varphi_1-E_{nz}+eV}}{2(\varphi_1+eV-\varphi_2)} -\frac{\sqrt{(\varphi_1-E_{nz}+eV)^3}-\sqrt{(\varphi_2-E_{nz})^3}}{(\varphi_1+eV-\varphi_2)^2}\right]. \quad (17)$$

Figure 2 shows the results of calculations of differential conductivity of a metal–insulator–thin metal film tunnel junction, which were made under the assumption that the

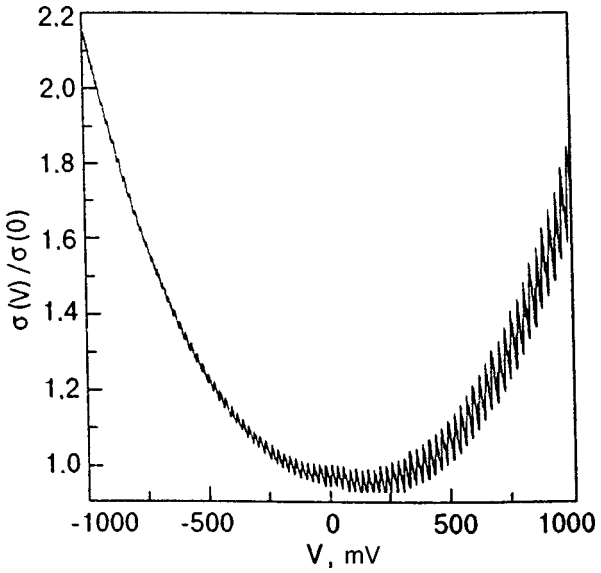

FIG. 2. Differential conductivity $\sigma(V)$ of a tunnel junction (solid curve) formed by a metal, insulator, and a quantized film of uniform thickness $L=1000$ Å. The electrodes are assumed to be made of a hypothetical metal with $E_F=4$ eV and the lattice constant $a=2$ Å. The height of the rectangular potential barrier $\varphi_1=\varphi_2=4$ eV and the thickness $d=11$ Å.

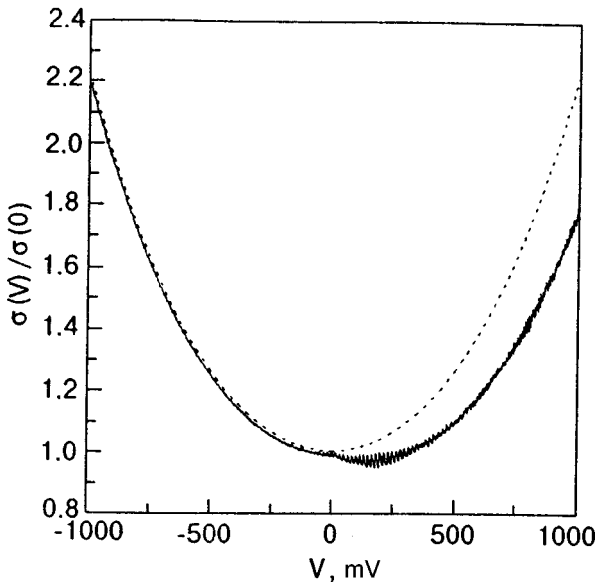

FIG. 3. Differential conductivity $\sigma(V)$ of a tunnel junction (solid curve) formed by a metal, insulator, and a heterogeneous quantized film with a Gaussian distribution over thickness. The electrodes are assumed to be made of a hypothetical metal with $E_F=4$ eV and the lattice constant $a=2$ Å. The film thickness varies from 470 to 530 Å, $\bar{L}=500$ Å, and $\alpha=1/6$. The height of the rectangular potential barrier $\varphi_1=\varphi_2=4$ eV and the thickness $d=11$ Å. The dashed curve corresponds to the differential conductivity of a junction with ordinary metal electrodes, which was calculated for the same parameters.

electrodes of the junction are made of a certain hypothetical metal with the Fermi energy $E_F=4$ eV and the lattice constant $a=2$ Å. The film was assumed to be uniform over the thickness L equal to 1000 Å and the barrier was assumed to be rectangular of height $\varphi=4$ eV and thickness $d=11$ Å. The curve clearly displays singularities located strictly in expected regions, but having an oscillating rather than step shape. This is in complete agreement with the assumptions made by Davis *et al.*,[4] according to which size quantization effects are superimposed on the parabolic voltage dependence of conductance, leading ultimately to oscillations of $\sigma(V)$. It should be noted, however, that the effects observed for a positive bias voltage corresponding to electron tunneling from an ordinary metal to a quantum-size film are much stronger than those observed for a negative voltage. In our opinion, the noticeable (although nonmonotonic) asymmetry of the curve should also be classified as an unexpected result.

For a heterogeneous film whose thickness varies from 470 to 530 Å according to the Gaussian law $L\sim\bar{L}\times\exp\{-[\alpha(L-\bar{L})/\bar{L}]^2\}$, where $\alpha=1/6$ and $\bar{L}=500$ Å, the results of similar calculations are presented by the solid curve in Fig. 3. In complete agreement with what has been said above, the welldefined oscillating structure was preserved only for the voltage $eV=178$ meV, which corresponds to the value of $S/Q=3/2$, and hence $k_z=3\pi/(2d)$. The dashed curve in Fig. 3 describes the tunneling conductivity calculated for the same barrier parameters, but under the assumption that both banks of the tunnel junction are bulk electrodes. A comparison of the two curves shows that the quantum size effect changes significantly the right branch of the $\sigma(V)$ curve, leaving its left branch corresponding to the tunneling from the quantized film to the metal virtually unchanged. In the case of the tunneling from the metal to the quantized film, the conductivity first decreases, passes through a minimum, and only after this increases at a noticeably lower rate than in the left branch. As a result, the entire $\sigma(V)$ dependence, which remains parabolic in general, is as if shifted by a certain finite quantity $V_{\rm sh}$ towards positive voltages. Similar shift effects for the $\sigma(V)$ are well known from experiments. For a long time, these effects were explained, as in Ref. 8, by the potential barrier asymmetry exclusively. It was proved recently[9,10] that this shift can also be due to the difference in the values of Fermi energy for the electrodes of the tunnel junction provided that one of these values is of the order of several volts, and the other value does not exceed one volt. It should be noted that the proposed model can readily give the values of $V_{\rm sh}$ of the order of several hundreds millivolts, which are observed in some cases and which can hardly be explained by the asymmetry of the trapezoidal barrier.

Let us consider the reason behind the asymmetry of tunneling parameters of symmetric junctions with a rectangular barrier and electrodes made of the same material. When the bias voltage V is supplied to the electrode with a quasicontinuous spectrum, the main contribution to conductivity comes from the subbands which lie below the Fermi energy and have transverse energy components E_{nz} belonging to the interval $E_F>E_{nz}>E_F-eV$. In the case of tunneling from the ordinary electrode, the tunneling conductivity is determined by the subbands lying above the Fermi energy ($E_F<E_{nz}<E_F-eV$). For a quadratic energy–momentum relation, the number of such subbands is smaller than in the previous case. It should be noted that their ratio depends on

the Fermi energy, lattice constant, and the interval being measured, but is generally independent on the thickness L of the quantized film. This means that, in the case of simple increase in the thickness L, our model does not indicate a limiting transition to the conventional metal–insulator–metal tunnel junction with nonquantized electrodes. Asymmetry in tunneling parameters will be preserved as long as the electron spectrum is continuous for one of the electrodes and discrete for the other electrode, which determines the conditions for the applicability of the proposed model.

The model under consideration predicts one more type of singularities associated with standing waves. It can be seen from formulas (14) and (15) that $\sigma(V)\to-\infty$ for a negative potential supplied to the bulk electrode for $eV\to E_{nz}$. This value of voltage across the junction corresponds to the instant of departure from the nth tunneling plane to the lower edge of the conduction band. Generally speaking, the fact that the receding subband can be responsible for a singularity in the tunneling conductivity is quite unexpected since the contribution of lower subbands to the total tunneling current is negligibly small as a rule. The contribution of higher-lying subbands is dominating. It follows from formulas (14) and (15), however, that this contribution in the immediate vicinity of the band edge tends to zero so rapidly that it overtakes the increase in all the remaining terms in formula (13). The resulting dip in the conductivity in this case must be extremely narrow. Indeed, according to numerical calculations, the width of the dip in tunnel conductivity shown in Fig. 3 varies from a few nanovolts (for subbands lying at the bottom of the conduction band) to several tens of microvolts (for subbands lying near the Fermi level). For this reason, the dips are not manifested in the $\sigma(V)$ dependence shown in Fig. 3, which is calculated with a step of 1 mV. However, the singularities under investigation start being manifested in the theoretical $\sigma(V)$ dependences (Fig. 4) under more favorable conditions, e.g., upon a further decrease in the Fermi energy, in the form of random peaks of resistance, which leaves a hope of their experimental observation under certain experimental conditions.

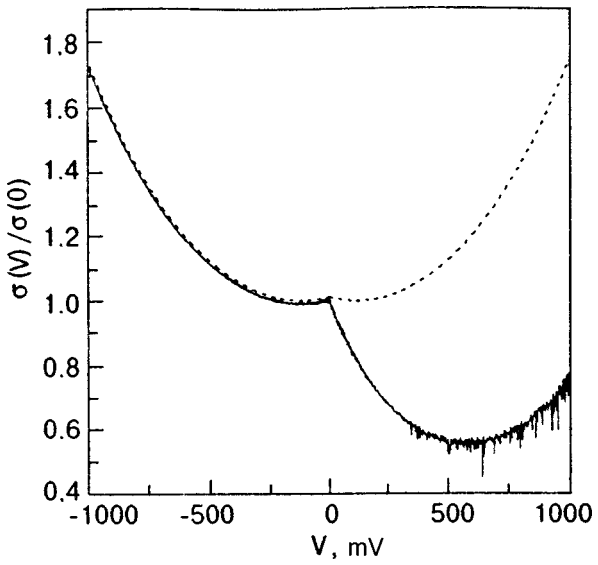

FIG. 4. Differential conductivity $\sigma(V)$ of a tunnel junction (solid curve) formed by a metal, insulator, and a heterogeneous quantized film with a Gaussian distribution over thickness. The Fermi energy of both electrodes is $E_F=1$ eV. The remaining calculated parameters coincide with corresponding values in Fig. 3. The dashed curve shows the differential conductivity of a junction with ordinary metal electrodes, which was calculated for the same parameters.

CONCLUSION

Thus, the theory of a tunnel junction with size quantization in one of the electrodes that has been constructed by us predicts a number of previously unknown effects. The first effect is associated with the general behavior of differential conductivity $\sigma(V)$ in a wide range of voltages. It was found that the branch of this curve corresponding to electron tunneling from the conventional to the quantized electrode behaves anomalously. At low voltages, the conductivity for this polarity first decreases, passes through the minimum, and then starts increasing, this increase occurring at a lower rate than for the opposite bias voltage across the junction. As a result, the entire dependence of conductivity on the bias voltage has in general the shape of a parabola shifted relative to zero voltage. It should be noted in connection with the second effect that resistive peaks are often observed in the tunneling conductivity of metal-oxide superconductors and can be explained exclusively on the basis of their superconducting properties (mainly as breaking of ''superconducting bridges''). Similar effects were also detected in the tunneling to the normal state of metal oxides[11] and have not been explained so far. The proposed model is the only model predicting narrow dips in the conductivity of tunnel junctions with nonsuperconducting banks. In our opinion, the quasiperiodic resistance peaks observed in tunneling parameters of metal-oxide compounds indicate the presence of quasi-two-dimensional subbands with a small number of charge carriers in their electron spectra.

This article was written to commemorate the 70th birth anniversary of Academician I. M. Dmitrenko who indicated the elegance of tunneling ''probing'' of solids even at the beginning of the sixties to one of the authors (V.M.S.).

This research was supported by a grant from TAO, the Telecommunications Advancement Organization of Japan.

*E-mail: svistuno@sts.dipt.donetsk.ua

[1] G. A. Gogadze and I. O. Kulik, Fiz. Tverd. Tela (Leningrad) **7**, 432 (1965) [Sov. Phys. Solid State **7**, 345 (1965)].
[2] R. C. Jaklevic and J. Lambe, Phys. Rev. B **B12**, 4146 (1975).
[3] V. N. Lutskii, D. N. Korneev, and M. I. Elinson, JETP Lett. **4**, 179 (1966).
[4] L. C. Davis, R. C. Jaklevic and J. Lambe, Phys. Rev. B **B12**, 798 (1975).
[5] V. M. Svistunov and V. Yu. Tarenkov, JETP Lett. **26**, 30 (1977).
[6] V. M. Svistunov, M. A. Belogolovskii, and O. I. Chernyak, Usp. Fiz. Nauk **151**, 31 (1987) [Sov. Phys. Usp. **30**, 1 (1987)].
[7] R. B. Floyd and D. G. Wamsley, J. Phys. C **11**, 4601 (1978).
[8] W. F. Brinkman, R. C. Dynes, and J. M. Rowell, J. Appl. Phys. **41**, 1915 (1970).

[9] A. I. Khachaturov, V. M. Svistunov, and M. A. Belogolovskii, Czech. J. Phys. **46**, Suppl. Part S2, 1031 (1996).
[10] V. M. Svistunov, A. I. Khachaturov, M. A. Belogolovskii, and O. I. Chernyak, Fiz. Nizk. Temp. **22**, 605 (1996) [Low Temp. Phys. **22**, 461 (1996)].
[11] V. M. Svistunov, Yu. F. Revenko, O. V. Grigut *et al.*, Mod. Phys. Lett. B **5**, 607 (1991).

Translated by R. S. Wadhwa

Phonon spectrum of Bi2223 for different carrier concentrations

V. M. Svistunov, V. Yu. Tarenkov, and A. I. D'yachenko

*A. Galkin Institute of Physics and Technology, National Academy of Sciences of the Ukraine, 340114 Donetsk, Ukraine**

R. Aoki

College of Industrial Technology, Amagasaki, Nishi-Koya, Japan
(Submitted March 2, 1998; revised March 24, 1998)
Fiz. Nizk. Temp. **24**, 668–671 (July 1998)

Tunneling experiments with Bi2223 reveal that a decrease in the carrier concentration shifts the boundary frequency ω_0 of the cuprate phonon spectrum towards higher frequencies from $\omega_0 = 98$ mV($T_c = 113$ K) to $\omega_0 = 106$ mV($T_c = 107$ K) with an insignificant suppression of the energy gap parameter Δ. © *1998 American Institute of Physics.* [S1063-777X(98)01007-X]

INTRODUCTION

The relation between the superconducting transition temperature and charge carrier concentration in metal oxides has been established quite reliably.[1] The relation between T_c and the phonon spectrum of cuprates has been studied less comprehensively. The establishment of such a relation can be a sound argument in an analysis of the high-T_c superconductivity mechanism. The carrier concentration in cuprates can be varied with the help of high pressure,[2] which increases[3] the ratio $2\Delta/kT_c$ and softens the high-frequency part of the phonon spectrum.[4,5] Such a behavior should be expected for the strong electron–phonon mechanism of superconductivity if the main contribution to the change in $2\Delta/kT_c$ comes from high-frequency phonon modes.[6] However, the mechanism of the effect of pressure on the carrier concentration is quite complicated.[2] Besides, pressure can only increase the carrier concentration in cuprates. Consequently, the inverse problem in which the carrier concentration decreases is of interest.

Here we use the hardening of samples, in which the carrier concentration is changed by varying the oxygen index δ, the cationic stoichiometry of the remaining core of a metal oxide remaining unchanged. The obtained results lead to a relation between $T_c(\delta)$ and the energy gap Δ and phonon frequencies of Bi2223.

EXPERIMENT

We studied tunnel junctions of the break junction type, prepared on ceramic plates of a Bi-based metal oxide of the 2223 phase. The initial ceramics (95% of the $Bi_{1.6}Pb_{0.4}Sr_{1.8}Ca_{2.2}Cu_3O_x$ phase with $T_c = 110$ K) was obtained by solid-phase synthesis from chemically pure oxides. Ten $1\times0.1\times12$ mm plates with silver current and potential contacts obtained by high-temperature annealing were prepared in each experimental cycle. The methods of preparing thin ceramic plates is described in detail in Ref. 5. The results of measurements proved that the superconducting transition temperatures of plates prepared in the same batch were virtually identical. In order to obtain samples with oxygen deficiency, half the plates in a batch were heated in a furnace to 845 °C and held there for 2 h. Then the plates were cooled rapidly (approximately during 3 min) to room temperature. As a result of such a quenching, the sample resistance increased, while the superconducting transition temperature decreased (Fig. 1). It is well known that the annealing temperature required for obtaining optimally doped (in oxygen) ceramics of the Bi2223 phase under atmospheric pressure lies in the range 820–830 °C.[7] According to the data of differential thermal analysis (DTA),[8] the oxygen concentration decreases at higher annealing temperatures. The annealing temperature chosen by us ensures oxygen removal. If we rapidly cool the sample, the oxygen concentration in it will be frozen at a level below the optimal value, and the carrier concentration decreases accordingly. This will lead to an increase in the sample resistance and a decrease in the transition temperature. The method of variation of the number density of charge carriers used by us has considerable limitations since the Bi2223 phase starts decomposing at $T \simeq 860$ °C (see, for example, Ref. 9). For this reason, the change in the superconducting transition temperature associated with quenching is less than ten degrees. It should be noted that a change in the superconducting transition temperature of the Bi2223 phase is also observed for an excess oxygen concentration in the sample. For this purpose, the sample should be annealed under a high oxygen pressure at 530 °C. The change in T_c in this case amounts to approximately 10 K.[10]

Thus, the conditions of sample treatment used by us lead to a decrease in the concentration p of hole carriers relative to the equilibrium concentration. Consequently, the values of p should be determined from the left-hand side of the well-known Gaussian dependence[1] $T_c(p)$:

$$T_c(p) = T_{c,\max}[1 - 82.6(p - 0.16)^2].$$

In order to obtain a tunnel junction, a ceramic sample was mounted on a flexible steel substrate and coated by a lacquer layer. The substrate was bent until a microcrack was formed in the ceramic, which was monitored by measuring the change in the sample resistance. The lacquer layer coating the ceramic plate not only protected the ceramic reliably

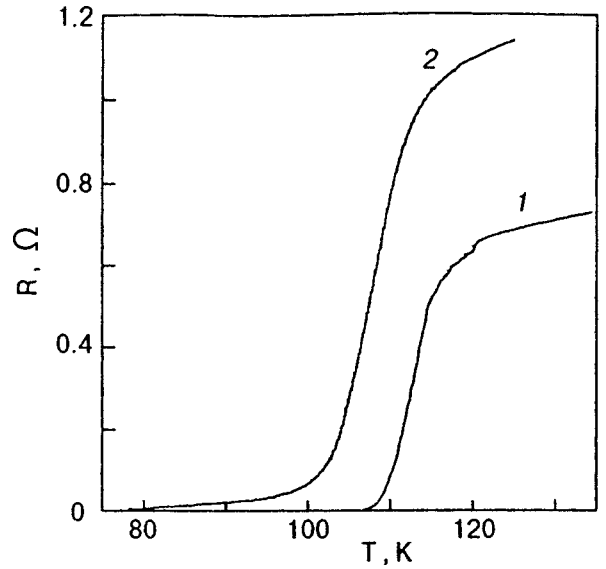

FIG. 1. Characteristics of the resistive $R(T)$ transition of the reference sample 1 ($T_c = 113$ K) and the annealed sample 2 ($T_c = 107$ K) of Bi2223 metal oxide. The value of T_c was determined from the middle of the $R(T)$ transition.

from degrading, but also fixed the parameters of the break junction, which allowed us to obtain tunnel junctions stable in resistance. For a small bias voltage $V = 5$ mV, the resistance of the obtained tunnel junctions increased upon cooling, reflecting the emergence of an energy gap. The ratio of the values of the resistance R_T of the junction for $eV < \Delta$ and $eV > \Delta$ in the temperature range $T \sim 4.2-20$ K was $R_T(0)/R_T(V>\Delta) \sim 10^2$. The resistance of the junctions in the normal state was $R_T \sim 50-100\ \Omega$.

Figure 2 shows the conductance of symmetric SIS junctions of the break junction type at $T = 4.2$ K. The values of energy gaps were determined from the separation of the peaks on the dI/dV curves. The spread in the values of energy gaps obtained for ceramics with equilibrium charge carrier concentration was small, and the mean value of Δ was $\Delta = 37 \pm 0.5$ meV. The spread in the value of Δ for ceramics with a deficiency of charge carriers was much larger ($\Delta = 33.5 \pm 2.5$ meV). The increase in the spread in the values of parameter Δ in oxygen-depleted samples is of universal nature. Such a spread was observed in the spectra of break junctions[11] as well as in the characteristics of these metal oxides obtained with the help of scanning tunneling microscope (STM).[12] This spread is probably associated with local fluctuations of carrier concentration emerging at a temperature below a certain temperature T^* of the junction.[13,14] A certain decrease in the energy gap parameter upon a decrease in the carrier concentration is observed in our case even if we take into account the spread in the measured value of Δ, the ratio $2\Delta/kT_c$ decreasing thereby from 7.6 to 7.2. It was noted by several authors[11–14] that the parameter δ for underdoping does not change (or even increases) upon a decrease in the hole concentration p. Among other things, such a behavior can be due to strong energy gap anisotropy in bismuth cuprates. Strongly directional tunneling effect realized in an acute cone angle makes it possible to determine the parameter Δ only in one of crystallographic directions. For this reason, the energy gap Δ observed in tunnel junctions is not the maximum gap Δ_{max} as a rule. At the same time, the increase in the gap width noted in Refs. 11 and 12 does not exceed Δ_{max} for the equilibrium state of a bismuth cuprate.[4] The characteristics of energy gaps for the reference sample 1 as well as for the hardened sample 2 were blurred rapidly upon heating (see Fig. 2). For this reason, it is impossible to establish the extent to which the $\Delta(T)$ dependence corresponds to the BCS theory. The absence of a clearly manifested $\Delta(T)$ dependence for tunnel samples was noted by some authors and is attributed at present to the emergence of a ''pseudogap.'' [13,14] The singularity (dip) in the tunneling conductance of junctions for $eV \approx 3\Delta$ is apparently also connected with the emergence of a ''pseudogap'' (see Fig. 2).

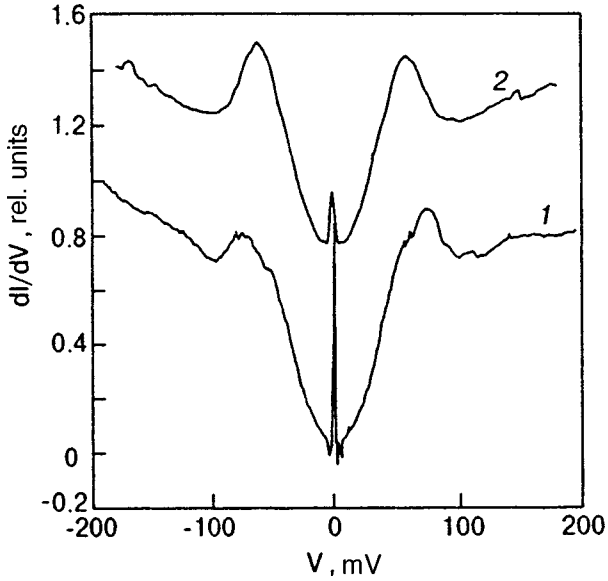

FIG. 2. Reflection of the energy gap in the tunneling conductance of Bi2223–I–Bi2223 junctions at $T = 4.2$ K for sample 1 ($T_c = 113$ K) and sample 2 ($T_c = 107$ K).

All tunnel junctions under investigation displayed a zero-point anomaly (peak) in conductance, which vanished upon a transition of the banks to the normal state. The amplitude of this anomaly increased linearly upon cooling in the entire temperature range $T = 4.2-100$ K. The magnetic field up to 3 kOe did not produce any noticeable effect on the anomaly.

The minima in the tunnel conductance derivative d^2I/dV^2 (Fig. 3) for bias voltages satisfying the relation $eV_i = 2\Delta + \hbar\omega_i$ correspond to phonons of frequencies ω_i in the cuprate. The spectroscopic nature of these singularities is confirmed by the constancy of their position on the energy scale for the entire series of the junctions under investigation as well as by the independence of their position of temperature in the range of $T = 4.2-77$ K. It should be noted that different samples from the same batch can display amplitude variations in the tunneling spectrum, but the position of singularities on the energy scale (measured from the gap) remains unchanged in this case. It can be seen that, for ceramic samples with different concentrations p of holes, the minima in the initial region of the spectra of d^2I/dV^2 virtually coin-

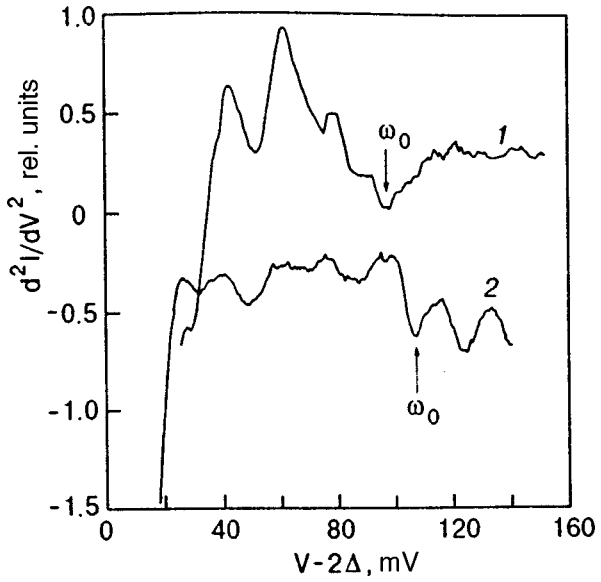

FIG. 3. Phonon spectra in characteristics of tunnel break junctions ($T=4.2$ K). Curve *1* corresponds to the optimal concentration of charge carriers for $T_c=113$ K, curve *2* describes the sample with oxygen deficiency and $T_c=107$ K; ω_0 is the boundary frequency of the spectrum subjected to considerable variations upon a change in the charge carrier concentration.

cide, The strongest difference is observed in the high-frequency region, in which the shift in the boundary frequency of the phonon spectrum for an underdoped sample towards higher energies amounts to 8 mV.

CONCLUSIONS

The experimental results obtained by us indicate that high-frequency phonons associated with optical oscillations of oxygen atoms and their surroundings in the Bi2223 cuprate experience the most significant variation upon a change in the carrier concentration. Acoustic and optical modes of the phonon spectrum with energies $\hbar\omega<40$ meV virtually remain unshifted, which is in accord with the known data of neutron and Raman spectroscopy.[2,15] The decrease in the hole concentration in cuprates in neutron diffraction experiments[16–19] was accompanied by an increase in the energy of high-frequency modes in the phonon spectrum. A similar effect was also observed by us here: a decrease in T_c upon a decrease in the charge carrier concentration is accompanied by an increase in the energy corresponding to upper frequencies of the phonon spectrum. An additional mode appears in the boundary region of the spectrum (Fig. 3). A similar behavior of this mode was also noted in tunneling experiments under pressure.[5] The bifurcation effect is probably of quite universal nature: the bifurcation of the high-frequency mode in YBCO associated with vibrations of apical oxygen O4 was observed by using optical spectroscopy for an oxygen-deficient composition $YBa_2Cu_3O_{6.9}$.[20]

The authors are grateful to N. A. Chernoplekov for numerous fruitful discussions on the electron–phonon interaction in high-temperature superconductors.

This research was supported by a grant from the Telecommunication Advancement Organization of Japan.

This article was written to commemorate the 70th birth anniversary of Academician I. M. Dmitrenko. One of the authors (V.M.S.) warmly recalls the breathtaking years 1962–65 during which he worked in the department headed by Acad. Dmitrenko who guided us to the fascinating world of superconductivity through an elegant, and yet enigmatic tunnel.

*E-mail: svistuno@sts.dipt.donetsk.ua

[1] W. A. Groen, D. M. de Leeuw, and L. F. Feiner, Physica C **165**, 55 (1990).
[2] J. S. Schilling and S. Klotz, in *Physical Properties of High-Temperature Superconductors*, Vol. III (edited by D. M. Ginsberg), World Scientific, Singapore (1992).
[3] V. Yu. Tarenkov, A. V. Abaleshev, A. I. D'yachenko *et al.*, Fiz. Nizk. Temp. **22**, 613 (1996) [Low Temp. Phys. **22**, 467 (1996)].
[4] V. M. Svistunov, V. Yu. Tarenkov, A. I. D'yachenko, and R. Aoki, Fiz. Nizk. Temp. **23**, 1183 (1997) [Low Temp. Phys. **23**, 886 (1997)].
[5] V. M. Svistunov, V. Yu. Tarenkov, A. I. D'yachenko, and R. Aoki, Fiz. Tverd. Tela (St. Petersburg) **39**, 1764 (1997) [Phys. Solid State **39**, 1572 (1997)].
[6] V. L. Ginzburg and E. G. Maksimov, Supercond., Phys. Chem. Technol. **5**, 1543 (1992).
[7] S. P. Tirumala, D. F. Lee, D. M. Kroeger, and K. Salama, Preprint No. 97:090, University of Houston, Houston (1997).
[8] F. Gan and G. Li, J. Non-Cryst. Solids **130**, 67 (1991).
[9] Y. C. Guo, H. K. Liu, and S. X. Dou, Physica C **200**, 147 (1992).
[10] J. Ma, C. Qutmann, R. J. Kelly *et al.*, Phys. Rev. B **51**, 3832 (1995).
[11] J. M. Harris, A. G. Loser, D. S. Marshall *et al.*, Phys. Rev. B **54**, 15665 (1996).
[12] H. Hancotte, R. Deltour, D. N. Davydov *et al.*, Phys. Rev. B **55**, R3410 (1997).
[13] D. Mihailovic, T. Mertelj, and K. A. Muller, Phys. Rev. B **57**, 9 (1998).
[14] Ch. Renner, B. Revaz, J.-Y. Genoud *et al.*, Phys. Rev. Lett. **80**, 149 (1998).
[15] A. P. Litvinchuk, C. Thompson, and M. Cardona, in *Physical Properties of High-Temperature Superconductors* (edited by D. M. Ginsberg), World Scientific, Singapore (1994).
[16] R. J. McQueeney, T. Egami, G. Shirane, and Y. Endoh, Phys. Rev. B **54**, R9689 (1996).
[17] L. Pintschovius and W. Reichardt, in *Physical Properties of High-Temperature Superconductors* (edited by D. M. Ginzberg), World Scientific, Singapore (1994).
[18] B. Renker, F. Compf, D. Ewert *et al.*, Z. Phys. B **77**, 65 (1989).
[19] P. P. Parshin, M. G. Zemlyanov, A. V. Irodova *et al.*, Fiz. Tverd. Tela (St. Petersburg) **38**, 1665 (1996) [Phys. Solid State **38**, 1665 (1996)].
[20] C. C. Homes, T. Timusk, D. A. Bonn *et al.*, Can. J. Phys. **73**, 663 (1995).

Translated by R. S. Wadhwa

LOW-DIMENSIONAL AND DISORDERED SYSTEMS

On spin wave scattering by a soliton in a two-dimensional isotropic ferromagnet

B. A. Ivanov and V. M. Muravyov

*Institute of Magnetism, National Academy of Sciences of the Ukraine, 252142 Kiev, Ukraine**

(Submitted January 4, 1998)
Fiz. Nizk. Temp. **24**, 672–676 (July 1998)

Scattering of magnons by a two-dimensional topological Belavin–Polyakov soliton in an isotropic ferromagnet is studied analytically. It is shown that the problem of spin wave scattering by a soliton with an arbitrary value of the topological charge ν can be analyzed completely in the longwave limit. General principles of the soliton–magnon interaction are studied, especially the relation between scattering and the behavior of the mode as the magnon wave vector $\mathbf{k}$ approaches zero. It is found that the scattering intensity has its maximum value for partial waves with the azimuthal number $m=0,\pm 1,\pm 2$ $(m=\nu-1)$. Although the mode with the maximum scattering always passes to a local mode for $k\to 0$ according to the general law, this fact is not crucial for the scattering intensity. In particular, the scattering intensity is stronger for a partial wave with $m=-1$ for $\nu=1$ (there is no local mode for $k\to 0$) than for a partial wave with $m=+1$ (a local mode exists for $k\to 0$). © *1998 American Institute of Physics.* [S1063-777X(98)01107-4]

1. It is well known that solitons play a special role in the thermodynamics of one- and two-dimensional ($1D$ and $2D$) nonlinear models of ordered media, including magnets. A systematic analysis of the thermodynamic quantities requires a knowledge not only of the structure of solitons, but also of the properties of magnon modes in the presence of a soliton. Local modes (LM), especially the zeroth modes, are quite important for constructing the soliton thermodynamics in the $1D$ case (see Refs. 1–3). For example, these modes determine the temperature dependence of the density of $1D$ solitons in soliton phenomenology.[4] Resonance in LM can be observed directly in experiments.[5,6] A number of exact solutions are known for $1D$ magnets, and solitons as well as magnon modes can be described against their background.

The situation is much more complicated in the two-dimensional case. As a rule, an analysis of solitons was carried out by using numerical methods. Studies of magnon modes against the background of soliton modes have only just begun. In this connection, it becomes especially important to analyze models for which analytical results can be obtained and general laws governing the soliton–magnon interaction can be determined.

For physically interesting models of $2D$ magnets, we are aware of only the exact solution obtained by Belavin and Polyakov[7] to describe a topological soliton in an isotropic ferromagnet (FM) whose energy can be presented in the form

$$W=A=\int (\nabla m)^2 dxdy, \tag{1}$$

where A is the exchange constant and $\mathbf{m}=\mathbf{M}/M_0$ is a unit vector defining the direction of the magnetization $\mathbf{M}$ ($M_0=|\mathbf{M}|$). In view of the gauge invariance of the model and the existence of self-duality equations, general static N-soliton solutions are also known for this model (see Refs. 7, 8 for details). The magnon spectrum in the presence of this soliton was studied in Ref. 9, where it was shown that a soliton with a topological charge ν possesses 2ν local magnon modes with zero frequency. These modes are limiting points of partial cylindrical waves with an azimuthal number $-\nu<m\leqslant\nu$ for $k\to 0$.

We shall show that for the Landau–Lifshitz equation (LLE) describing an FM with energy (1), the problem of scattering of a spin wave by a soliton can be analyzed completely in the long-wave approximation.

2. In order to analyze small oscillations of magnetization, it is convenient to introduce a rotating system of unit vectors $\mathbf{e}_1,\mathbf{e}_2,\mathbf{e}_3$, where $\mathbf{e}_3=\mathbf{e}_2\cos\theta+\sin\theta(\mathbf{e}_x\cos\varphi+\mathbf{e}_y\sin\varphi)$ coincides with $\mathbf{m}$ in a soliton, and $\mathbf{e}_2=-\mathbf{e}_x\sin\varphi+\mathbf{e}_y\cos\varphi$, $\mathbf{e}_1=[\mathbf{e}_1\times\mathbf{e}_3]$. Here, θ and φ are angular variables for $\mathbf{m}$. The soliton solution can be represented in an explicit form as follows:[7] $\tan(\theta/2)=(R/r)^{|\nu|}$, $\varphi=\nu\chi+\varphi_0$, where $\nu=\pm 1,\pm 2,\ldots$ is the topological charge, r and χ are polar coordinates in the FM plane, while the soliton radius R and φ_0 are arbitrary parameters. Linearizing the LLE in m_1 and m_2, we can represent the equation for spin waves against a soliton background in the form of a two-dimensional Schrödinger equation for the quantity $\psi=m_1+im_2$:

$$\left(-\nabla^2+\frac{\nu^2}{r^2}\cos 2\theta\right)\psi-2i\cos\theta\,\frac{\nu}{r^2}\frac{\partial\psi}{\partial\chi}+i\,\frac{2A}{\gamma M_0}\frac{\partial\psi}{\partial t}=0, \tag{2}$$

where γ is the gyromagnetic ratio. The solution of this equation has the form of a superposition of cylindrical waves:

$$\psi=\sum_{m=-\infty}^{m=\infty} F_m(r)\exp(im\chi-i\omega t), \tag{3}$$

where m is the azimuthal quantum number. The function $F_m(r)$ satisfies an equation having the form of a radial Schrödinger equation:

$$-\frac{1}{r}\frac{d}{dr}\left(r\,\frac{d}{dr}\right)F_m+\frac{1}{r^2}\,[m^2+2m\nu\,\cos\,\theta+\nu^2\,\cos 2\theta]$$
$$=F_m=k^2F_m,$$

$$k^2=\frac{\omega M_0}{2\gamma A}. \tag{4}$$

The ''potential'' in this equation is not low, but it can be analyzed quite comprehensively in the longwave limit $kR\ll 1$. For this purpose, we use the fact that for $\omega=0$ Eq. (4) possesses an exact solution:[9]

$$F_m^{(0)}=[\tan(\theta/2)]^{m/\nu}\,\sin\,\theta=(R/r)^{\sigma m}\,\sin\,\theta,$$

$$\sigma=\nu/|\nu|. \tag{5}$$

The existence of these exact solitons is associated with the restoration of the gauge invariance for $\omega\to 0$ and the validity of the self-duality equation characteristic of a static $2D$ LLE (see Ref. 9 for a detailed analysis of this problem).

An analysis of Eq. (5) reveals that for $r\to 0$ the solution $F_m^{(0)}(r)\propto(r/R)^{\nu-m}$ (for definiteness, we shall discuss in the following the case $\nu>0$; to analyze solitons with $\nu<0$, it is sufficient to replace m by $-m$). This means that for $m\leqslant\nu$, this solution does not have a singularity for $r\to 0$, and can be used for analyzing magnon modes in a soliton ($r\leqslant R$). Away from the soliton ($r\to\infty$), $F_m^{(0)}\propto(r/R)^{-(\nu+m)}$. For $\nu>-m$, the function $F_m^{(0)}$ decreases as we go away from the soliton. This at once leads to the existence of $2|\nu|$ zeroth modes with $-|\nu|<m\leqslant|\nu|$ localized in the vicinity of the soliton.[9]

The physical meaning of two such modes is obvious: for $m=1$, the function $F_1^{(0)}\propto\theta_0'$ and describes translational modes, i.e., the displacement of a soliton as a whole. The case $m=0$ corresponds to the variation of free soliton parameters φ_0 and R. As regards the remaining LM with $\omega=0$, which may exist for $\nu>1$, their emergence is associated with a high latent symmetry of the static LLE in model (1), i.e., with the fact that the general Belavin–Polyakov solution with the topological charge ν depends on 2ν free parameters (see Refs. 1–3, 8).

For $m<-\nu$, the function $F_m^{(0)}(r)$ decreases as $r\to\infty$. Hence it can be used only as an asymptotic solution for regions $r\leqslant R$. The case $m=-\nu$ is special since $F_{-\nu}^{(0)}\to$const as $r\to\infty$. It will be proved below that a singularity in the magnon scattering by a soliton exists in this case also.

For $m>\nu$, the solution $F_m^{(0)}$ has a singularity at zero and is not applicable for describing regions in the vicinity of the soliton center. In this case, we can use the second linearly independent solution (4) which can be easily represented for $k=0$ in the form

$$F_m^{(1)}=\sin\,\theta\left(\frac{r}{R}\right)^m\left[\frac{1}{m+\nu}\left(\frac{r}{R}\right)^{2\nu}+\frac{2}{m}+\frac{1}{m-\nu}\left(\frac{R}{r}\right)^{2\nu}\right]. \tag{6}$$

Thus, for $\omega=0$ (or $k=0$), we can construct at least one solution of the problem (4) that does not have a singularity at zero. For small but finite values of frequency, this solution can be used as an approximate solution in the region $r\ll 1/k$, when the term ψk^2 in (4) is small in comparison with terms containing $d^2\psi/dr^2$ or ψ/r^2. If, however, r is quite large (to be more precise, $r\gg R$), another simplification is possible: for $r\gg R$, the angle $\theta\to 0$ and (4) is transformed into the standard Bessel equation whose solution is well known:

$$F_m=J_n(kr)+\sigma_n(k)N_n(kr),\quad n=m+\nu, \tag{7}$$

where $J_n(x)$ and $N_n(x)$ are the Bessel and Neumann functions of the integral index n (the notation $n=m+\nu$ will be used at later stages also).

3. The quantity $\sigma_n(k)$ can be associated easily with the magnon scattering matrix. For this purpose, we must consider the asymptotic form of solution (7) at extremely large distances from the soliton (for $r\gg\max\{(1/k),R\}$) and compare it with the solution of the problem on free movement of magnons, i.e., on magnon states without a vortex.[10] To compare the solutions of this problem, it is convenient to introduce the variable $\tilde{\psi}=\psi\exp(i\nu\chi-i\omega t)$ which is transformed for $r\to\infty$ into $(m_x+im_y)\exp(-i\omega t)$ and describes a spin wave against the background of the homogeneous state $\mathbf{m}\|\mathbf{e}_z$. Taking formulas (3) and (7) into consideration, we can write the asymptotic form of the solution in terms of this variable for $r\gg R$ as follows:

$$\tilde{\psi}=\sum_{n=-\infty}^{n=\infty} C_n[J_n(kr)+\sigma_n(k)N_n(kr)]\exp(in\chi-i\omega t), \tag{8}$$

where C_n are arbitrary constants. Obviously, this expression for free motion must be valid for all r including $r=0$. In other words, free motion corresponds to $\sigma_n(k)=0$. In this case, for an appropriate choice of the constant C_n, we obtain the wave function for free motion $\psi\sim\exp(i\mathbf{k}\cdot\mathbf{r})$. On the other hand, for $\sigma_n(k)\neq 0$, the asymptotic form of ψ for $r\gg 1/k$ can be represented as

$$\tilde{\psi}=\sum_{n=-\infty}^{n=\infty} C_n[e^{-ikr}+S_n(k)e^{ikr}]\exp(in\chi-i\omega t), \tag{9}$$

where

$$S_n(k)=\frac{1-i\sigma_n(k)}{1+i\sigma_n(k)}. \tag{10}$$

The quantity $S_n(k)$ has the meaning of an element of the **S**-matrix for scattering of a partial wave with a given n.

4. Let us now calculate the scattering matrix in the longwave limit ($k\gg 1/R$). It was mentioned above that the functions (5) or (6) describe correctly the solution in the region $r\ll 1/k$. In other words, the solution in this region can be sought for small but finite values of k in the form

$$F_m(r)=F_m^{(0,1)}(r)[1+\alpha(r)], \tag{11}$$

where $F_m^{(0,1)}$ is one of the functions (5) or (6), $\alpha(r)\ll 1$. Substituting (11) into (4) and retaining terms with $k^2F_m^{(0)}$ or $\alpha(r)$ only, we obtain for $\alpha(r)$ an inhomogeneous equation

$$F^{(0)}\left[\frac{d^2\alpha}{dr^2}+\frac{1}{r}\frac{d\alpha}{dr}\right]+2\frac{d\alpha}{dr}\frac{dF^{(0)}}{dr}=k^2F^{(0)}. \tag{12}$$

The solution of this equation without a singularity at zero can be presented in the form

$$\alpha(r)=-k^2\int_0^r\frac{du}{u[F^{(0)}(u)]^2}\int_0^u v[F^{(0)}(v)]^2dv. \tag{13}$$

As $r\to 0$, the function $\alpha(r)\to 0$. Hence the above correction is obviously small for small values of r ($kr\ll 1$, but perhaps $r\sim R$). For large r, this function increases and for quite large r, when $kr\sim 1$, the quantity $\alpha(r)F_m^{(0)}$ cannot be treated as a small correction to $F_m^{(0)}$, and Eq. (12) is no longer applicable. However, this region is not significant for our problem, i.e., for determining the scattering amplitude for $kR\ll 1$. Indeed, over a wide range of values of r, for $R\ll r\ll 1/k$, we can use the asymptotic form (8) on one hand, assuming on the other hand that $\alpha(r)\ll 1$, and describe $\alpha(r)$ with the help of Eq. (13). Moreover, we can use for cylindrical functions in this region their asymptotic forms for small arguments $z=kr\ll 1$, $J_n(z)=(1/n!)(z/2)^nN_n(z)=-[(n-1)!/\pi](2/z)^n$, which simplifies the specific task of computing $\sigma_n(k)$.

5. Let us discuss some specific results. For a translational mode ($m=1$ or $n=\nu+1$), $\alpha(r)$ can be calculated exactly and the required asymptotic solution can be represented in the form

$$F_m=\left(\frac{R}{r}\right)\sin\theta\left[1-\frac{(kR)^2}{4\nu}\left(\frac{r}{R}\right)^2-\frac{(kR)^2}{4\nu(\nu+1)}\left(\frac{r}{R}\right)^{\nu+1}\right].$$

It can easily be seen that, for $R\ll r\ll 1/k$, the second term in the brackets is small in comparison with the other two terms. For $r\gg R$, we can write

$$F_m=\left(\frac{R}{r}\right)^{\nu+1}-\frac{(kR)^2}{4\nu(\nu+1)}\left(\frac{r}{R}\right)^{\nu+1}. \tag{14}$$

Using the asymptotic form of the cylindrical functions $J_n(z),N_n(z)$, we find that

$$\sigma(k)=\frac{\pi}{\nu!(\nu-1)!}\left(\frac{kR}{2}\right)^{2\nu} \tag{15}$$

for $m=1$, and the scattering intensity decreases for $k\to 0$ even more rapidly than for solitons with a large topological charge.

We can also carry out overall computations for any ν and $n=1$, i.e., for $m=-\nu+1$. In this case, computations are more cumbersome, and we shall directly present the result of calculations:

$$\sigma(k)=\frac{\pi}{2\ln(1/kR)}. \tag{16}$$

An analysis shows that for this mode the intensity of scattering of magnons is maximum, although $\sigma(k)\to 0$ as $k\to 0$, and $d\sigma(k)/dk$ diverges for small k. Such a behavior was detected during a numerical analysis of magnon scattering for $m=0$ by a magnetic vortex in an easy-plane antiferromagnet.[10]

For other values of ν and m, it is not possible to obtain general formulas for $\sigma(k)$. However, this problem can be solved for any specific values of ν and m after simple (albeit cumbersome at times) calculations.

We present below the results of calculations for $\nu=1,2,3$ and for certain values of m which cannot be described by general formulas (15) and (16).

For $\nu=1$ and $m=-1,-2$, we can write

$$\sigma_{-1}(k)=\pi(kR)^2\ln[1/(kR)],$$

$$\sigma_{-2}(k)=(\pi/4)(kR)^2\{1-(kR)^2\ln[1/(kR)]\}.$$

In the region of existence of quasilocal modes ($-\nu<m\leqslant\nu$), we can restore the general dependence

$$\sigma_m(k)\propto(kR)^{2(\nu+m-1)}. \tag{17}$$

In particular, for a soliton with $\nu=2$, the values of σ_m for certain values of m are defined by formulas $\sigma_0(k)=(kR)^2$, $\sigma_2(k)=(1/9)(kR/2)^6$. For $\nu=3$, we obtain

$$\sigma_{-1}(k)=3^{5/2}(kR/4)^2,\quad \sigma_0(k)=(3^{5/2}/8)(kR/2)^4,$$

$$\sigma_2(k)=2\times 3^{1/2}(kR/4)^8.$$

Together with formulas (15) and (16), which give the values of $\sigma(k)$ for $m=1$ and any ν, as well as the values of $\sigma(k)$ for $m=0,-1,-2$ and $\nu=1,2,3$, these results also lead to certain general conclusions concerning the nature of magnon scattering by a soliton.

It was found that the scattering intensity is not maximum for partial waves with the smallest $m=\pm 1,0$ (this assumption is also valid for magnetic vortices[10,11]).

The fact that the limiting point $k=0$ is a local mode for partial waves with a given m is not critical for scattering intensity. In particular, for a soliton with $\nu=1$, the scattering intensity of a partial wave with $m=-1$ (there is no local mode for $k\to 0$) is stronger than with $m=+1$ (a local mode exists for $k\to 0$). The only regularity is that the mode with the maximum scattering always passes into a local mode for $k\to 0$.

The third singularity lies in that for Belavin–Polyakov solitons there are no simple laws describing the connection of scattering intensities for $m=+|m|$ and $m=-|m|$. For magnon scattering by vortices in easy-plane magnets, such regularities were found by numerical analysis: $\sigma_m(k)=\sigma_{-m}(k)$ for antiferromagnets,[10] while for ferromagnets, the values of $\sigma_m(k)$ and $\sigma_{-m}(k)$ are obtained from each other by reversing the sign of the magnon frequency.[11]

The authors are indebted to D. D. Sheka for help and discussions, and to V. G. Bar'yakhtar, A. K. Kolezhuk, F. H. Mertens, H. J. Schnitzer, and G. M. Wysin for a discussion of the results. This research was partially supported by a grant (No. 2.4./27) from the Ukrainian State Foundation for Fundamental Research.

We are pleased to dedicate this publication to the jubilee of Prof. A. M. Kosevich, the author of fundamental works on the theory of magnetic solitons.

*E-mail: vbaryakhtar@gluk.apc.org

[1] A. M. Kosevich, B. A. Ivanov, and A. S. Kovalev, *Nonlinear Magnetization Waves. Dynamic and Topological Solitons* [in Russian], Naukova Dumka, Kiev (1983); A. M. Kosevich, B. A. Ivanov, and A. S. Kovalev, Phys. Rep. **194**, 117 (1990).
[2] H.-J. Mikeska and M. Steiner, Adv. Phys. **40**, 191 (1991).
[3] V. G. Bar'yakhtar and B. A. Ivanov, in *Soviet Science Reviews Sec. A—Physics* (edited by I. M. Khalatnikov), Vol. 61 (1992).
[4] J. R. Currie, J. A. Krumhansl, A. R. Bishop, and S. E. Trullinger, Phys. Rev. B **22**, 477 (1980).
[5] G. A. Kraftmakher, V. V. Meriakri, A. Ya. Chervonenkis, and V. I. Sheglov, Zh. Éksp. Teor. Fiz. **63**, 1353 (1972) [Sov. Phys. JETP **36**, 714 (1972)].
[6] J.-P. Boucher, G. Rius, and Y. Henry, Europhys. Lett. **4**, 1073 (1987).
[7] A. A. Belavin and A. M. Polyakov, JETP Lett. **22**, 245 (1975).
[8] A. M. Perelomov, Usp. Fiz. Nauk **134**, 557 (1981) [*sic*].
[9] B. A. Ivanov, JETP Lett. **61**, 917 (1995).
[10] B. A. Ivanov, A. K. Kolezhuk, and G. M. Wysin, Phys. Rev. Lett. **76**, 511 (1996).
[11] B. A. Ivanov, H. J. Schnitzer, F. H. Mertens, and G. M. Wysin, Phys. Rev. B (in press).

Translated by R. S. Wadhwa

Giant oscillations of the sound attenuation decrement in organic conductors in a magnetic field

O. V. Kirichenko and V. G. Peschansky

*B. Verkin Institute for Low Temperature Physics and Engineering, National Academy of Sciences of the Ukraine, 310164 Kharkov, Ukraine**

(Submitted February 24, 1998)
Fiz. Nizk. Temp. **24**, 677–682 (July 1998)

Attenuation of sound wave energy in low-dimensional organic conductors with several charge carrier groups is investigated theoretically. It is shown that the existence of a Fermi surface sheet in the form of a corrugated plane affects considerably the behavior of the sound attenuation rate Γ in a magnetic field $\mathbf{H}$. Giant oscillations of Γ as a function of $1/H$, which are not associated with quantization of charge carrier energy, are predicted. Oscillations with a period dependent on the wavelength of sound appear in a quantizing magnetic field in addition to the oscillations described by the Lifshitz–Kosevich formula. © *1998 American Institute of Physics.* [S1063-777X(98)01207-9]

Many organic conductors have a metal type conductivity, and their electron energy spectrum can be studied with the help of methods developed for metals. Independently of Onsager,[1] Lifshitz and Kosevich[2] formulated the inverse problem of reconstructing the electron energy spectrum by studying experimentally the magnetic susceptibility of metals at low temperatures in a strong magnetic field. Subsequently, other methods were also proposed for reconstructing the main characteristic of the spectrum (Fermi surface) by experimental investigation of galvanomagnetic effects[3] and propagation of electromagnetic and acoustic waves in a magnetic field.[4–7]

Organic conductors have a layered or filamental structure with a sharp anisotropy of the electrical conductivity resulting apparently from the sharp anisotropy of velocities at the Fermi surface. This considerably narrows the class of possible types of Fermi surface. The specific nature of low-dimensional electron energy spectrum leads to a large number of diverse effects which are not observed in ordinary metals. This simplifies considerably the solution of the inverse problem of reconstructing the energy spectrum of charge carriers.

From topological point of view, the simplest model of the Fermi surface of a quasi-two-dimensional conductor is a weakly corrugated cylinder, which is in good accord with the results of experimental studies of galvanomagnetic phenomena and Shubnikov–de Haas oscillations in some salts of tetrathiafulvalene.[8–13] However, the replacement of halogens in them by a more sophisticated complex of the type $MHg(SCN)_4$ where M is one of the metals from the group (K, Rb, Tl), leads to a quite complicated dependence of resistance on the magnetic field. According to the band calculations of the electron energy spectrum, the Fermi surface of the salts $(BEDT\text{-}TTF)_2MHg(SCN)_4$ consists of a weakly corrugated cylinder and weakly corrugated planes.[14–15] The authenticity of such a version for the spectrum of charge carriers can be verified by studying the attenuation of acoustic waves in such conductors.

Let us consider the propagation of acoustic waves in layered conductors placed in a magnetic field, whose electron energy spectrum consists of two bands with an energy–momentum relation

$$\varepsilon(\mathbf{p})=\sum_{n=0}^{\infty}\varepsilon_n(p_x,p_y)\cos\left(\frac{anp_z}{\hbar}\right); \tag{1}$$

$$\varepsilon'(\mathbf{p})=\sum_{n,m,q}^{\infty}A_{nmq}\cos\left(\frac{a_1np_x}{\hbar}\right)\cos\left(\frac{a_2mp_y}{\hbar}\right)\cos\left(\frac{aqp_z}{\hbar}\right). \tag{2}$$

The coefficients of cosines in formulas (1) and (2) decrease rapidly with increasing indices over which summation is carried out, and hence the maximum value of the function $\varepsilon_1(p_x,p_y)$ on the Fermi surface $\varepsilon(\mathbf{p})=\varepsilon_F$, which is equal to $\max\varepsilon_1(p_x,p_y)=\eta\varepsilon_F$, is much smaller than ε_F. The coefficients $A_{010}=\eta_1 U$ and $A_{001}=\eta U$ are much smaller than $A_{100}=U$, while all the remaining coefficients in (2) except A_{000} are assumed to be equal to zero in specific calculations. Such a choice of the dispersion relation for charge carriers takes into account a weak dependence of the charge carrier energy on the projection of the momentum $p_z=\mathbf{n}\cdot\mathbf{p}$ onto the normal $\mathbf{n}$ to the layers and the preferred motion of charge carriers with a quasi-one-dimensional spectrum (2) along the x-axis. In many layered organic conductors, the normal to the layers does not coincide with the symmetry axis of the crystal, and the arguments of cosines in formulas (1) and (2) must be supplemented by a phase taking into account the deviation of the axes p_x, p_y, p_z from the symmetry axes of the crystal. However, the results obtained by us did not change significantly when these phases or terms in formula (2) with higher indices of summation were taken into consideration.

The acoustic wave attenuation decrement in a conductor can be determined by solving the equation in the theory of elasticity

$$-\omega^2\rho u_i=\lambda_{ijlm}\frac{\partial u_{lm}}{\partial x_j}+F_i, \tag{3}$$

where ρ and λ_{ijlm} are the density and elastic moduli tensor of the crystal and u_{lm} is the deformation tensor. The force $\mathbf{F}$ acts on the crystal lattice from the side of the electron system excited by a spin wave which we shall assume to be monochromatic with a frequency ω.

The electric field $\mathbf{E}$ excited by an acoustic wave should be sought from the Maxwell equation

$$\text{curl curl }\mathbf{E}=\frac{4\pi i\omega}{c^2}\mathbf{j}+\left(\frac{\omega}{c}\right)^2\mathbf{E} \tag{4}$$

and the condition of electroneutrality of the conductor, which is equivalent to the condition of continuity of the electric current:

$$\text{div }\mathbf{j}=0. \tag{5}$$

The current density $\mathbf{j}$ and force $\mathbf{F}$ are determined by solving the kinetic equation for the distribution function $f_0\{\varepsilon(\mathbf{p})-\mathbf{p}\cdot\dot{\mathbf{u}}\}-\psi\partial f_0/\partial\varepsilon$, which can be presented in linear approximation in weak perturbation of the electron system of an acoustic wave in the form

$$\mathbf{v}\frac{\partial\psi}{\partial\mathbf{r}}+\frac{\partial\psi}{\partial t}+\left(\frac{1}{\tau}-i\omega\right)=g, \tag{6}$$

where e and $\mathbf{v}$ are the electron charge and velocity, t the duration of its motion in a magnetic field, c the velocity of light, and $g=-i\omega\Lambda_{ij}(\mathbf{p})u_{ij}+e\tilde{\mathbf{E}}\cdot\mathbf{v}$.

The collision integral, which vanishes as a result of the substitution of the equilibrium Fermi function $f_0\{\varepsilon(\mathbf{p})-\mathbf{p}\cdot\dot{\mathbf{u}}\}$ in a reference frame moving with the ion velocity $\dot{\mathbf{u}}$, is taken into account in the approximation of the mean free time τ of charge carriers, i.e., in the form of the operator of multiplication of the nonequilibrium correction $-\psi\partial f_0/\partial\varepsilon$ to the Fermi distribution function f_0 by the collision frequency $1/\tau$.

At quite low temperatures, when the temperature blurring of the Fermi distribution function of charge carriers is much smaller than the separation between their quantized levels in a magnetic field $\hbar\Omega$, the response of the electron system to the external perturbation should be sought by solving the quantum kinetic equation[16–20] or by using Kubo's method[21] ($\Omega=eH/m^*c$ is the rotational frequency of an electron around a closed orbit, and m^* is its cyclotron effective mass). We shall assume that the energy spectrum of charge carriers is not too close to two-dimensional, so that

$$\hbar\Omega/\varepsilon_F\ll\eta\ll1 \tag{7}$$

and the Fermi surface contains many electron states with quantized momentum projection p_H in the direction of the magnetic field. In this case, the semiclassical description of nonequilibrium processes is valid for the electron system, and the use of Boltzmann's kinetic equation (6) is fully justified for determining the acoustoelectron coefficients.

Perturbation of the conduction electrons of an acoustic wave is associated not only with the action of the electric field

$$\tilde{\mathbf{E}}=\mathbf{E}-\frac{i\omega}{c}[\mathbf{u}\times\mathbf{H}]+\frac{m\mathbf{u}\omega^2}{e} \tag{8}$$

on them in the reference frame associated with the vibrating lattice, but also with renormalization of the energy spectrum under the action of crystal deformation

$$\delta\varepsilon=\lambda_{ij}(\mathbf{p})u_{ij}. \tag{9}$$

The tensor components of the deformation potential $\lambda_{ij}(\mathbf{p})$ appear in the kinetic equation in which the number of charge carriers is preserved, i.e., in the form

$$\Lambda_{ik}(\mathbf{p})=\lambda_{ik}(\mathbf{p})-\langle\lambda_{ik}(\mathbf{p})\rangle/\langle1\rangle, \tag{10}$$

where angle brackets denote averaging over the Fermi surface and m is the free electron mass.

Using the solution of the kinetic equation (6), we obtain a relation connecting the current density

$$j_i=-\frac{2}{(2\pi\hbar)^3}\int ev_i\psi\frac{\partial f_0}{\partial\varepsilon}d^3p\equiv\langle ev_i\psi\rangle \tag{11}$$

and the force

$$F_i=\frac{1}{c}[\mathbf{j}\times\mathbf{H}]_i+\frac{m}{e}i\omega j_i+\frac{\partial}{\partial x_k}\langle\Lambda_{ik}\psi\rangle \tag{12}$$

with the displacement $\mathbf{u}$ of ions and the electric field $\tilde{\mathbf{E}}$.

Let an acoustic wave propagate in the plane of layers along the x-axis.

In Fourier representation, Eqs. (3)–(5) can be reduced to a system of linear algebraic equations for Fourier components of the displacement $\mathbf{u}(k)$ of ions and the electric field $\tilde{\mathbf{E}}(k)$. The condition for the existence of a nontrivial solution of this system of equations (equality of its determinant to zero) is the energy-momentum relation. The imaginary parts of the roots of this equation define the decrement of attenuation of an acoustic wave and an electromagnetic wave generated by it, while the real parts of these roots describe renormalizations of the wave velocities.

The solution of the kinetic equation in Fourier representation has the form

$$\psi=\int_{-\infty}^{t}dt'g(t')\exp\{ik[x(t')-x(t)]+\nu(t'-t)\}=\hat{R}g. \tag{13}$$

Formula (13) where $\nu=1/\tau-i\omega$, $g(t)=\omega\Lambda_{ji}(t)k_iu_j(k)+e\mathbf{v}(t)\cdot\tilde{\mathbf{E}}(k)$ can be used to present the fluxes characterizing the response of the electron system to the perturbation caused by sound in the following form:

$$j_i(k)=\sigma_{ij}(k)\tilde{E}_j(k)+a_{ij}(k)k\omega u_j(k), \tag{14}$$

$$\langle\Lambda_{ix}\psi(k)\rangle=b_{ij}(k)\tilde{E}_j(k)+c_{ij}(k)k\omega u_j(k), \tag{15}$$

where the Fourier transforms of the electrical conductivity $\sigma_{ij}(k)$ and acoustoelectronic tensors $a_{ij}(k)$, $b_{ij}(k)$, and $c_{ij}(k)$ are described by the expressions

$$\begin{aligned}&\sigma_{ij}(k)=\langle e^2v_i\hat{R}v_j\rangle;\quad a_{ij}(k)=\langle ev_i\hat{R}\Lambda_{jx}\rangle,\\&b_{ij}(k)=\langle e\Lambda_{ix}\hat{R}v_j\rangle;\quad c_{ij}(k)=\langle\Lambda_{ix}\hat{R}\Lambda_{jx}\rangle.\end{aligned} \tag{16}$$

The attenuation of acoustic waves is described by a root of the dispersion equation that is close to ω/s. Presenting it in the form

$$k=\frac{\omega}{s}+k_1 \tag{17}$$

and confining ourselves in the solution of the dispersion equation just to the main approximation in the small quantity k_1, we arrive at the following expression for the damping decrement Γ of a longitudinal acoustic wave:

$$\Gamma=\mathrm{Im}\ k_1=\mathrm{Im}\ \frac{ik^2}{2\rho s}\frac{1}{(1-\xi\tilde{\sigma}_{yy})}\left\{\xi(\tilde{a}_{yx}\tilde{b}_{xy}-\tilde{c}_{xx}\tilde{\sigma}_{yy})+\tilde{c}_{xx}-i(\tilde{a}_{yx}-\tilde{b}_{xy})\frac{H_z}{kc}+\tilde{\sigma}_{yy}\frac{H_z^2}{k^2c^2}\right\}\Bigg|_{k=\omega/s}. \tag{18}$$

Here,

$$\xi=\frac{4\pi i\omega}{k^2c^2-\omega^2},\quad \rho s^2=\lambda_{xxxx},$$

$$\tilde{\sigma}_{\alpha\beta}=\sigma_{\alpha\beta}-\frac{\sigma_{\alpha x}\sigma_{x\beta}}{\sigma_{xx}},\quad \tilde{a}_{\alpha j}=a_{\alpha j}-\frac{a_{xj}\sigma_{\alpha x}}{\sigma_{xx}},$$

$$\tilde{b}_{i\beta}=b_{i\beta}-\frac{b_{ix}\sigma_{x\beta}}{\sigma_{xx}},\quad \tilde{c}_{ij}=c_{ij}-\frac{b_{ix}a_{xj}}{\sigma_{xx}},\quad \alpha,\beta=y,z. \tag{19}$$

If the magnetic field $\mathbf{H}=(0,H\sin\theta,H\cos\theta)$ does not lie in the plane of the layers, i.e., if θ is not equal to $\pi/2$, the charge carriers with the quasi-two-dimensional energy–momentum relation (1) move along a closed orbit in a magnetic field. For magnetic fields in which the electron orbit radius r exceeds considerably the acoustic wavelength, but is much smaller than the electron mean free path l, the contributions from this group of electrons to the electrical conductivity tensor components and all acoustoelectronic coefficients oscillate upon a variation of the inverse magnetic field (Pippard effect[5]). If $kr\eta\ll 1$, the oscillations are formed practically by all charge carriers with a quasi-two-dimensional energy spectrum and the oscillation amplitude is comparable with the part of the acoustoelectronic coefficients varying smoothly with the magnetic field.

Conduction electrons with a quasi-one-dimensional energy spectrum respond weakly to the presence of a magnetic field, but their presence may considerably affect the dependence of the decrement of sound attenuation on magnetic field for $1\ll kr\ll kl$.

If the acoustic wave propagates along the x-axis, the asymptotic behavior of the decrement of sound attenuation remains the same as in the case of just one group of charge carriers with a quasi-two-dimensional energy spectrum, and the sound attenuation decrement experiences resonance oscillations upon a variation of the inverse magnetic field.

If the energy–momentum relation for quasi-two-dimensional conduction electrons has the form

$$\varepsilon(\mathbf{p})=\frac{p_x^2+p_y^2}{m}+\eta\frac{\hbar}{a}v_0\cos\left(\frac{ap_z}{\hbar}\right),\quad v_0=\frac{2\varepsilon_F}{m}, \tag{20}$$

and a strong magnetic field is directed at right angles to the layers along the z-axis, the following relation holds for the sound attenuation decrement for indefinitely small values of the parameter η_1^2:

$$\Gamma=\frac{Nm\omega v_0}{4\pi\rho s^2}\Omega\tau\ \mathrm{Re}\left[\frac{(\pi\gamma)^2+(kR\eta)^2/2+i\mu[1+\sin(2kr_0)]}{1-\sin(2kr_0)+(\pi\gamma)^2/2+(kR\eta)^2/2+1/2(3/4kr_0)^2+i\mu}\right]_{k=\omega/s}, \tag{21}$$

where $\mu=\pi v_0c^2\omega/2s^3\omega_0^2\Omega\tau$, ω_0 is the frequency of plasma oscillations, $r_0=v_0/\Omega$; $\Omega=eH/mc$; $R=2\hbar c/eHa$; and N is the number density of charge carriers.

If η_1 differs considerably from zero, the numerator and denominator of formula (21) acquire additional terms proportional to η_1^2.

However, upon a deviation of the acoustic wave vector from the preferred direction of the velocity of charge carriers with energy–momentum relation (2), their role in the acoustic wave attenuation increases sharply. This is due to the fact that the contribution of these electrons to electrical conductivity in a direction orthogonal to the wave vector increases with the angle φ between the vector $\mathbf{k}$ and the x-axis, thus causing a decrease in the resonance denominator. For $\varphi\gg(kr)^{-1/2}$, there will be no resonance if the number densities of both types of charge carriers are of the same order of magnitude. Instead of resonance, we now obtain giant oscillations of sound attenuation decrement which has the following form for $\varphi=\pi/2$:

$$\Gamma=\frac{Nm\omega v_0}{4\pi\rho s^2}\Omega\tau\left\{1+\sin(2kr_0)+\frac{(\pi\gamma)^2}{2}+\frac{(kR\eta)^2}{4}+\frac{7}{2}\frac{1}{(kr_0)^2}\right\}\Bigg|_{k=\omega/s}. \tag{22}$$

Instead of sharp peaks which are observed for $\varphi=0$ in the dependence of sound attenuation decrement on $1/H$ for $\sin(2kr_0)=1$, the peak of Γ for the same values of $2kr_0$ is attained upon a smooth variation of the magnetic field. The asymptotic behavior of the sound attenuation decrement (22) in magnetic fields satisfying the condition $1\ll kr\ll 1/\eta$ remains unchanged for an arbitrary quasi-two-dimensional electron energy spectrum also, and only numerical factors of the order of unity in the last three terms are sensitive to the type of energy–momentum relation for charge carriers.

In high-purity conductors with $kl\eta\gg 1$, a decrease in the magnetic field for any orientation of the acoustic wave vector leads to a replacement of the resonance and giant oscillations of Γ by Pippard oscillations for $kr\eta\gg 1$, their amplitude be-

ing $(kr\eta)^{1/2}$ times smaller than the part of Γ varying smoothly with magnetic field.

At low temperatures, when energy quantization of charge carriers in a magnetic field is significant, the quantum oscillations described by the Lifshitz–Kosevich formula[2]

$$\frac{\Gamma_{\rm osc}}{\Gamma_{\rm mon}}=\sum_{n=1}^{\infty}\psi(n\xi)\left(\frac{\hbar\Omega}{n\varepsilon_F\eta}\right)^{1/2}\cos\left(\frac{ncS_0}{eH\hbar}+\frac{\pi}{4}\right)\cos\frac{\pi nm}{m^*}, \tag{23}$$

are supplemented by quantum oscillations of the sound attenuation decrement with a phase shift of $2kr_0$ and a period

$$\Delta\left(\frac{1}{H}\right)=\frac{2\pi\hbar e}{cS_0(1\pm k\lambda_B)}, \tag{24}$$

differing from the period of oscillations defined in (23) by a small amount $k\lambda_B$, equal to the ratio of the de Broglie wavelength of an electron to the acoustic wavelength.

Here, S_0 is the extremal area of cross-section of a corrugated cylinder by the plane $p_H=\text{const}$; $\psi(\xi)=\xi/\sinh\xi$; and $\xi=2\pi^2\Theta/\hbar\Omega$, where Θ is the temperature of blurring of the Fermi function of distribution of conduction electrons, i.e., temperature in energy units.

For $\Theta\ll\hbar\Omega$, the acoustic wave energy is absorbed mainly by charge carriers with an energy–momentum relation (2), for which states at the Fermi surface with a drift velocity along **k** equal to the velocity of sound are allowed for almost any value of the magnetic field. For electrons in closed orbits, the momentum projection p_H assumes discrete values, and the absorption of an acoustic phonon having an energy $\hbar\omega$ by a charge carrier with a drift velocity $\overline{v_x}\cos\alpha=s$ is possible only for certain values H_n of the magnetic field (α is the angle between the vectors **k** and **H**). For $H=H_n$, this leads to the emergence of sharp absorption peaks of acoustic wave energy at the instants when conduction electrons with a quasi-two-dimensional energy spectrum participate in this process.

Thus, in the case of existence of a Fermi surface sheet in the form of a corrugated plane, quantum oscillations predicted by Gurevich *et al.*[7] occur against the background of a smooth dependence of Γ on $1/H$.

The authors are indebted to A. M. Kosevich for fruitful discussions of the obtained results. We also take the opportunity to congratulate him on his jubilee and wish him sound health and creative achievements. This research was partially financed by the Ukrainian Ministry of Science (Grant No. 2.4/192).

*E-mail: peschansky@ilt.kharkov.ua

[1] L. Onsager, Philos. Mag. **43**, 1006 (1952).
[2] I. M. Lifshitz and A. M. Kosevich, Zh. Éksp. Teor. Fiz. **29**, 730 (1955) [Sov. Phys. JETP **2**, 636 (1955)].
[3] I. M. Lifshitz and V. G. Peschansky, Zh. Éksp. Teor. Fiz. **35**, 1251 (1958) [Sov. Phys. JETP **8**, 875 (1958)].
[4] M. Ya. Azbel' and E. A. Kaner, Zh. Éksp. Teor. Fiz. **33**, 896 (1957) [Sov. Phys. JETP **6**, 730 (1957)].
[5] A. B. Pippard, Philos. Mag. **2**, 1147 (1957).
[6] E. A. Kaner, V. G. Peschansky, and I. A. Privorotskii, Zh. Éksp. Teor. Fiz. **40**, 214 (1961) [Sov. Phys. JETP **13**, 147 (1961)].
[7] V. L. Gurevich, V. G. Skobov, and Yu. A. Firsov, Zh. Éksp. Teor. Fiz. **40**, 786 (1961) [Sov. Phys. JETP **13**, 552 (1961)].
[8] M. V. Kartsovnik, V. N. Laukhin, V. I. Nizhankovskii, and A. A. Ignat'ev, Pis'ma Zh. Éksp. Teor. Fiz. **47**, 302 (1988) [JETP Lett. **47**, 363 (1988)].
[9] M. V. Kartsovnik, P. A. Kononovich, V. N. Laukhin, and I. F. Shchegolev, Pis'ma Zh. Éksp. Teor. Fiz. **48**, 498 (1988) [JETP Lett. **48**, 541 (1988)].
[10] N. Tojota, T. Sasaki, K. Murata *et al.*, J. Phys. Soc. Jpn. **57**, 2616 (1988).
[11] W. Kang, G. Montambaux, J. R. Cooper *et al.*, Phys. Rev. Lett. **62**, 2559 (1989).
[12] M. V. Kartsovnik, P. A. Kononovich, V. N. Laukhin *et al.*, Zh. Éksp. Teor. Fiz. **97**, 1305 (1990) [Sov. Phys. JETP **70**, 735 (1990)].
[13] R. Jagi, Y. Iye, T. Osada, and S. Kagoshima, J. Phys. Soc. Jpn. **59**, 3069 (1990).
[14] R. Rossenau, M. L. Doublet, E. Canadell *et al.*, J. Phys. (France) **6**, 1527 (1996).
[15] T. Sasaki, H. Ozawa, H. Mori *et al.*, J. Phys. Soc. Jpn. **65**, 213 (1996).
[16] I. M. Lifshitz, Zh. Éksp. Teor. Fiz. **32**, 1509 (1957) [Sov. Phys. JETP **5**, 1227 (1957)].
[17] I. M. Lifshitz, J. Phys. Chem. Solids **4**, 11 (1958).
[18] E. N. Adams and T. D. Holstein, J. Phys. Chem. Solids **10**, 254 (1959).
[19] A. M. Kosevich and V. V. Andreev, Zh. Éksp. Teor. Fiz. **38**, 882 (1960) [Sov. Phys. JETP **11**, 637 (1960)].
[20] A. M. Kosevich and V. V. Andreev, Zh. Éksp. Teor. Fiz. **43**, 1061 (1962) [Sov. Phys. JETP **16**, 750 (1963)].
[21] R. Kubo, J. Phys. Soc. Jpn. **12**, 570 (1957).

Translated by R. S. Wadhwa

PHYSICAL PROPERTIES OF CRYOCRYSTALS

Broken symmetry phase transition in solid HD: a manifestation of quantum orientational melting

Yu. A. Freiman and S. M. Tretyak

*B. Verkin Institute for Low Temperature Physics and Engineering, 47 Lenin Ave., 310164 Kharkov, Ukraine**

A. Jeżowski

*Trzebiatowski Institute for Low Temperatures and Structure Research, Polish Academy of Sciences, P.O. Box 937, 50-950 Wroclaw 2, Poland***

R. J. Hemley

*Geophysical Laboratory and Center for High Pressure Research, Carnegie Institution of Washington, 5251 Broad Branch Road, NW Washington, DC 20015, USA****

(Submitted March 19, 1998)
Fiz. Nizk. Temp. **24**, 683–688 (July 1998)

Theoretical study of the broken symmetry phase (BSP) transition line in solid HD reveals that its anomalous features provide evidence for quantum orientational melting. The observations of unusual reentrant behavior is a consequence of the symmetry properties of the system, namely, the fact that in HD all rotational states and transitions between them are allowed, in contrast to the behavior of the homonuclear isotopes H_2 and D_2. The systematic underestimation of the transition pressure characteristic of all theories of the BSP transition can be removed if crystal-field effects are taken into account. [S1063-777X(98)01307-3]

1. INTRODUCTION

The large isotopic family of hydrogens (H_2, HD, D_2, HT, DT, T_2) presents a unique possibility for studying the diversity of quantum isotopic effects.[1] The differences in properties of the isotopic substances cannot be, as a rule, related solely to the de Boer quantum parameter, and symmetry-related nuclear-spin effects turn out to be far more essential. Due to symmetry requirements, hydrogen and deuterium have two species: para-H_2 and ortho-D_2 correspond to the even rotational quantum number J, whereas ortho-H_2 and para-D_2 correspond to odd J states. In the case of HD molecules, the nuclei are distinguishable and the molecules do not possess a center of inversion. As a result, the HD molecules do not have ortho-para species and all angular momentum states $J=0,1,2,...$ and transitions between all of them are allowed.

To a very good approximation, the electron density distributions in the H_2 and HD molecules are the same. But in the HD molecule the center-of-charge does not coincide with the center-of-mass. Since the molecule rotates around its center-of-mass but the intermolecular interactions are related to the center-of-charge, rotations of the molecules are accompanied by translational displacements of the center-of-mass. Thus, the rotation and translation of the molecule are coupled dynamically. As a result of such off-center rotation, an additional Heisenberg-like term appears in the anisotropic part of the intermolecular potential, as first has been shown by van Kranendonk.[2] Evidence for differences in properties of asymmetric and symmetric hydrogens, which are a consequence of the coupling of the rotation and translation of the molecule in the condensed state, has been reported since the sixties.[3] A large negative deviation of the c/a ratio from the ideal hcp value of $\sqrt{8/3}$ found by Prokhvatilov *et al.*[4] for HD at zero pressure by x-ray diffraction was attributed by the authors to features of the intermolecular interaction of HD molecules. Subsequent calculations by Strzhemechny[5] support this conclusion.

But the most striking differences between the homonuclear hydrogens (H_2 and D_2) and HD are evident by properties of the solids under very high pressures. At low pressure, the free rotor quantum numbers JM remain good quantum numbers for molecules in solid H_2 and D_2, and at low temperatures only lowest states $J=0$ in the even J species are occupied. Since the $J=0$ state has a spherically symmetric spatial distribution, there is no orientational order in p-H_2 and o-D_2 at low pressures down to $T=0$ K. The intermolecular interaction admixes the higher rotational states into the ground state wave function, but this admixture is too small to produce the ordering at zero pressure. With increasing pressure, the anisotropic intermolecular interaction increases, and admixtures of higher rotational states into the ground state wave function become more appreciable, eventually resulting in the transition into a phase characterized by orientational order. This transition has been called the broken

symmetry phase (BSP) transition. This transition was foretold by Raich and Etters in 1972 [Ref. 6] and found experimentally by Silvera and Wijngaarden in 1981 in o-D_2[7] and then by Lorenzana, Silvera and Goettel in 1989 in p-H_2.[8] Moshary, Chen and Silvera[9] experimentally studied the BSP transition in HD and reported evidence for a non-monotonic phase line (i.e., a P-T minimum and thus reentrant behavior) that contrasted markedly with that found for p-H_2 and o-D_2.

The BSP transition in HD was found at 68.3 GPa and 3 K, which gave by extrapolating the temperature dependence a transition pressure $P_{\rm tr}$ at $T=0$ K of $P_0 \approx 69.0$ (± 2) GPa. The minimum point was located at $P_m \approx 53$ GPa and $T_m \approx 30$ K or in reduced units at $T_m/B \approx 1/2$ (B is the rotational constant). The disordered phase is reentrant, that is, for fixed pressure in the range between P_m and P_0, as temperature is increased, the solid goes from a disordered to an ordered and then to a disordered phase once again. The slope of the orientational melting curve $dP_{\rm tr}/dT$ is negative at temperatures less than T_m and positive at $T > T_m$. At $T \approx 65$ K $(T/B \approx 1)$ the transition pressure becomes equal to P_0. Above this temperature, the studied portion of the transition curve is approximately linear with temperature.

The peculiar features of HD responsible for the remarkable behavior of its BSP transition line and the nature of the transition itself are thus of obvious interest. Two different mechanisms have been proposed in the literature. One of them, called quantum orientational melting,[10,11] was studied for the model system of all-J quantum rotors before the phase transition in HD was found experimentally. A different approach to the problem was proposed by Strzhemechny.[5] According to the latter model, the mechanism of the pressure-driven orientational ordering in solid HD is completely different from that in H_2 and D_2, and is related to the creation of a single delocalized $J=1$ state that is a direct analog of the zero-point vacancy waves in quantum crystals. Thus, this mechanism is directly tied with the Heisenberg-like term in the intermolecular potential that is specific to HD and its off-center rotation.

The BSP transition has attracted considerable interest from both experiment and theory for many years (see, for example,[1,12–14] and references therein). The main efforts in theory have been made either to calculate the transition pressure at zero temperature[15–20] or to predict the lattice structure for the BS phase.[21–26] After the BSP transition was found experimentally, it became clear that the critical densities determined in the first theoretical studies[6,15,16] were considerably underestimated relative to experiment. In more recent work, several basic assumptions and simplifications of these early treatments have been subjected to careful analysis, and attempts were made to go beyond the most questionable approximations. One of the most significant approximations is the mean field (MF) approximation. The effect of correlations neglected in the MF approximation was taken into account (in different ways) by Lagendijk and Silvera[18] and by Sprik and Klein,[19] the effect of translation-rotation coupling was studied by Janssen and van der Avoird,[20] and the consequences of different forms of the intermolecular potential were tested by Aviram *et al.*[17] Though a number of important results emerged from these studies, only small changes were found in the predicted transition pressure. It was suggested[20] that many-body effects are responsible for the systematic underestimation of the transition pressure. In the present paper, we propose a new approach to this problem. It is shown that the main discrepancy between theory and experiment can be removed even in the MF approximation if crystal field effects are taken into account.

Another problem that has been intensively studied in the context of the BSP transition is the question of the structure of the BS phase. In early theoretical studies,[6,15,17,18] the structure assumed to be $Pa3$ α-nitrogen structure. The crystal structure of the high-temperature phase to 120 GPa (phase I) was found to be hcp,[21] but the structure of the BS is still unknown. Recent theoretical search for the lowest-energy structure of the BS phase based on the local density approximation[22–24] and *ab initio* molecular dynamics simulations[25,26] suggest a four-molecular orthorhombic structure of $Pca2_1$ symmetry. On the other hand, recent spectroscopic data do not rule out $Pa3$, at least for p-H_2.[27]

In the present paper the phase diagram of solid HD has been calculated. We show that quantum orientational melting can readily account for the unusual features of the BSP transition in this system. The behavior of the phase transition line in solid HD as compared with H_2 and D_2 is a consequence of the symmetry properties of the system, namely of the fact that in HD transitions between all the rotational states are allowed in contrast to H_2 and D_2.

2. BASIC EQUATIONS

In the MF approximation, the Hamiltonian of the system of linear rotors interacting via quasiquadrupolar forces can be written in the following form:[28]

$$\mathscr{H} = BL^2 - (U_0\eta + U_1)Y_{20} + U_0\eta^2/2, \tag{1}$$

where L is the operator of angular momentum; U_0 and U_1 are molecular and crystal field constants; B is the rotational constant; $\eta = \sqrt{4\pi/5}\langle Y_{20}\rangle$ is the order parameter; and $\langle ... \rangle$ denotes thermodynamic averaging with the Hamiltonian [Eq. (1)].

The MF constant

$$U_0 = -\sum_{ff'}\sum_{\alpha\beta\gamma\delta} V_{ff'}^{\alpha\beta\gamma\delta} Q_f^{\alpha\beta} Q_{f'}^{\gamma\delta}, \tag{2}$$

where $V_{ff'}^{\alpha\beta\gamma\delta}$ is the interaction matrix, defined by the parameters of the intermolecular potential and by the lattice parameters; $Q_f^{\alpha\beta} = \Omega_\alpha \Omega_\beta - (1/3)\delta_{\alpha\beta}$, f numbers the lattice sites; Ω is a unit vector along the equilibrium orientation of the molecule in the site f.

While the molecular field is generated by the coupling terms in the intermolecular interaction potential, the crystal-field term[2]

$$U_1 = -\frac{4\pi}{5}\sum_{\delta} B(R_\delta) Y_{20}(\Omega_\delta) \tag{3}$$

originates from single-molecular terms in the intermolecular potential. Here $B(R_\delta)$ is the radial function characterizing

the anisotropic pair potential;[2] $\mathbf{R}_\delta$ is the radius-vector of the nearest neighbors, $\Omega_\delta = \mathbf{R}_\delta / R_\delta$, and δ are indices of the nearest neighbors.

The orientational state of the system is determined by values and signs of the molecular and crystal constants, and can be described by positive and negative order parameters. In the case of α-N_2 and the low-temperature phase of o-H_2, $U_0 > 0$ and $U_1 = 0$ (more precisely, the second-degree term is zero, but higher-degree terms do exist); for β-O_2, $U_0 < 0$ and $U_1 > |U_0|$ and the order parameter is positive. For γ-O_2, both molecular and crystal field constants are negative, a negative order parameter describes precession of disc-like molecules. The states with the negative order parameter can be treated as the orientational analog of the easy-plane-type ordering in magnets.

As shown in Ref. 28, even very small crystal fields can substantially change the behavior of the system. For positive U_1, the main difference with the case of $U_1 = 0$ lies in the fact that the orientational phase transitions, instead of separating orientationally ordered and disordered states having generally speaking different symmetry, separate more and less ordered states of the same symmetry. Thus, these phase transitions are of the order-order type.

The most characteristic feature of the system at negative values of the crystal field (compared with that at $U_1 = 0$) is that states with a negative order parameter can exist as thermodynamically stable states of the system along with the states having a positive order parameter. The phase transitions occurring in the system at negative crystal fields are the transitions between two different ordered states, the easy-axis orientational states with the positive order parameter and the easy-plane orientational states with $\eta < 0$.

In principle, the crystal-field term can be deduced from Eq. (3). It is proportional to a product of such quantities as $\xi_c = c/a - \sqrt{8/3}$, the deviation of c/a from the ideal hcp value; $\xi_m = b/a - \sqrt{3}$, the deviation of b/a from the ideal hcp value in the case of the monoclinic distortion, and $P_2(\cos\theta_0) = (3/2)\cos^2\theta_0 - 1/2$, where θ_0 is the polar angle of the central molecule with respect to the c-axis. None of these quantities are known to sufficient accuracy either from experiment or theory. That is why the reduced crystal field will be treated in the present study as a parameter of theory.

3. RESULTS AND DISCUSSION

To find the phase diagram of the system of rotors described by the Hamiltonian [Eq. (1)], we used the same computational scheme as in Refs. 10 and 11. First, the energy spectrum of the linear rotors in the field VY_{20} was calculated, where $V = -(U_0\eta + U_1)$. We used the basis of spherical functions Y_{lm} in which the kinetic energy operator L^2 is diagonal. The basis set was restricted to $l = 7$, which, within the studied range of V, ensures sufficient accuracy of calculations for lower levels of the system. Making use of the spectrum obtained, we have calculated the free energy F as a function of the order parameter and of the temperature at given values of the molecular field and crystal field constants U_0 and U_1. Then we found the temperature dependence of the order parameter from the condition that the free energy of the system is a minimum ($dF/d\eta = 0$). Data on the variation of the order parameter with temperature and molecular field constant U_0 allow us to obtain the phase transition line for the given value of the crystal field constant in the coordinates $U_0 - T$. The locus of equation $d\eta/dT = \infty$ for different U_0 is the curve of absolute instability of the orientationally ordered phase. The locus of equation $F(\eta_{tr}) = F(\eta = 0)$ for different U_0 is the curve of the thermodynamically equilibrium transitions (η_{tr} is the value of the order parameter for which the free energy of the ordered phase becomes equal to the free energy of the disordered phase).

Using van Kranendonk's analytical representation[1,2] of the short-range valence potential of Ree and Bender,[29] we have calculated the molecular field constant U_0 as a function of relative compression R_0/R, where R_0 and R are the nearest neighbor distances at zero pressure and pressure P, respectively. It was assumed that the BS phase in solid HD has the same supposedly lowest energy structure $Pca2_1$ as was predicted for solid H_2.[22–26] Finally, to map the BSP transition line into P-T space, we must use the pressure-volume equation of state. Although no P-V experimental data have been reported for solid HD at these pressures, isotopic differences (at least between H_2 and D_2) in the megabar range are very small. Thus, we use the recent x-ray pressure-volume equation of state for H_2 and D_2 measured by Loubeyre *et al.*[21] (Vinet functional form).

As expected, the phase transition pressure calculated under the assumption of zero crystal field underestimates the experimental value by a factor of four. As shown in our study of the model system given by the Hamiltonian [(Eq. (1)],[28] negative values for the crystal field shift the phase transition line upward to higher pressures. Figure 1a, shows a set of theoretical curves that give the best agreement with the experimental data from Ref. 9. These curves correspond to reduced crystal fields U_1/U_0 of -0.13, -0.14, and -0.15. The theory succeeds in reproducing the distinguishing feature of the HD phase transition line, i.e., the nonmonotonicity of the curve and a correct position of the minimum. The steeper temperature dependence characteristic of the experimental data is principally due to the effect of orientational correlations, and in part to the Heisenberg-like term in the HD-HD intermolecular potential omitted in this study.

In the present paper we consider the crystal field as a parameter in the theory, and thus the question exists as to the value and the sign of this parameter required to gain agreement between theory and experiment. As follows from the analysis of Eq. (3), the negative sign of the crystal field is definite, and the values given above correspond to the value of $\xi_c = c/a - \sqrt{8/3}$, the deviation of c/a from the ideal hcp value, which was found in the recent x-ray high-pressure study.[21] A detailed analysis of this point will be given elsewhere. Here we would like to point out that the deformation of the lattice that gives rise to the negative crystal field as a response of the lattice to the applied pressure is in accord with the general Le–Chatelier–Braun principle.

As one can see, the BSP transition line in solid HD is similar to the P-T melting curve of ^{3}He (Fig. 1b). It is established that the presence of the minimum in the ^{3}He melt-

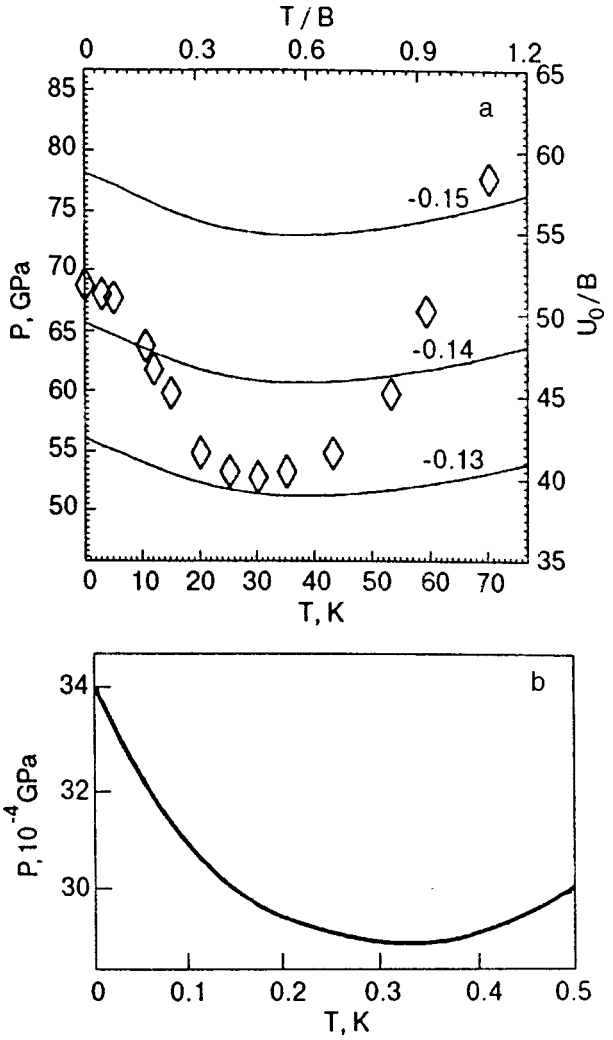

FIG. 1. Broken phase transition line in solid HD. Symbols:experimental data by Moshary, Chen, and Silvera.[9] Solid curves: present theory. Different curves are labeled by values of the reduced crystal field (a). Melting curve in ^{3}He (b).

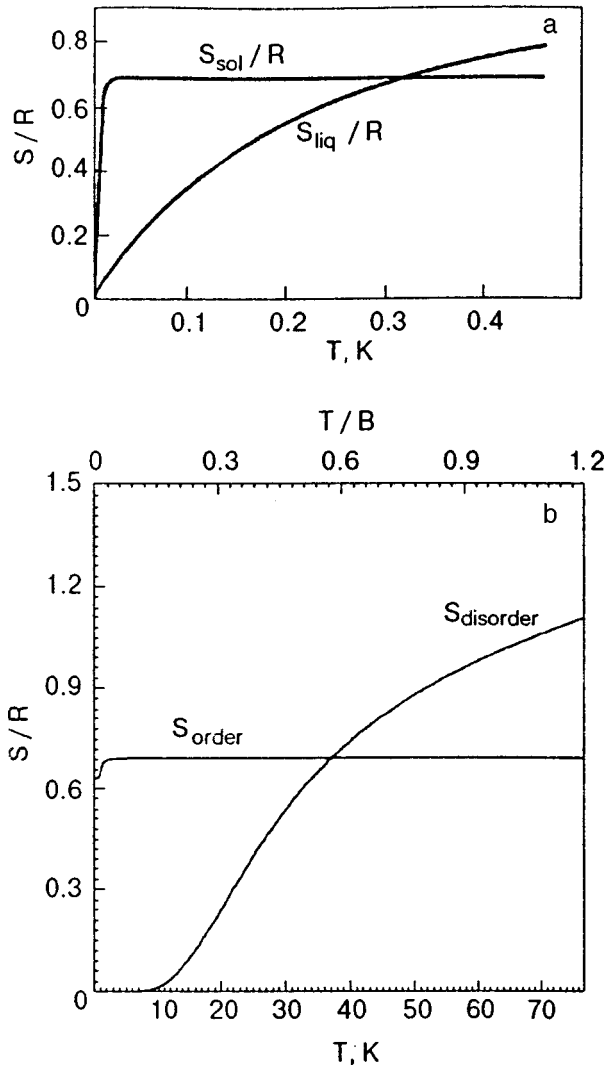

FIG. 2. Entropies of liquid and solid ^{3}He (a) and ordered and disordered phases of solid HD (b).

ing curve stems from the fact that the entropy of the solid phase exceeds the entropy of the liquid at low temperatures, where the thermal properties of the condensed phases are dominated by spin properties. Liquid ^{3}He obeys Fermi statistics, with the entropy proportional to the temperature. On the other hand, the entropy of solid ^{3}He is that of weakly interacting spin 1/2 nuclei; that is, the entropy of solid ^{3}He is independent of temperature and equals to R ln 2 (Fig. 2a). In this temperature region, the entropy contribution to the free energy is an additional factor that stabilizes the solid phase.

A similar situation occurs in the case of the system of rotors. The molecular field gives a doublet-shape ground state of the system; this provides an extra contribution to the entropy of the ordered phase, which is equal to R ln 2. As a result, in the low-temperature region the entropy of the orientationally ordered phase is larger than that of the disordered phase (Fig. 2b). Similar to the case of ^{3}He, this is an additional factor that stabilizes the ordered phase. Above the point of intersection, the situation becomes ''normal'' and the entropy factor stabilizes the disordered phase.

4. CONCLUSIONS

The broken symmetry phase transition line in solid HD has been shown to be an example of quantum orientational melting. The unusual behavior of the phase transition line (i.e., its P-T minimum) is a consequence of the symmetry properties of the system, namely, the fact that in HD all rotational states and transitions between them are allowed, in contrast to homonuclear isotopes H_2 and D_2. The systematic underestimation of the transition pressure characteristic of all theories of the BSP transition can be removed if crystal-field effects are taken into account. It was suggested that the effect of orientational correlations, and specifically for HD, the Heisenberg-like term in the intermolecular potential, should be taken into account to obtain quantitative agreement between theory and experiment.

ACKNOWLEDGMENTS

This research was supported by the NSF (DMR-9624050). The authors dedicate this work to Prof. Yu. Kagan on the occasion of his 70th birthday.

*E-mail: freiman@ilt.kharkov.ua
**E-mail: an–je@int.pan.wroc.pl
***E-mail: hemley@gl.ciw.edu

[1] V. G. Manzhelii and M. A. Strzhemechny, in *Physics of Cryocrystals*, V. G. Manzhelii and Yu. A. Freiman (Eds.), AIP Press, Woodbury, New York (1997).
[2] J. van Kranendonk, *Solid Hydrogen*, Plenum Press, New York–London (1982).
[3] J. Bigeleisen, J. Chem. Phys. **39**, 769 (1963).
[4] A. I. Prokhvatilov, M. A. Strzhemechny, and G. N. Shcherbakov, Fiz. Nizk. Temp. **19**, 622 (1993) [Low Temp. Phys. **19**, 445 (1993)].
[5] M. A. Strzhemechny, Fiz. Nizk. Temp. **22**, 130 (1996) [Low Temp. Phys. **22**, 92 (1996)].
[6] J. C. Raich and R. D. Etters, J. Low Temp. Phys. **6**, 229 (1972).
[7] I. F. Silvera and R. J. Wijngaarden, Phys. Rev. Lett. **47**, 39 (1981).
[8] H. E. Lorenzana, I. F. Silvera, and K. A. Goettel, Phys. Rev. Lett. **64**, 1939 (1990).
[9] F. Moshary, N. H. Chen, and I. F. Silvera, Phys. Rev. Lett. **71**, 3814 (1993).
[10] Yu. A. Freiman, V. V. Sumarokov, A. P. Brodyanskii, and A. Jeżowski, J. Phys. Condens. Matter **3**, 3855 (1991).
[11] A. P. Brodyanskii, V. V. Sumarokov, Yu. A. Freiman, and A. Jeżowski, Fiz. Nizk. Temp. **19**, 520 (1993) [Low Temp. Phys. **19**, 368 (1993)].
[12] Ho-kwang Mao and R. J. Hemley, Rev. Mod. Phys. **66**, 671 (1994).
[13] R. J. Hemley, A. F. Goncharov, H. K. Mao, E. Karmon, and J. H. Eggert, J. Low Temp. Phys. **110**, 75 (1998).
[14] N. H. Chen, E. Sterer, and I. F. Silvera, Phys. Rev. Lett. **76**, 1663 (1996).
[15] W. England, J. C. Raich, and R. D. Etters, J. Low Temp. Phys. **22**, 213 (1976).
[16] J. Felsteiner and Z. Friedman, Phys. Rev. B **8**, 3996 (1973).
[17] I. Aviram, S. Goshen, and R. Thieberger, J. Low Temp. Phys. **38**, 371 (1980); *ibid.* **43**, 549 (1981); *ibid.* **52**, 397 (1983); *ibid.* **55**, 349 (1984); Phys. Lett. **88A**, 410 (1982); J. Chem. Phys. **80**, 5337 (1984).
[18] Ad Lagendijk and I. F. Silvera, Phys. Lett. **84A**, 28 (1981).
[19] M. Sprik and M. L. Klein, J. Chem. Phys. **81**, 6207 (1984).
[20] W. B. J. M. Janssen and A. van der Avoird, Phys. Rev. B **42**, 838 (1990).
[21] P. Loubeyre, R. LeToullec, D. Hausermann, M. Hanfland, R. J. Hemley, H. K. Mao, and L. W. Finger, Nature (London) **383**, 702 (1996).
[22] H. Nagara and T. Nakamura, Phys. Rev. Lett. **68**, 2468 (1992).
[23] H. Chacham, L. M. Falikov, and B. Koiller, Phys. Rev. B **50**, 7195 (1994).
[24] K. Nagao, H. Nagara, and S. Matsubara, Phys. Rev. B **56**, 2295 (1997).
[25] M. P. Surh, K. J. Runge, T. W. Barbee III, E. L. Pollock, and C. Mailhiot, Phys. Rev. B **55**, 11330 (1997).
[26] J. Kohanoff, S. Scandolo, G. L. Chiarotti, and E. Tosatti, Phys. Rev. Lett. **78**, 2783 (1997).
[27] A. F. Goncharov, R. J. Hemley, H. K. Mao, and J. Shu, Phys. Rev. Lett. **80**, 101 (1998).
[28] Yu. A. Freiman, S. Tretyak, and A. Jeżowski, J. Low Temp. Phys. **110**, 147 (1998).
[29] F. H. Ree and C. F. Bender, J. Chem. Phys. **71**, 5362 (1979).

This article was published in English in the original Russian journal. It was edited by R. T. Beyer.

LATTICE DYNAMICS

Theory of orientational relaxation in the low-temperature phase of fullerite C_{60}

V. D. Natsik and A. V. Podolskiy

*B. Verkin Institute for Low Temperature Physics and Engineering, National Academy of Sciences of the Ukraine, 310164 Kharkov, Ukraine**

(Submitted February 25, 1998; revised March 23, 1998)
Fiz. Nizk. Temp. **24**, 689–703 (July 1998)

A microscopic extension of the phenomenological model of double-well orientational states, viz., pentagonal and hexagonal configurations of molecules, which is widely used for describing the low-temperature phase of fullerite C_{60}, is proposed. A simple kinetic equation and a set of thermodynamic relations connecting the crystal lattice deformation, the concentration of orientational excitations of molecules, and temperature are derived. Basic physical properties of the low-temperature phase, including orientational glass transition, heat capacity, thermal expansion, rheological properties and damping of elastic vibrations are described on a unified basis. The conclusions of the theory are compared with the experimental data, and empirical estimates are obtained for the parameters of double-well states and the lattice–orientational interaction. It is shown that the large values of thermal expansion and acoustic damping above the orientation glass-transition temperature of fullerite are due to high-intensity lattice–orientational interaction. © *1998 American Institute of Physics.*
[S1063-777X(98)01407-8]

INTRODUCTION

Recent studies following the synthesis of crystalline fullerene (fullerite) C_{60} in 1990 revealed peculiarities in the structural parameters as well as in thermal, acoustical, and mechanical characteristics of this crystal in the low-temperature range, which are associated with the thermal excitation of rotational degrees of freedom of molecules.[1–11] These peculiarities were explained qualitatively on the basis of phenomenological concepts of the structural–orientational phase transition near 260 K and double-well orientational states in the low-temperature phase, which are referred to as the pentagonal (p) and hexagonal (h) configurations.[5] This research aims at a microscopic extension of phenomenological concepts concerning double-well orientational states of molecules and at constructing of a simple kinetic theory providing a description of peculiarities in the temperature behavior of most physical properties of the low-temperature phase of fullerite C_{60} on a unified basis. In order to avoid terminological ambiguity and formulate the problem more clearly, it is expedient to characterize briefly the structural features of fullerite, which are associated with rotational degrees of freedom and orientational states of molecules.

A molecule of fullerene C_{60} has the shape of a truncated icosahedron whose surface is formed by 12 pentagons framed by single covalent bonds C–C and by 20 hexagons framed by alternating single C–C and double C=C bonds. The large set of symmetry axes of the molecule contains 10 third-order axes passing through the centers of diametrically opposite hexagons. Pentagon and hexagon configurations of electron orbitals and third-order symmetry axes of the molecule play a significant role in the classification of structural states of crystalline fullerene.

The formation of a crystal from C_{60} molecules is ensured by the forces of paired Van der Waals (dispersion) interaction, which have a significant noncentral component determined by the mutual orientation of molecules and associated with the nonuniformity of electron density on the surfaces of molecules. Fullerite C_{60} exists in three structural modifications differing in the ordering of molecular orientation. The critical temperature[4] $T_c \approx 260$ K separates two crystallographic modifications: the high-temperature face-centered cubic (fcc) phase and the low-temperature simple cubic (sc) phase. Thermal excitation of rotational degrees of freedom at $T > T_c$ leads to random rotation of molecules, which effectively ''smooths'' the angular dependence of pair molecular interaction potential and ensures the energy expedience of densely packed fcc structure. In the region of low temperatures $T < T_c$, the centers of gravity of molecules also form a lattice of sites of the fcc structure, but their third-order symmetry axes acquire ordered orientations in view of the increasing role of the noncentral component of dispersion forces: nearest neighbors are divided into symmetrically equivalent groups containing four molecules each (tetrahedra) with different orientations of third-order axes along spatial diagonals of an elementary cube within a group (the $\langle 111 \rangle$ type directions), and the centers of such tetrahedra form a lattice of sites of a sc structure.

At the same time, the sc phase possesses one more important structural feature, viz., partial orientational disorder associated with the possible retarded rotations of molecules about ordered axes between two orientational configurations

nonequivalent from the energy point of view: pentagonal (p) and hexagonal (h). Both configurations correspond to the minima in the angular dependence of molecular interaction energy: a deeper (global) minimum is attained as the double bond of a molecule approaches the center of a pentagon on the surface of a neighboring molecule (p-configuration); a shallower (local) minimum takes place when a double bond approaches the center of a hexagon on the surface of a neighboring molecule (h-configuration). The difference in the energies of p- and h-configurations per intermolecular bond is of the order of 0.01 eV, and the energy barrier separating the configurations is of the order of 0.3 eV.[2,3,6] For this reason, molecular rotations (i.e., transitions between these configurations) can be stimulated by thermal fluctuations at moderately low temperatures. Thus, the ideal thermodynamically equilibrium structure of the sc phase of fullerite C_{60} corresponds to p-configurations of all molecules, while h-configurations should be regarded as thermally excited local orientational defects of the crystal structure. Various experimental methods of structural analysis and theoretical estimates show that a thermodynamically equilibrium relative concentration of defective h-configurations in a wide temperature range 90–260 K has a high value of the order of 20–40%, and thermally activated local transitions (rotations) between p- and h-configurations occur during time periods of the order of or less than 10 s, i.e., rapidly on the laboratory time scale. Consequently, the orientational subsystem of the sc phase in this temperature range can be regarded as a sort of orientational liquid (OL). On the other hand, in the case of cooling of fullerite below $T_g \approx 90$ K, thermodynamic equilibrium between p- and h-configurations has no time to be established over reasonable laboratory time intervals. This allows us to treat the sc phase under these conditions as orientational glass (OG) with a relative concentration of frozen defective h-configurations of the order of 20% and to refer to the temperature T_g as the temperature of orientational glass transition.[4]

1. PHYSICAL MODEL AND KINETIC EQUATION FOR DESCRIBING ORIENTATIONAL RELAXATION IN SC PHASE

The orientational structure of the sc phase of fullerite C_{60} described in Introduction can be put in correspondence (conditionally to a certain extent) with the energy states of neighboring molecules shown in Fig. 1.[3–5,9] Strictly speaking, orientational states of molecules and transitions between them in a crystal are of cooperative nature, and hence the angle θ has the meaning of a generalized coordinate describing local disorientation of neighboring molecules. The introduction of such a coordinate in the description of orientational molecular dynamics in fullerite C_{60} has not been substantiated microscopically. Nevertheless, the phenomenological model of local ''one-particle'' double-well states illustrated in Fig. 1 is found to be constructive and makes it possible to construct a description of thermal, acoustic, and mechanical properties of the low-temperature sc phase of fullerite which matches the experimental results.

An individual unit cell of fullerite contains four molecules each of which has 12 nearest neighbors.

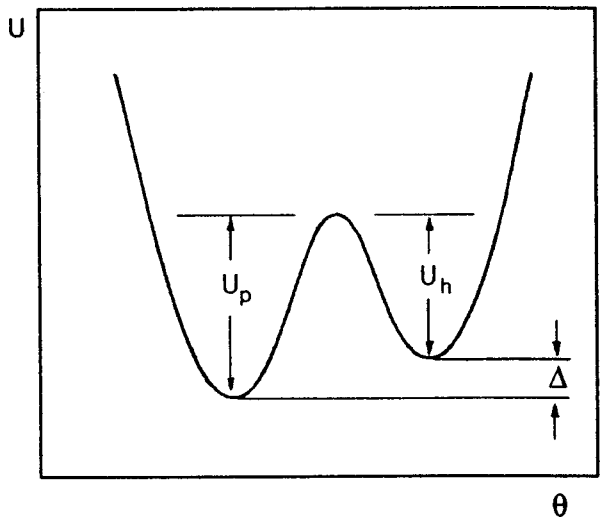

FIG. 1. Schematic diagram of a double-well potential $U(\theta)$ characterizing the dependence of the interaction energy of adjacent fullerite molecules on the generalized angular variable.

Consequently, the volume concentration of N_0 paired intermolecular bonds satisfies the relation $N_0 a^3 = 24$, where a is the length of an edge of an elementary cube. Since each intermolecular bond can be in two metastable states, we can also introduce in our model instantaneous local concentrations $N_p(\mathbf{r},t)$ and $N_h(\mathbf{r},t)$ of pentagon and hexagon configurations respectively, which satisfy the balance equation (conservation law)

$$N_p(\mathbf{r},t) + N_h(\mathbf{r},t) = N_0, \tag{1}$$

where the spatial coordinate $\mathbf{r}$ is determined to within the lattice parameter a.

Refining the model of double-well states formulated above, we note that its application presumes that it is possible to single out a set of identical independent collective angular variables θ among the aggregate of rotational degrees of freedom of crystalline C_{60} molecules, whose number is normalized to the parameter N_0, and classical dynamics for each such variable is determined by an equation of motion of the type

$$I \frac{d^2}{dt^2}\theta = -\frac{d}{d\theta} U(\theta) + K_s(t). \tag{2}$$

Here I is the effective moment of inertia corresponding to the variable θ, and $K_s(t)$ is the moment of forces describing the interaction of the singled out degree of freedom with the remaining degrees of freedom of the crystal. The macroscopically large number of the remaining degrees of freedom allows us to consider their effect on the singled out ''particle'' with the dynamic variable θ as an action of a certain effective medium (thermostat) and to treat the function $K_s(t)$ as a complex random process whose statistical parameters are determined by the state of thermal motion of the medium.

The phenomenological model described above makes it possible to analyze the orientational relaxation in the sc phase of fullerite C_{60} by using the results of the theory of one-dimensional Brownian motion of a particle in a potential relief of a complex shape.[12] We shall assume that the

medium (the majority of degrees of freedom of the crystal) is in thermodynamic equilibrium with temperature T and consider only relaxation processes associated with deviation of the dynamic variable θ from equilibrium. According to Kramers,[12] we can introduce for each of the potential wells depicted in Fig. 1 a mean time τ_p or τ_h over which a particle which was first localized near the bottom of the corresponding well leaves it through the barrier U_p or U_h under the action of thermal impacts exerted by the medium. For low temperatures $kT \ll U_p'', U_h$ (k is the Boltzmann constant), these times are determined by an activation formula of the form

$$\tau_{p,h} = \tau_0 \exp \frac{U_{p,h}}{kT}. \tag{3}$$

In the general case, the pre-exponential factor τ_0 in this formula has a complex structure. The typical values of τ_0 are of the order of effective period $2\pi(I/U_{p,h}'')^{1/2}$ of molecular librations, where $U_{p,h}''$ is the value of the second derivative of the function $U(\theta)$ near the bottom of the corresponding well. This means that, strictly speaking, τ_0 has different values for pentagonal and hexagonal configurations. Besides, exact values of τ_0 also depend on the parameters of the medium, viz., the temperature of the crystal and the viscous friction emerging if we take into account the relation between molecular librations and translational vibrations of the crystal (phonons) and vibrations of the atomic core of the molecule. A quantitative description of such dependences on the basis of the phenomenological model under investigation is impossible; we can only expect that the dependence of the pre-exponential factor $\tau_0^{(p,h)}$ on temperature and parameters of the potential $U(\theta)$ is much weaker than the dependence determined by the exponent. For this reason, we shall henceforth assume that the factor $\tau_0^{(p,h)}$ in (3) is a constant the which is the same for both configurations ($\tau_0^{(p)} \approx \tau_0^{(h)} = \tau_0 = \text{const}$) and treat the parameters U_p, U_h, $\Delta = U_p - U_h$, and τ_0 as microscopic characteristics of the phenomenological model under investigation.

Using the times τ_p and τ_h and the balance equation (1), we can easily write a simple kinetic equation describing the time variation of the concentration N_h or $N_p = N_0 - N_h$:

$$\frac{\partial}{\partial t} N_h = -\frac{N_h}{\tau_h} + \frac{N_0 - N_h}{\tau_p}. \tag{4}$$

The effect of orientational transitions in the system of molecules on the thermal, acoustic, and mechanical properties of fullerite can be taken into account in the model under investigation by supplementing this model with some more relations and parameters which also have microscopic or semimicroscopic meaning. In order to describe the relation between rotational degrees of freedom of molecules with the fullerite lattice, we must introduce corrections associated with elastic deformations of the lattice to the parameters of the double-well potential $U(\theta)$. Assuming that the deformations are small, we can neglect their effect on the parameter τ_0 in the first approximation and to confine our analysis of a linear approximation for the dependence of the barriers U_p and U_h on the components of the symmetric strain tensor ε_{ik}:

$$U_{p,h}^{(\varepsilon)} = U_{p,h} - v_{ik}^{(p,h)} \varepsilon_{ik}, \tag{5}$$

where $v_{ik}^{(p,h)}$ is the symmetric matrix whose components have the dimensions of energy. Here and below, recurring coordinate indices indicate summation. For a crystal of cubic symmetry, the matrix of deformation potential constants $v_{ik}^{(p,h)}$ in crystallographic coordinates must have the form $v_{ik}^{(p,h)} = v_{p,h}\delta_{ik}$ (δ_{ik} is the Kronecker symbol), i.e., linear corrections to scalar energy parameters are determined by only one scalar combination, i.e., the sum of diagonal component of the strain tensor $\varepsilon_{ll} = \delta_{ik}\varepsilon_{ik}$. Thus, taking into account the cubic symmetry of fullerite, we can write the deformation corrections (5) to the parameters of the double-well potential in the form

$$\begin{aligned} U_{p,h}^{(\varepsilon)} &= U_{p,h} - v_{p,h}\varepsilon_{ll}, \\ \Delta^{(\varepsilon)} &= \Delta - v_\Delta \varepsilon_{ll}, \end{aligned} \tag{6}$$

where $v_\Delta = v_p - v_h$.

It should be noted that the dependence of the scalar parameters $U_{p,h}$ on the shear components of elastic strain in the linear approximation in the case of a cubic crystal can appear only if we take into account the rotational modes of deformation in the nonsymmetric theory of elasticity.[13] This presumes a correction to the right-hand sides of relations (6) of the scalar terms proportional to spatial derivatives of the field of rotational vectors for macroscopic elements of the crystalline medium, which is equivalent to the inclusion of spatial dispersion effects in the continuum mechanics of the crystal.

Replacing the times $\tau_{p,h}$ in the kinetic equation (4) by $\tau_{p,h}^{(\varepsilon)} = \tau_0 \exp(U_{p,h}^{(\varepsilon)}/kT)$ we obtain an equation determining the kinetics of orientational relaxation of molecules in the presence of macroscopic elastic deformations in the fullerite crystal. In the further analysis, it is convenient to go over to the relative concentrations $n_p = N_p/N_0$ and $n_h = N_h/N_0$ of pentagon and hexagon configurations. The variation of these quantities is described by the following equations:

$$\begin{cases} \tau^{(\varepsilon)} \dfrac{\partial}{\partial t} n_h + n_h = \dfrac{\tau^{(\varepsilon)}}{\tau_p^{(\varepsilon)}}, \\ n_p + n_h = 1 \end{cases} \tag{7}$$

$$\tau_{p,h}^{(\varepsilon)} = \tau_0 \exp\left(\frac{U_{p,h} - v_{p,h}\varepsilon_{ll}}{kT}\right), \quad \tau^{(\varepsilon)} = \frac{\tau_p^{(\varepsilon)}\tau_h^{(\varepsilon)}}{\tau_p^{(\varepsilon)} + \tau_h^{(\varepsilon)}}. \tag{8}$$

Let us consider one more important aspect pertaining to the conditions of applicability of Eqs. (7) for describing processes associated with varying strain fields $\varepsilon_{ik} = \varepsilon_{ik}(\mathbf{r}, t)$. Expression (3) for the mean time of emergence of a particle from a potential well was derived by Kramers[12] for the time-independent potential $U(\theta)$. In this case, the role of minimal time intervals appearing in the corresponding diffusion problem is played by the time of correlation of a random process $K_s(t)$ and the period τ_0 of oscillations of the particle near the bottom of the well; these time intervals are equal to characteristic molecular time and are of the order of or less than 10^{-12} s. This means that the quantity $\tau_{p,h}$ defined by

formula (3) preserves the meaning of ''instantaneous'' value of the mean time of emergence of the particle from the potential well for time-dependent values of the barriers $U_{p,h}$ only if the characteristic time of their variation is much longer than these minimal time intervals. Consequently, we can expect that the kinetic equation (7) is also applicable for describing orientational relaxation processes excited by the varying strain fields $\varepsilon_{ik}(\mathbf{r},t)$ if these strains vary insignificantly over time intervals of the order of the molecular libration period τ_0.

The effectiveness of the microscopic refinement of the phenomenological model of double-well orientational states in fullerite C_{60} proposed in this section is determined by the possibility of indicating and carrying out experiments whose results make it possible to obtain empirical estimates for all the model parameters introduced above: the barrier heights U_p and U_h and their difference $\Delta = U_p - U_h$, the effective libration period τ_0, the deformation potential constants v_p and v_h, and their difference $v_\Delta = v_p - v_h$.

2. THERMODYNAMIC EQUILIBRIUM AND ORIENTATIONAL GLASS FORMATION

If the temperature of the crystal and local deformations remain unchanged for a long time, the local densities of pentagon and hexagon configurations assume thermodynamically equilibrium values $\overline{n}_p(\mathbf{r};T)$ and $\overline{n}_h(\mathbf{r};T)$ which are described by the time-independent solutions of Eq. (7):

$$\overline{n}_h(\mathbf{r};T) = \overline{n}_h^{(\varepsilon)}(T) = \left[1+\exp\left(\frac{\Delta - v_\Delta \varepsilon_{ll}(\mathbf{r})}{kT}\right)\right]^{-1},$$
$$\overline{n}_p(\mathbf{r};T) = \overline{n}_p^{(\varepsilon)}(T) = \left[1+\exp\left(-\frac{\Delta - v_\Delta \varepsilon_{ll}(\mathbf{r})}{kT}\right)\right]^{-1}. \tag{9}$$

It should be noted that equilibrium nonuniformities of orientational ordering in fullerite emerging due to static nonuniform strains $\varepsilon_{ik}(\mathbf{r})$ of the crystal can appear in the analysis of the fullerite structure by the x-ray and neutron spectroscopy method; their inclusion can be essential in describing acoustic and mechanical properties of the crystal. For example, considerable nonuniformity of orientational ordering must be observed in fullerite containing dislocations. Formulas (9) make it possible to describe nonuniform distributions of pentagon and hexagon configurations appearing around stationary dislocation lines (an analog of the Cottrell or Snoek impurity atmospheres which are encountered in the physics of alloys).[14] For this purpose, we must substitute into formulas (9) the expressions for the strain fields of individual dislocations.

For pure and well-annealed fullerite samples, we can neglect nonuniform strains ($\varepsilon_{ik} \equiv 0$). In this case, the relation between $\overline{n}_h$ and $\overline{n}_p$ is determined only by the value of the temperature T and the parameter $\Delta = U_p - U_h$:

$$kT \ln \frac{\overline{n}_p(T)}{\overline{n}_h(T)} = \Delta. \tag{10}$$

This formula makes it possible to obtain an empirical estimate of the parameter Δ by using the results of experimental study of the temperature dependence of orientational order in fullerite (e.g., the results of x-ray of neutron diffraction spectroscopy). The generally accepted estimate at the present time is $\Delta \simeq (11-13)\times 10^{-3}$ eV.[2–6]

The factor $\tau^{(\varepsilon)}$ appearing in front of the time derivative in the kinetic equation (7) has the meaning of relaxation time over which the local thermodynamic equilibrium in molecular orientation is restored if it was violated by a fast change in internal stresses or external conditions (e.g., change in temperature). Indeed, it can easily be seen that, for time-independent values of T and ε_{ik}, the approach to orientational equilibrium is described by solutions of equations (7) of the type

$$n_{p,h}(t) - \overline{n}_{p,h}^{(\varepsilon)} = [n_{p,h}(0) - \overline{n}_{p,h}^{(\varepsilon)}]\exp\left(-\frac{t}{\tau^{(\varepsilon)}}\right), \tag{11}$$

where $n_{p,h}(0)$ are the initial nonequilibrium concentrations of pentagonal and hexagonal configurations. The explicit dependence of $\tau^{(\varepsilon)}$ on temperature and coordinates is given by

$$\tau^{(\varepsilon)} = \frac{\tau_0 \exp[\{U_h - v_h \varepsilon_{ll}(\mathbf{r})\}/kT]}{1+\exp\left(-\dfrac{\Delta - v_\Delta \varepsilon_{ll}(\mathbf{r})}{kT}\right)}. \tag{12}$$

Relations (11) and (12) form the basis of the formal description of the orientational glass transition in fullerite. We shall consider this phenomenon for quite perfect crystals, neglecting random strain fields, but presuming the presence of bulk compression ε_{ll} by the hydrostatic pressure $P = -B^{(0)}\varepsilon_{ll}$, where $B^{(0)}$ is the isothermal bulk compression modulus. Let t_{lab} be the characteristic laboratory time, i.e., the total time of temperature stabilization for the sample and of carrying out the physical experiment at a given constant temperature. Reasonable values of this quantity can be estimated as $t_{\text{lab}} \sim 10^3$ s with a possible spread within an order of magnitude. The orientational glass transition temperature $T_g(P)$ can be naturally determined as the solution of the equation

$$\tau^{(P)}(T) = t_{\text{lab}}. \tag{13}$$

Using formula (12) and taking into account the inequality $\Delta \ll U_h$ and a considerable indeterminacy of the numerical values of the parameters τ_0 and t_{lab}, we can write the approximate solution of Eq. (13) determining the temperature T_g with a relative error of the order of 10%:

$$T_g(P) \simeq \left(k \ln \frac{t_{\text{lab}}}{\tau_0}\right)^{-1}\left(U_h + \frac{v_h}{B^{(0)}} P\right). \tag{14}$$

In experimental investigation of the temperature dependence of the physical parameters of fullerite, certain singularities, whose recording makes it possible to obtain empirical values of T_g, are observed in some cases in the vicinity of the orientational glass-transition temperature. For example, such a singularity was observed in experiments on the thermal conductivity of fullerite C_{60} under pressure;[11] these experiments confirm the linear form of the function $T_g(P)$ in a very wide range of pressures, while under zero pressure we obtain the value of $T_g(0) \simeq 90$ K. Formula (14) together with experimental data on the $T_g(P)$ dependence can be used for obtaining empirical values of the parameters U_h and v_h of

the theory. The positive slope of the $T_g(P)$ curve recorded in Ref. 11 indicates the positive sign of the deformation potential constant $v_h > 0$.

Assuming that $t_{\text{lab}} \simeq 3 \times 10^3$ s and using the empirical estimates $\tau_0 \approx 3 \times 10^{-14}$ s and $B \approx 10$ GPa obtained in acoustic experiments,[15,16] as well as the estimate $dT_g/dP \approx 60$ K/GPa obtained in Ref. 11, we obtain the values of $U_h \simeq 0.3$ eV and $v_h \simeq 2.0$ eV.

3. THERMODYNAMICS OF DEFORMATION, THERMAL EXPANSION, AND HEAT CAPACITY OF THE SC PHASE

In this section, we propose a thermodynamic description of the influence of rotational degrees of freedom of molecules on deformation and thermal properties of fullerite in the temperature range (T_g, T_c). In an analysis of this phenomenon, we shall use basic principles of the thermodynamics of irreversible processes, the phenomenological model of double-well orientational states, and microscopic refinement of this model described in Sec. 1.

We shall assume that a thermodynamically equilibrium state of the fullerite lattice is undeformed at a certain preset temperature T and in the absence of external forces. Let us suppose that fullerite becomes nonequilibrium as a result of quite small long-wave strains $\varepsilon_{ik}(\mathbf{r},t)$. These strains cause small local deviations of temperature from its initial value T and violate the equilibrium orientational ordering of molecules, i.e., generate small deviations of local concentrations of hexagonal and pentagonal configurations from their equilibrium values $\overline{n_h^{(0)}}(T)$ and $\overline{n_p^{(0)}}(T) = 1 - \overline{n_h^{(0)}}(T)$. In order to describe these deviations, we introduce the variable temperature $T + \Theta(\mathbf{r},t)$ and the nonequilibrium correction to the number density of hexagon excitations: $n_h(\mathbf{r},t) = \overline{n_h^{(0)}} + \nu_h(\mathbf{r},t)$. According to the basic concepts of the thermodynamics of irreversible processes (see, for example, Ref. 17), we can describe a nonequilibrium state of the crystal by introducing the free energy density $\widetilde{F}(T + \Theta, \varepsilon_{ik}, \nu_h)$ which is regarded as a function of temperature, extrinsic parameters ε_{ik} and the intrinsic parameter ν_h, the latter being treated as an independent thermodynamic variable, For the given initial temperature T, the total differential of free energy is defined by the thermodynamic identity

$$d\widetilde{F} = \frac{\partial \widetilde{F}}{\partial \Theta}\, d\Theta + \frac{\partial \widetilde{F}}{\partial \varepsilon_{ik}}\, d\varepsilon_{ik} + \frac{\partial \widetilde{F}}{\partial \nu_h}\, d\nu_h, \tag{15}$$

while equilibrium states of the crystal must correspond to the minima of the function $\widetilde{F}(T + \Theta, \varepsilon_{ik}, \nu_h)$ under preset external conditions.

For example, for given values of the strain tensor components ε_{ik}, the thermodynamic equilibrium state is defined by the equation

$$\left[\frac{\partial \widetilde{F}(T + \Theta, \varepsilon_{ik}, \nu_h)}{\partial \nu_h}\right]_{\Theta, \varepsilon_{ik}} = 0. \tag{16}$$

The solution of this equation for the variable ν_h must describe an equilibrium distribution of hexagonal configurations $\overline{n_h^{(\varepsilon)}}(T) = \overline{n_h^{(0)}}(T) + \overline{\nu_h^{(\varepsilon)}}(T)$, in a statically deformed crystal, which is equivalent to distribution (9) obtained from microscopic considerations in statistical mechanics.

The mechanical stress tensor components σ_{ik} are defined in thermodynamics as generalized forces conjugate to the strain tensor components ε_{ik}:

$$\sigma_{ik} = \left[\frac{\partial \widetilde{F}(T + \Theta, \varepsilon_{ik}, \nu_h)}{\partial \varepsilon_{ik}}\right]_{\Theta, \nu_h}. \tag{17}$$

Specific calculations require the knowledge of the explicit form of the function $\widetilde{F}(T + \Theta, \varepsilon_{ik}, \nu_h)$. For small values of nonequilibrium corrections Θ, ε_{ik}, and ν_h, this function can be approximated by the truncated power series

$$\begin{aligned}\widetilde{F} = {} & F_0(T) - \alpha(T)\Theta\varepsilon_{ik}\delta_{ik} - \beta(T)\Theta\nu_h - \gamma(T)\nu_h\delta_{ik}\varepsilon_{ik} \\ & - (1/2)\xi(T)\Theta^2 + (1/2)\eta(T)\nu_h^2 + (1/2)\lambda_{iklm}(T)\varepsilon_{ik}\varepsilon_{lm} \\ & + \ldots .\end{aligned} \tag{18}$$

In order to describe the thermal and rheological properties of fullerite in the approximation of linear response, it is sufficient to confine our analysis only to the quadratic terms in this expansion. The free energy F_0 of the initial state and the coefficient of expansion (18) are certain functions of the initial temperature T, and their explicit form can be obtained only from an analysis of the thermal motion of the crystal on microscopic level by using the methods of statistical mechanics. It should also be noted that the tensor structure of the terms proportional to the strain tensor ε_{ik} presumes the cubic symmetry of the crystal and disregard of spatial dispersion effects associated with the interaction of hexagonal excitations with gradients of local lattice rotations (see the discussion of this question in Sec. 1).

The physical meaning of individual coefficients in expansion (18) can be clarified by analyzing several reversible processes corresponding to different external conditions by using this expansion. We shall carry out such an analysis following the procedure described by Landau and Lifshitz.[18]

Let us first consider two processes of reversible deformation of the crystal: (1) quasistatic deformation at a constant temperature $(\Theta \equiv 0)$, and (2) extremely rapid deformation during which heat exchange between different regions of the crystal and the relaxation of local values of number density of hexagonal excitations cannot take place $(\nu_h \equiv 0)$. In the first case, minimization of the free energy (18) in ν_h gives the change in the quasiequilibrium concentration of hexagonal excitations, which follows after the slow variation of strain:

$$\nu_h^{(\varepsilon)} = \frac{\gamma}{\eta}\, \delta_{ik}\varepsilon_{ik}. \tag{19}$$

Substituting (19) into (18) and putting $\Theta \equiv 0$, we obtain the free energy of a reversible isothermal deformation, which can be written in the form

$$\begin{aligned}\widetilde{F}^{(T)} &= F_0(T) + (1/2)\lambda_{iklm}^{(0)}\varepsilon_{ik}\varepsilon_{lm}, \\ \lambda_{iklm}^{(0)} &= \lambda_{iklm} - \frac{\gamma^2}{\eta}\, \delta_{ik}\delta_{lm}.\end{aligned} \tag{20}$$

It can be seen that the parameters $\lambda_{iklm}^{(0)}$ have the meaning of tensor components of isothermal elastic moduli.

For the second process under investigation, the entropy $\tilde{S}=-[\partial\tilde{F}/\partial T]_{\varepsilon_{ik}}$ of individual regions of the crystal must remain unchanged, while local values of temperature change in proportion to strains. From the conditions of vanishing of the parameter ν_h and the entropy increment $\partial(\tilde{F}-F_0)_{\varepsilon_{ik}}/\partial\Theta=0$ we obtain

$$\Theta^{(\varepsilon)}=-\frac{\alpha}{\xi}\,\delta_{ik}\varepsilon_{ik}. \tag{21}$$

Substituting (21) into (18) and putting $\nu_h=0$, we obtain the free energy of adiabatic deformation, which can be written in the form

$$\begin{aligned}&\tilde{F}^{(S)}=F_0(T)+(1/2)\lambda_{iklm}^{(\infty)}\varepsilon_{ik}\varepsilon_{lm},\\&\lambda_{iklm}^{(\infty)}=\lambda_{iklm}+\frac{\alpha^2}{\xi}\,\delta_{ik}\delta_{lm}.\end{aligned} \tag{22}$$

Here $\lambda_{iklm}^{(\infty)}$ are the tensor components of adiabatic elastic moduli. According to (20) and (22), the difference between adiabatic and isothermal moduli is defined as

$$\lambda_{iklm}^{(\infty)}-\lambda_{iklm}^{(0)}=\left(\frac{\alpha^2}{\xi}+\frac{\gamma^2}{\eta}\right)\delta_{ik}\delta_{lm}. \tag{23}$$

The elastic moduli tensor for a cubic crystal has three independent components. In the crystallographic system of coordinates, we normally use $\lambda_{1111}=C_{11}$, $\lambda_{1122}=C_{12}$ and $\lambda_{1212}=\lambda_{2323}=C_{44}$, as independent components, while the bulk modulus B is defined by the relation $3B=C_{11}+2C_{12}$. Thus, the shear modulus C_{44} in the approximation used here has the same value for isothermal and adiabatic deformation, the only difference appearing for the compression modulus:

$$B^{(\infty)}-B^{(0)}=\frac{\alpha^2}{\xi}+\frac{\gamma^2}{\eta}. \tag{24}$$

Let us consider two more reversible processes: slow heating of the crystal at constant volume (i.e., in the absence of strains $\varepsilon_{ik}\equiv0$) and under constant pressure (in the absence of stresses $\sigma_{ik}\equiv0$). In the former case, minimization of (18) with respect to the variable ν_h gives the variation of the concentration of hexagonal excitations, which is proportional to the temperature increment:

$$\nu_h^{(\Theta)}=\frac{\beta}{\eta}\,\Theta. \tag{25}$$

Substituting (25) into (18) and putting $\varepsilon_{ik}=0$, we obtain the following expression describing the variation of free energy as a result of slow heating at constant volume:

$$\tilde{F}^{(V)}=F_0(T)-\frac{1}{2}\left(\xi+\frac{\beta^2}{\eta}\right)\Theta^2. \tag{26}$$

This formula leads to the relation connecting the coefficient of expansion (18) with the heat capacity of the crystal at constant volume $C_V=-T\partial^2F^{(V)}/\partial\Theta^2$ (this quantity is reduced to unit volume of the crystal):

$$C_V=T\left(\xi+\frac{\beta^2}{\eta}\right). \tag{27}$$

In the case of slow heating of the unstressed crystal ($\sigma_{ik}\equiv0$), the increase in temperature is accompanied by a change in the concentration of hexagonal excitations $\nu_h^{(\Theta)}$, and the thermal expansion strain $\varepsilon_{ik}^{(\Theta)}$ is generated. These quantities are solutions of the system of two equations corresponding to the minimization of the free energy (18) over the variables ν_h and ε_{ik}:

$$\begin{cases}\lambda_{iklm}\varepsilon_{lm}-\gamma\nu_h\delta_{ik}=\alpha\Theta\,\delta_{ik},\\ \gamma\delta_{ik}\varepsilon_{ik}-\eta\nu_h=-\beta\Theta.\end{cases} \tag{28}$$

Going over to isothermal moduli in accordance with (20), we obtain

$$\begin{aligned}&\varepsilon_{ik}^{(\Theta)}=\frac{\alpha\eta+\gamma\beta}{3\eta B^{(0)}}\,\Theta\,\delta_{ik},\\&\nu_h^{(\Theta)}=\frac{B^{(0)}\beta\eta+\gamma(\alpha\eta+\gamma\beta)}{\eta^2B^{(0)}}\,\Theta.\end{aligned} \tag{29}$$

The substitution of these quantities into (18) leads to the expression describing the variation of free energy as a result of slow heating of the crystal under constant pressure ($\sigma_{ik}\equiv0$):

$$\tilde{F}^{(P)}=F_0(T)-\frac{1}{2}\left[\xi+\frac{\beta^2}{\eta}+\frac{(\alpha\eta+\gamma\beta)^2}{\eta^2B^{(0)}}\right]\Theta^2. \tag{30}$$

This leads to the following expressions for the heat capacity at constant pressure $C_P=-T\partial^2\tilde{F}^{(P)}/\partial\Theta^2$ and the difference C_P-C_V in heat capacities:

$$\begin{aligned}&C_P=T\left[\xi+\frac{\beta^2}{\eta}+\frac{(\alpha\eta+\gamma\beta)^2}{B^{(0)}\eta^2}\right],\\&\frac{C_P-C_V}{T}=\frac{(\alpha\eta+\gamma\beta)^2}{B^{(0)}\eta^2}.\end{aligned} \tag{31}$$

Using formulas (29) and (31), we can also obtain easily the expressions for the thermal expansion coefficient $\kappa=\partial\varepsilon_{ll}^{(\Theta)}/\partial\Theta$ and the well-known thermodynamic relation between κ and the heat capacity difference[18] C_P-C_V:

$$\kappa=\frac{\alpha\eta+\gamma\beta}{B^{(0)}\eta},\quad C_P-C_V=TB^{(0)}\kappa^2. \tag{32}$$

The formulas (24), (27), (31), and (32) derived above make it possible to connect the formally introduced coefficients α, β, γ, ξ, η, and λ_{iklm} of expansion (18) with the macroscopic parameters $\lambda_{iklm}^{(\infty)}$, $\lambda_{iklm}^{(0)}$, C_V, C_P, κ, of the crystal which have a clear physical meaning as can be measured experimentally. It should also be noted that the terms in these formulas depending on the coefficients β, γ, and η describe the contribution of thermal excitations of the rotational degrees of freedom of molecules to physical parameters of fullerite, while the terms depending on the coefficients α and ξ describe the purely lattice (phonon) contribution. The possibility and expedience of such a separation in the theoretical formulas and in the experimental

data processing are due to qualitatively different forms of the temperature dependences of each of these contributions.

It is also useful to establish the relation between the coefficient β, γ, and η characterizing the orientational contribution to the thermodynamics of fullerite and the parameters of the model of double-well orientational states of molecules, which was described in Sec. 1. For this purpose, we must compare some of the results of the thermodynamic analysis with microscopic relations presented in Sec. 1. For the given time-independent strain ε_{ik} and a given temperature $T+\Theta$, the minimization of the free energy (18) over the variable ν_h leads to the equilibrium distribution

$$\overline{\nu_h}(\Theta,\varepsilon_{ik})=\overline{n_h^{(\varepsilon)}}(T+\Theta)-\overline{n_h^{(0)}}(T)=\frac{\gamma}{\eta}\,\varepsilon_{ll}+\frac{\beta}{\eta}\,\Theta, \quad (33)$$

which is equivalent to the distribution (9) derived from the kinetic equation (7). If we write (9) for the temperature $T+\Theta$ and linearize in ε_{ik} and Θ, we obtain

$$\overline{n_h^{(\varepsilon)}}(T+\Theta)-\overline{n_h^{(0)}}(T)=f\left(\frac{\Delta}{kT}\right)\left(\frac{v_\Delta}{\Delta}\,\varepsilon_{ll}+\frac{\Theta}{T}\right), \quad (34a)$$

$$f(x)=\frac{xe^x}{(1+e^x)^2}. \quad (34b)$$

Comparing (34a) and (33), we arrive at the following relations:

$$\frac{\gamma}{\eta}=\frac{v_\Delta}{\Delta}\,f\left(\frac{\Delta}{kT}\right), \quad \frac{\beta}{\eta}=T^{-1}f\left(\frac{\Delta}{kT}\right). \quad (35)$$

In an analysis of experimental data, one more relation connecting the coefficient γ with the orientational component $\kappa_{\rm or}=\kappa-\alpha/B^{(0)}$ of the thermal expansion coefficient can be found helpful. Using formulas (32) and (35), we obtain

$$\gamma=\frac{B^{(0)}\kappa_{\rm or}T}{f(\Delta/kT)}. \quad (36)$$

According to (18), the value of the coefficient γ characterizes the intensity of interaction of orientational states of C_{60} molecules with the lattice deformation. Consequently, the direct proportionality of γ to the orientational component $\kappa_{\rm or}$ of thermal expansion is quite natural.

Experiments[19] show that orientational ordering of molecules strongly affects the lattice parameter of fullerite: the value of $a(T)$ changes strongly at the phase-transition point T_c as well as for gradual ''freezing out'' of hexagonal excitations during cooling of fullerite in the temperature interval (T_g,T_c), while the $a(T)$ dependence in the region $T<T_g$ is much weaker. This observation suggests that $\kappa\approx\kappa_{\rm or}$ in the range corresponding to orientational liquid. Besides, the thermal expansion coefficient at these temperatures virtually remains unchanged and equal to $\kappa\simeq 6\times10^{-5}$ K^{-1} (except a weak anomaly near 100 K). Relations (35) and (36) lead to the following simple formula for the orientational contribution to the heat capacity per unit volume, which is valid for $\kappa\approx\kappa_{\rm or}$:

$$C_P^{(\rm or)}=C_P-T\xi(T)=\frac{B^{(0)}\kappa_{\rm or}\Delta}{v_\Delta}\left(1+\frac{v_\Delta\kappa_{\rm or}T}{\Delta}\right). \quad (37)$$

In the case when the lattice and orientational contributions in the measured values of C_P are separable, formula (37) can be used for obtaining an empirical estimate of the ratio v_Δ/Δ.

4. EFFECT OF ORIENTATIONAL RELAXATION ON RHEOLOGICAL PROPERTIES OF FULLERITE

A description of acoustic and deformation properties of solids in the continuum mechanics presumes the knowledge of the basic rheological equation connecting internal stresses $\sigma_{ik}(\mathbf{r},t)$ and the strains $\varepsilon_{ik}(\mathbf{r},t)$ generating them. For perfectly elastic linear bodies, such a relation is determined by the classical Hooke's law $\sigma_{ik}(\mathbf{r},t)=\lambda_{iklm}\varepsilon_{lm}(\mathbf{r},t)$, where λ_{iklm} is the tensor of elastic moduli of the material. It is important that this relation is local in space and time, i.e., long-range effects as well as aftereffects are absent. However, the presence of quasi-independent internal degrees of freedom associated with lattice deformations in the solid violates the local nature of the relation between stresses and strains. The basic rheological equation for such bodies in the linear approximation assumes the form[20,21]

$$\sigma_{ik}(\mathbf{r},t)=\int_{-\infty}^{t}dt'\int d^3\mathbf{r}'\,\Lambda_{iklm}(\mathbf{r}-\mathbf{r}',t-t')\varepsilon_{lm}(\mathbf{r}',t). \quad (38)$$

This equation takes into account aftereffect and internal friction inherent in actual solids, and the role of elastic moduli in such a generalized Hooke's law is played by an integral operator with the kernel $\Lambda_{iklm}(\mathbf{r},t)$.

Equation (38) assumes the conventional form of Hooke's law if instead of the fields $\varepsilon_{ik}(\mathbf{r},t)$ and $\sigma_{ik}(\mathbf{r},t)$ we consider their Fourier components $\tilde{\varepsilon}_{ik}(\mathbf{q},\omega)$ and $\tilde{\sigma}_{ik}(\mathbf{q},\omega)$ (here $\mathbf{q}$ and ω are the wave vector and cyclic frequency respectively). Applying to (38) the Fourier transformation in spatial and time variables, we obtain the linear algebraic relation

$$\tilde{\sigma}_{ik}(\mathbf{q},\omega)=\tilde{\lambda}_{iklm}(\mathbf{q},\omega)\tilde{\varepsilon}_{lm}(\mathbf{q},\omega), \quad (39)$$

in which, in contrast to Hooke's law, the components of the tensor $\tilde{\lambda}_{iklm}$ are generally complex-values quantities depending on $\mathbf{q}$ and ω:

$$\tilde{\lambda}_{iklm}(\mathbf{q},\omega)=\int_0^\infty dt\int d^3\mathbf{r}\Lambda_{iklm}(\mathbf{r},t)\mathrm{e}^{-i(\mathbf{q}\cdot\mathbf{r}-\omega t)}. \quad (40)$$

We can find the explicit form of the kernel $\Lambda_{iklm}(\mathbf{r},t)$ or complex elastic moduli $\tilde{\lambda}_{iklm}(\mathbf{q},\omega)$ from an analysis of joint evolution of dynamic variables of the crystal lattice and internal degrees of freedom of the crystal associated with it by the methods of thermodynamics and statistical mechanics of irreversible processes (see, for example, Ref. 21). While describing the aftereffects and internal friction in fullerite, we must take into account the relation between dynamic deformations of the lattice and rotational degrees of freedom of molecules or orientational excitations corresponding to them. Using the formal thermodynamic definition of the stress tensor (17) and the expansion of free energy (18), we can obtain a relation connecting σ_{ik} with the strain tensor components ε_{ik}, temperature increment Θ, and concentrations ν_h of hexagonal excitations. In order to establish the one-to-one cor-

respondence between the mechanical stress $\sigma_{ik}(\mathbf{r},t)$ and the strain $\varepsilon_{ik}(\mathbf{r},t)$ varying according to a preset law, this relation should be supplemented with two kinetic equations: the equation of thermal conductivity that makes it possible to describe the relaxation of local temperature variations $\Theta(\mathbf{r},t)$ emerging due to varying strain $\varepsilon_{ik}(\mathbf{r},t)$, and the equation describing the relaxation of the nonequilibrium concentration $\nu_h(\mathbf{r},t)$ which is also associated with the strain $\varepsilon_{ik}(\mathbf{r},t)$. Thus, the problem is reduced to an analysis of the system of three equations which have the following form in the linear response approximation:

$$\sigma_{ik}(\mathbf{r},t)=\lambda_{iklm}\varepsilon_{lm}(\mathbf{r},t)-\alpha\Theta(\mathbf{r},t)\,\delta_{ik}-\gamma\nu_h(\mathbf{r},t)\,\delta_{ik}, \tag{41a}$$

$$\dot{\Theta}(\mathbf{r},t)-\chi\delta_{ik}\nabla_i\nabla_k\Theta(\mathbf{r},t)=-\frac{\alpha}{\xi}\,\delta_{ik}\dot{\varepsilon}_{ik}(\mathbf{r},t), \tag{41b}$$

$$\tau^{(0)}\dot{\nu}_h+\nu_h=f\left(\frac{\Delta}{kT}\right)\left(\frac{v_\Delta}{\Delta}\,\delta_{ik}\varepsilon_{ik}+\frac{\Theta}{T}\right). \tag{41c}$$

Here the dot over a variable indicates the time differentiation operator, ∇_i is the operator of differentiation with respect to the coordinate, $\chi\delta_{ik}$ is the thermal diffusivity tensor for a cubic crystal (the parameter χ together with the coefficients of expansion (18) is a certain function of the initial temperature T), and the right-hand side of the thermal conductivity equation (41b) describes the rate of variation of local values of temperature as a result of adiabatic deformation (see formula (21)). Equation (41c) was obtained by linearizing the kinetic equation (7) with respect to the strain tensor components ε_{ik} and temperature increment Θ.

The choice of single-values solutions of the system of equations (41) is ensured by its supplementing with a few additional relations: the initial condition for Eq. (41c), and the initial and boundary conditions for Eq. (41b). If we assume that the strain tensor components ε_{ik} vary according to a preset law from the initial values $\varepsilon_{ik}(\mathbf{r},-\infty)\equiv 0$, it is natural to take the initial conditions in the form $\Theta(\mathbf{r},-\infty)\equiv 0$ and $\nu_h(\mathbf{r},-\infty)\equiv 0$. In the case of an unbounded crystal, we can assume that the strains $\varepsilon_{ik}(\mathbf{r},t)$ are equal to zero at an infinitely long distance. In this case, the boundary conditions to Eq. (41b) should be chosen as the natural requirement that $\Theta(\mathbf{r},t)$ vanishes at infinity. An analysis of aftereffects in finite fullerite crystals can be carried out only if we know the conditions of the force and thermal contact between the crystal surface and the ambient.

If we solve solutions of Eqs. (41b) and (41c) assuming that the function $\varepsilon_{ik}(\mathbf{r},t)$ is given and substitute them into (41a), we obtain the integral relation (38) with an explicit form of the coordinate and time dependence of the kernel $\Lambda_{iklm}(\mathbf{r},t)$. However, it is most convenient to analyze specific physical problems by converting equations (41) into a system of algebraic equations. This can be done by expanding $\varepsilon_{ik}(\mathbf{r},t)$ and the required functions $\sigma_{ik}(\mathbf{r},t)$, $\Theta(\mathbf{r},t)$ and $\nu_h(\mathbf{r},t)$ in the eigenfunctions of the corresponding boundary-value problem and by carrying out the Fourier and Laplace transformations in the time coordinate. By way of an example, we consider deformations of an unbounded crystal and seek solutions of Eqs. (41) in the form of Fourier expansions in plane waves $\exp^{(\mathbf{q}\cdot\mathbf{r}-\omega t)}$, which leads to Hooke's law in the form (39) with complex moduli of elasticity described by the formula

$$\tilde{\lambda}_{iklm}(\mathbf{q},\omega)=\lambda^{(\infty)}_{iklm}-\left[\frac{q^2\chi R_W}{q^2\chi-i\omega}+\frac{R_{\mathrm{or}}}{1-i\omega\tau^{(0)}}+\frac{i\omega R_{W0}}{(q^2\chi-i\omega)(1-i\omega\tau^{(0)})}\right]B^{(\infty)}\delta_{ik}\delta_{lm}. \tag{42}$$

Here we have used the notation

$$R_W=\frac{\alpha^2}{B^{(\infty)}\xi},\quad R_{\mathrm{or}}=\frac{\gamma f v_\Delta}{B^{(\infty)}\Delta},\quad R_{W0}=\frac{\alpha\gamma f}{B^{(\infty)}\xi T}. \tag{43}$$

These dimensionless parameters determine the relative variation of elastic moduli associated with relaxation processes: R_W and R_{or} characterize the contribution of thermal and orientational relaxation moduli to dispersion, while R_{W0} describes the interference contribution. As expected, the value of R_{or} is proportional to the coefficient γ of orientational–lattice interaction.

It should be noted that the relaxation processes considered here lead only to a renormalization of the elastic moduli tensor components λ_{1111} and λ_{1122} (i.e., the crystal rigidity to extension–compression), but do not affect the shear modulus λ_{1212}. We must also pay attention to spatial dispersion (dependence on $\mathbf{q}$) of elastic moduli associated with thermal relaxation; the emergence of aftereffects in the given case is quite natural since a relaxation process is the heat exchange between spatially separated extension and compression regions in a strain wave.

5. ACOUSTIC PROPERTIES OF THE SC PHASE

In a description of acoustic properties of solids, spatial and temporal delocalization of the kernel in the integral relation (38) appear in the form of damping effects of acoustic waves and dispersion in the velocity of their propagation. The velocities and damping factors of acoustic waves are determined by the solutions $\omega(\mathbf{q})$ of the dispersion equation

$$\det|\rho\omega^2\delta_{ik}-\tilde{\lambda}_{iklm}(\mathbf{q},\omega)q_lq_m|=0, \tag{44}$$

where ρ is the crystal density. In the presence of dispersion and imaginary corrections to elastic moduli, the real component $\mathrm{Re}\,\omega(\mathbf{q})$ of the solutions acquire a more complicated dependence on $\mathbf{q}$ (dispersion in the velocities of sound), and imaginary corrections $\mathrm{Im}\,\omega(\mathbf{q})\neq 0$ describing attenuation appear.

Acoustical properties of single crystals are often studied by using the high-frequency echo-pulse method: excitation and detection of waves having a given frequency ω and propagating along individual crystallographic directions. In this case, $\mathbf{q}=\mathbf{n}q$, where $\mathbf{n}$ is a unit vector with preset components, and it is convenient to seek the solution of the dispersion equation (44) in the form

$$q(\mathbf{n},\omega)=\frac{\omega}{s(\mathbf{n},\omega)}+i\Gamma(\mathbf{n},\omega)=\frac{\omega}{s(\mathbf{n},\omega)}\left[1+i\,\frac{\delta(\mathbf{n},\omega)}{2\pi}\right], \tag{45}$$

where s, Γ, and δ are the wave velocity, damping factor per unit length, and logarithmic decrement respectively. In a crystal with the cubic symmetry, the propagation of high-frequency elastic waves is studied most often along the following three directions: $\langle 100\rangle$, $\langle 110\rangle$, and $\langle 111\rangle$.

At first sight, the use of the complex moduli (42) leads to the dispersion equation (44) of a complex form. The main difficulty in the search for exact solutions of this equation is the dependence of the components of the tensor $\tilde{\lambda}_{iklm}$ on the magnitude q of the wave vector. However, the method of echo-pulse spectroscopy gives interesting results in the case of a small dispersion of elastic moduli, which is formally described by the inequalities $R_W \ll 1$ and $R_{\rm or} \ll 1$. These inequalities make it possible to obtain approximate solutions of the dispersion equations by perturbation theory methods by putting $\tilde{\lambda}_{iklm}=\lambda^{(\infty)}_{iklm}$ in the zeroth approximation. If we are interested only in linear corrections in the parameters R_W and $R_{\rm or}$, we can make the replacement

$$\chi q^2 = \chi\left[\frac{\omega}{s^{(\infty)}(\mathbf{n})}\right]^2$$

for the substitution (42) into (44), i.e., consider the values of the wave number corresponding to the energy–momentum relation in the zeroth approximation, i.e., $\omega = s^{(\infty)}(\mathbf{n})q \times (s^{(\infty)}(\mathbf{n})$ are the values of the velocities of sound determined by adiabatic moduli of elasticity). After such a substitution, the difficulties encountered in the solution of the dispersion equation (44) for the variable q are the same as for the zeroth approximation (see, for example, Ref. 22).

If we consider oscillations with the wave vector $\mathbf{q}$ oriented along the crystallographic directions $\langle 100\rangle$, $\langle 110\rangle$, and $\langle 111\rangle$, two transverse and one longitudinal waves[22] will propagate in each of these directions without damping in the zeroth approximation. Since the thermal and orientational relaxation do not lead to a renormalization of the shear modulus ($\lambda_{1212} \equiv C^{(\infty)}_{44}$), their inclusion leads to frequency dispersion of velocity and attenuation of only longitudinal waves.[1)] For each of these directions, Eq. (44) splits into three simple equation as in the absence of dispersion. Two of these equations describe undamped transverse waves (subscript t), and the third equation describes an attenuating longitudinal wave (subscript l). In the linear approximation in the parameters R_W and $R_{\rm or}$, these equations have the form

$$\omega = s^{(\infty)}_{t1}(\mathbf{n})q, \quad \omega = s^{(\infty)}_{t2}(\mathbf{n})q \tag{46}$$

for transverse waves and

$$\omega = \left\{1 - A(\mathbf{n})\left[\frac{R_{\rm or}}{1 - i\tau_{\rm or}\omega} + \frac{i\omega\tau_W R_W}{1 + i\tau_W\omega} - \frac{R_{W0}}{(1 - i\tau_{\rm or}\omega)(1 + i\tau_W\omega)}\right]\right\}^{1/2} s^{(\infty)}_l(\mathbf{n})q \tag{47}$$

for the longitudinal wave. Here $A(\mathbf{n})$ is a dimensionless combination of the tensor components $\lambda^{(\infty)}_{iklm}$, which has a positive value of the order of unity. This relation also contains two parameters having dimensions of time: the orientational relaxation time $\tau_{\rm or} = \tau^{(0)}(T)$ which depends on time, and the thermal relaxation time $\tau_W = \tau_W(\mathbf{n}, T)$ which depends both on temperature and on the direction of wave propagation. The relaxation times are defined as

$$\tau_{\rm or}(T) = \frac{\tau_0 \exp(U_p/kT)}{1 + \exp(\Delta/kT)},$$

$$\tau_W(\mathbf{n}, T) = \chi(T)[s^{(\infty)}_l(\mathbf{n})]^{-2}. \tag{48}$$

The formulas connecting the velocities $s^{(\infty)}_{t1}(\mathbf{n})$, $s^{(\infty)}_{t2}(\mathbf{n})$ and $s^{(\infty)}_l(\mathbf{n})$ of acoustic waves with adiabatic moduli of elasticity are well known for the crystallographic directions under investigation (see, for example, Ref. 22). The relation between the coefficient $A(\mathbf{n})$ and the moduli is given by

$$A = \frac{C^{(\infty)}_{11} + 2C^{(\infty)}_{12}}{3C^{(\infty)}_{11}} \text{ in the } \langle 100\rangle \text{ direction},$$

$$A = \frac{2(C^{(\infty)}_{11} + 2C^{(\infty)}_{12})}{3(C^{(\infty)}_{11} + C^{(\infty)}_{12} + 2C^{(\infty)}_{44})} \text{ in the } \langle 110\rangle \text{ direction},$$

$$A = \frac{C^{(\infty)}_{11} + 2C^{(\infty)}_{12}}{C^{(\infty)}_{11} + 2C^{(\infty)}_{12} + 4C^{(\infty)}_{44}} \text{ in the } \langle 111\rangle \text{ direction}. \tag{49}$$

Comparing the dispersion equation (47) with expression (45), we can easily derive formulas describing the frequency dispersion of velocity and attenuation of the longitudinal wave. In the approximation linear in the parameters R_W, $R_{\rm or}$, and R_{W0}, we have

$$\frac{s^{(\infty)}_l(\mathbf{n}) - s_l(\mathbf{n},\omega)}{s^{(\infty)}_l(\mathbf{n})} = \frac{A(\mathbf{n})}{2}\left[\frac{R_{\rm or}}{1 + \tau^2_{\rm or}\omega^2} + \frac{R_W\tau^2_W\omega^2}{1 + \tau^2_W\omega^2} - \frac{R_{W0}(1 + \tau_{\rm or}\tau_W\omega^2)}{(1 + \tau^2_{\rm or}\omega^2)(1 + \tau^2_W\omega^2)}\right], \tag{50}$$

$$\delta(\mathbf{n},\omega) = \pi A(\mathbf{n})\left[\frac{R_{\rm or}\tau_{\rm or}\omega}{1 + \tau^2_{\rm or}\omega^2} + \frac{R_W\tau_W\omega}{1 + \tau^2_W\omega^2} - \frac{R_{W0}(\tau_{\rm or} - \tau_W)\omega}{(1 + \tau^2_{\rm or}\omega^2)(1 + \tau^2_W\omega^2)}\right]. \tag{51}$$

The velocity and decrement of a wave are determined by its frequency ω and the direction of propagation $\mathbf{n}$, but the temperature dependence of these quantities is more significant. The latter is determined by the relatively weak dependences $R_{\rm or}(T)$, $R_W(T)$, $R_{W0}(T)$ and much stronger dependences $\tau_{\rm or}(T)$ and $\tau_W(T)$. Most informative results can be obtained by acoustic spectroscopy of crystals in the vicinity of temperatures $T_m(\omega)$ defined by the relaxation resonance condition $\omega\tau(T) \approx 1$: these temperatures of the crystal correspond to peaks of the $\delta(T)$ dependence and blurred steps on the $s(T)$ dependence.

In the case of fullerite C_{60}, each relaxation effect considered here (orientational and thermal relaxation) must generally correspond to its own relaxation resonance at temperatures $T^{(\rm or)}_m(\omega)$ and $T^{(W)}_m(\omega,\mathbf{n})$, defined by the equations

$$\omega\tau_{\rm or}(T) \approx 1, \quad \omega\tau_W(\mathbf{n}, T) \approx 1. \tag{52}$$

According to Eqs. (51) and (52), the heights of absorption peaks are proportional to the parameters $R_{\rm or}$ and R_W and are connected through them with the initial parameters of the theory as well as a few parameters accessible to direct experimental measurements:

$$\delta_m^{(\rm or)}=\delta(T_m^{(\rm or)})=\frac{\pi A f \gamma v_\Delta}{2B^{(\infty)}\Delta}, \tag{53}$$

$$\delta_m^{(W)}=\delta(T_m^{(W)})=\frac{\pi A \alpha^2}{2B^{(\infty)}\xi}. \tag{54}$$

The recording of relaxation peaks extends the potentialities for obtaining empirical estimates of phenomenological parameters of the theory. For example, using relations (36) and (53) and neglecting the difference between $B^{(0)}$ and $B^{(\infty)}$, we obtain

$$\frac{v_\Delta}{\Delta}=\frac{2\delta_m^{(\rm or)}}{\pi A \kappa_{\rm or} T_m^{(\rm or)}}. \tag{55}$$

In the first approximation in small relaxation parameters, formulas (37) and (55) also lead to a relation containing only the quantities accessible to direct experimental measurements:

$$C_P^{(\rm or)}\simeq\frac{\pi A B T_m^{(\rm or)}\kappa_{\rm or}^2}{2\delta_m^{(\rm or)}}. \tag{56}$$

This relation makes it possible to estimate the relative contribution of orientational excitations of molecules to the thermal parameters of fullerite in the range of orientational liquid (T_g,T_c).

The low-temperature phase of fullerite C_{60} has been studied comprehensively by high-frequency acoustic spectroscopy methods, although most of the results unfortunately pertain to polycrystals. In order to compare the relations derived above with the experimental data, we shall use the results obtained in Refs. 15 and 16 as well as the results of other authors presented in these publications. Experimental data lead to the following estimates: $A\approx 0.5-0.6$, $B\approx 10$ GPa, $T_m^{(\rm or)}\simeq 215$ K, and $\delta_m^{(\rm or)}\approx 2\times 10^{-2}$. Substituting these values and $\kappa_{\rm or}\approx 6\times 10^{-5}$ K^{-1} into formula (56), we obtain the following estimate for the orientational contribution to heat capacity of fullerite: $C_P^{(\rm or)}\approx 3.3\times 10^5$ J·m^{-3}·K^{-1}≈150 J·mole^{-1}·K^{-1} (the possible error in this estimate is of the order of 20%). The results of experiments[15] show that the heat capacity C_P in the temperature range 100–200 K remains unchanged and has the value coinciding with the estimate obtained above. Such a coincidence leads to the conclusion that the thermal characteristics of fullerite C_{60} in the range (T_g,T_c) of orientational liquid are mainly determined by thermal excitations of hexagonal configurations of molecules: in the first approximation, $\kappa\simeq\kappa_{\rm or}=$const and $C_P=C_P^{(\rm or)}=$const in this range. Naturally, this conclusion is not valid for the immediate vicinity of the temperature T_c where anomalies in thermal parameters associated with the phase transition are manifested.

Substituting the above experimental values of parameters of fullerite into formula (55), we obtain the estimate $v_\Delta\approx 2\Delta$ for the deformation potential constant. Taking into account the estimates obtained in Sec. 2, we arrive at the conclusion that $v_p>v_h$, and we can write with an accuracy to within 20%

$$v_p\approx v_h\approx 2\ \text{eV},\quad v_\Delta\approx 24\times 10^{-3}\ \text{eV}.$$

Experimental data on the dependence of the peak temperature $T_m^{(\rm or)}$ on the ultrasonic frequency[15,16] together with the resonance condition (52) and formula (48) for $\tau_{\rm or}(T)$ lead to the following estimates for the parameters of a double-well potential:

$$U_p\approx U_h\approx 0.3\ \text{eV},\quad \tau_0=3\times 10^{-14}\ \text{s}.$$

It is also expedient to estimate the value of the lattice–orientational interaction parameter γ, or the dimensionless parameter ε_h corresponding to it:

$$\varepsilon_h=\frac{\gamma}{B}=\frac{\kappa_{\rm or}\Delta}{k}\,\varphi\left(\frac{\Delta}{kT}\right),\quad \varphi(x)=\frac{(1+e^x)^2}{x^2e^x}. \tag{57}$$

In the temperature range (T_g,T_c) we are interested in, the function $\varphi(x)$ varies approximately from 3 to 17, and hence the following estimate is valid for the midpoint of this interval: $\varepsilon_h\sim 8\times 10^{-2}$. The large value of this parameter is actually responsible for the decisive effect of orientational excitations on the thermal and acoustic properties of fullerite.

Concluding this section, we note the highly damping properties of the low-temperature phase of fullerite C_{60}. According to the existing classification,[23] solids for which the logarithmic damping factor attains values of $\delta\geqslant 10^{-2}$ belong to highly damping materials. As a rule, such properties are inherent in complex metal alloys at temperatures of the order of or above the room temperature. Fullerite C_{60} belongs to a few materials preserving highly damping properties over a wide temperature range. The above analysis shows that a physical reason behind this property is the large value of the lattice–orientational interaction parameter.

CONCLUSIONS

1. The microscopic extension proposed for the phenomenological model of doublewell orientation states (pentagonal or hexagonal configurations) is used extensively for describing various physical properties of the low-temperature phase of fullerite C_{60} which exists below the phase transition temperature $T_c=260$ K. A set of microscopic parameters characterizing the thermally activated transitions between p and h configurations (barriers U_p,U_h, their difference $\Delta=U_p-U_h$, and the characteristic molecular libration period τ_0) is proposed as well as a set of deformation potential constants v_p, v_h and v_Δ characterizing the effect of fullerite lattice deformations on these barriers and their difference. A simple kinetic equation describing the relaxation of nonequilibrium concentrations of p and h configurations is obtained.

2. A semimicroscopic model of double-well orientational states and their corollaries are compared with the thermodynamic relations for macroscopic physical characteris-

tics of fullerite obtained from an analysis of the boundary properties of free energy for the processes of heating, as well as quasistatic and dynamic deformation.

3. Relations connecting the structural and experimentally measurable thermodynamic characteristics of fullerite with the microscopic parameters of the double-well state parameters are derived.

4. Expressions are obtained for complex elastic moduli of fullerite, connecting its mechanical characteristics with the double-well state model parameters, and relaxation corrections to the velocities and sound wave attenuation rate are calculated and analyzed.

5. A comparison of the conclusions of the theory with the results of experimental measurements of structural, thermal and acoustic characteristics of fullerite leads to empirical estimates for microscopic parameters of double-well orientation states: $U_p \approx U_h \approx 0.3$ eV, $\Delta \approx 12\times 10^{-3}$ eV, $v_p \approx v_h \approx 2.0$ eV, $v_\Delta \approx 24\times 10^{-3}$ eV.

6. It is shown that significant effects of thermal expansion and acoustic absorption, which are characteristic of the low-temperature phase of fullerite C_{60}, are due to the relatively large intensity of interaction of rotational degrees of freedom of molecules with the crystal lattice deformations. A formula describing the magnitude and temperature dependence of the dimensionless coefficient of lattice-orientational interaction in the range of existence of the orientational liquid is obtained as well as an empirical estimate $\varepsilon_h \simeq 8 \times 10^{-2}$ for the magnitude of this coefficient.

The authors are privileged to dedicate this publication to Prof. A. M. Kosevich on his 70th birth anniversary, and express their gratitude for the honor of belonging to his school.

Sincere thanks are due to S. V. Lubenets, V. G. Manzheli, and M. A. Strzhemechnyi for their interest in this research and for fruitful discussions.

This research was supported by Prof. H. Kostorz (Institute of Applied Physics, Zurich) and the Swiss National Science Foundation CEEC/NIS (Project No. 7UKPJ048645).

*E-mail: natsik@ilt.kharkov.ua

[1)]For sound propagation in other less symmetric directions along which waves cannot be classified strictly as longitudinal and transverse waves, thermal and orientational relaxation must lead to dispersion and attenuation of all three acoustic modes. Propagation of transverse waves in fullerite polycrystals must also be accompanied by relaxation effects, since individual grains in the field of transverse wave are subjected not only to shear strain, but also to compression i.e., extension strain.

[1] P. A. Heiney, J. A. Fischer, A. R. McGhie *et al.*, Phys. Rev. Lett. **66**, 2911 (1991).
[2] F. Gugenberg, R. Heid, C, Meingast *et al.*, Phys. Rev. Lett. **69**, 3774 (1992).
[3] R. C. Yu, N. Tea, M. V. Salanon *et al.*, Phys. Rev. Lett. **68**, 2050 (1992).
[4] M. I. F. David, R. M. Ibberson, T. J. S. Dennis *et al.*, Europhys. Lett. **18**, 219 (1992).
[5] M. I. F. David, R. M. Ibberson, and T. Matsuo, Proc. R. Soc. London **A442**, 129 (1993).
[6] W. Schranz, A. Fnith, P. Dolinar *et al.*, Phys. Rev. Lett. **71**, 1561 (1993).
[7] J. E. Fischer and P. A. Heiney, J. Phys. Chem. **54**, 1725 (1993).
[8] V. M. Loktev, Fiz. Nizk. Temp. **18**, 217 (1992) [Sov. J. Low Temp. Phys. **18**, 149 (1992)].
[9] J. D. Axe, S. C. Moss, and D. A. Neumann, in *Solid State Physics* (edited by H. Ehrenreich and F. Spaepan), Acad. Press, New York, Vol. **48**, 150 (1994).
[10] V. D. Natsik, S. V. Lubenets, and L. S. Fomenko, Fiz. Nizk. Temp. **22**, 337 (1996) [Low Temp. Phys. **22**, 264 (1996)].
[11] O. Anderson, A. Soldatov, and B. Sundqvist, Phys. Rev. B **54**, 3093 (1996).
[12] H. A. Kramers, Physica **7**, 284 (1940).
[13] W. Nowacki, *Theory of Elasticity*, Mir, Moscow (1975).
[14] J. Hirth and J. Lothe, *Theory of Dislocations* (McGraw-Hill, New York, NY, 1967).
[15] N. P. Kobelev, Ya. M. Soifer, I. O. Bashkin *et al.*, Phys. Status Solidi B **190**, 157 (1995).
[16] Ya. M. Soifer and N. P. Kobelev, Mol. Mater. **7**, 267 (1996).
[17] M. A. Leont'ev, *Introduction to Thermodynamics. Statistical Physics* (in Russian), Nauka, Moscow (1983).
[18] L. D. Landau and E. M. Lifshitz, *Theory of Elasticity* (in Russian), Nauka, Moscow (1987).
[19] L. S. Fomenko, V. D. Natsik, S. V. Lubenets *et al.*, Fiz. Nizk. Temp. **21**, 465 (1995) [Low Temp. Phys. **21**, 364 (1995)].
[20] A. M. Kosevich and V. D. Natsik, Fiz. Tverd. Tela (Leningrad) **8**, 1250 (1966) [Sov. Phys. Solid State **8**, 993 (1966)].
[21] V. S. Postnikov, *Internal Friction in Metals* (in Russian), Metallurgiya, Moscow (1969).
[22] C. Kittel, *Introduction to Solid State Physics*, Nauka, Moscow (1978).
[23] K. Sugimoto, Met. Inst. Sci. and Res. **35**, 31 (1978).

Translated by R. S. Wadhwa

CHRONICLES

Igor Mikhailovich Dmitrenko
(On his 70th birthday)

Fiz. Nizk. Temp. **24**, 704 (July 1998)
[S1063-777X(98)01507-2]

July 24, 1998, marks the 70th birthday of Igor Mikhailovich Dmitrenko, Member of the National Academy of Sciences of the Ukraine, Head of the Department at the B. Verkin Institute for Low Temperature Physics and Engineering, Kharkov, and a leading specialist in the field of superconductor physics. Dr. Dmitrenko gained wide recognition owing to his brilliant experiments on the transient Josephson effect, quantum interference, magnetic flux quantization, and macroscopic tunneling phenomena in superconducting systems. His name is associated with numerous applied investigations aimed at practical application of the achievements of superconducting technology in modern electronics. As regards his scientific organizational capabilities, it is hard to overestimate or overemphasize the role of Dr. Dmitrenko as one of the founders and supervisors of the Institute for Low Temperature Physics and Engineering in Kharkov, and also as an active member of the Editorial of our journal.

We heartily congratulate Igor Mikhailovich on his jubilee, and wish him health, prosperity and many years of fruitful scientific activity.

The Editorial Board

Translated by R. S. Wadhwa

Yurii Moiseevich Kagan
(On his 70th birthday)

Fiz. Nizk. Temp. **24**, 705 (July 1998)
[S1063-777X(98)01607-7]

The leading Russian theoretical physicist Yurii Moiseevich Kagan, Member of the Russian Academy of Sciences, turned 70 on July 5, 1998. The field of low-temperature physics research has been enriched greatly by his brilliant ideas and results, including the prediction of quasilocal vibrations of crystals with impurities, a microscopic analysis of the phonon spectra of metals, description of the metastable metallic phase of hydrogen and tunneling mechanism of phase transitions, prediction of the self-localization effect during quantum diffusion of defects in crystals, and a comprehensive analysis of the kinetics of spin-polarized hydrogen.

We sincerely wish Yurii Moiseevich many more years of his inherent scientific activity, dynamism and energy in research and his cordial relationship with colleagues and pupils.

The Editorial Board

Translated by R. S. Wadhwa

Arnold Markovich Kosevich
(On his 70th birthday)

Fiz. Nizk. Temp. **24**, 706 (July 1998)
[S1063-777X(98)01707-1]

Arnold Markovich Kosevich, Corresponding Member of the National Academy of Sciences of the Ukraine, Head of the Department at the B. Verkin Institute for Low Temperature Physics and Engineering, Kharkov, Professor at the Kharkov State University, and a talented theoretical physicist, turned 70 on July 7, 1998. His name is associated with the solution of numerous fundamental problems in the field of low-temperature solid state physics. He was one of the founders of the theory of quantum oscillatory effects in metals. The results obtained by A. M. Kosevich from investigations of phonon spectra and dynamic dislocation processes are widely used for describing thermal and mechanical properties of crystals. A profound and comprehensive analysis of dynamic nonlinear excitations in magnetically ordered media was carried out under his guidance. For many years, he has been an active member of the Editorial of our journal.

Arnold Markovich celebrates his 70th birthday at the zenith of his scientific career, with an irrepressible capacity to generate new original ideas and to develop them into important and brilliantly formulated results. We heartily congratulate Dr. Kosevich, and wish him health, prosperity and many years of fruitful scientific activity.

The Editorial Board

Translated by R. S. Wadhwa

